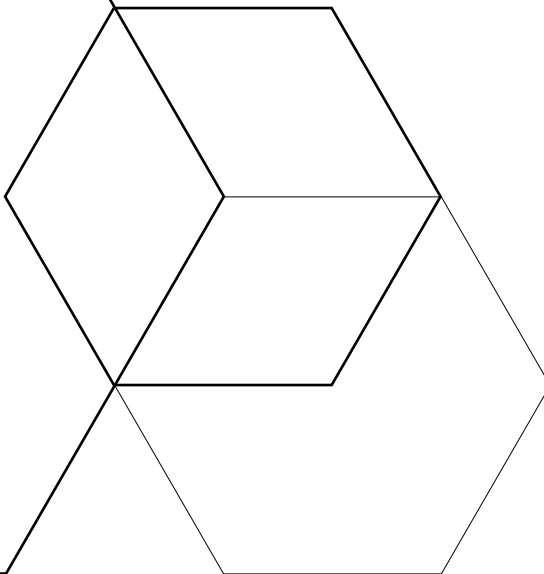
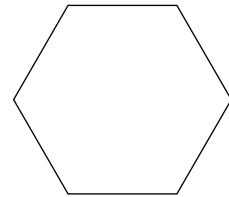


MRI-GUIDED PROSTATE BIOPSY: WHICH DIRECTION?

Martijn G. Schouten



Wat mij ontzettend heeft aangesproken tijdens het tot stand komen van dit proefschrift is het betrokken zijn bij de nieuwste technische ontwikkelingen en de implementatie hiervan in de klinische praktijk.

Martijn G. Schouten



MRI-guided prostate biopsy: which direction?

Proefschrift

ter verkrijging van de graad van doctor
aan de Radboud Universiteit Nijmegen
op gezag van de rector magnificus prof. dr. J.H.J.M. van Krieken,
volgens besluit van het college van decanen
in het openbaar te verdedigen op maandag 19 juni 2017
om 12.30 uur precies

door

Martijn Gerjan Schouten

geboren op 22 mei 1985
te Groningen

Colofon

© Martijn G. Schouten, Nijmegen, The Netherlands, Mei 2017

ISBN 9789462956469

Ontwerp Geert van Holland (www.geertvanholland.nl)

Print Proefschriftmaken, Nijmegen

The research in this thesis was funded by the Dutch Cancer Society (KWF Kankerbestrijding). The studies were performed at the Department of Radiology, Radboudumc, Nijmegen, the Netherlands.

Publication of this thesis was financially supported by Radboudumc, Health Valley Netherlands, Guerbet Nederland B.V. and Soteria Medical.

Promotoren

prof. dr. J.O. Barentsz
prof. dr. J.J. Fütterer (Universiteit Twente)

Copromotoren

dr. ir. T.W.J. Scheenen
dr. S. Misra (Universiteit Twente)

Manuscriptcommissie

prof. dr. J.A. Witjes
prof. dr. W.R. Gerritsen
dr. M. Moche (Universitätsklinikum Leipzig, Duitsland)

Paranimfen

dr. R.J. Klijn
drs. J. Doorduyn

TABLE OF CONTENTS

Chapter 1.0

Introduction

p 8

Chapter 2.0

Three-tesla magnetic resonance (MR)-guided prostate biopsy in men with increased prostate specific antigen and repeated, negative, random, systematic, transrectal ultrasound biopsies: detection of clinically significant prostate cancers

p 16

Chapter 3.0

Location of prostate cancers determined by multi-parametric and MR-guided biopsy in patients with elevated prostate specific antigen level and at least one negative transrectal ultrasound-guided biopsy

p 32

Chapter 4.0

Why and where do we miss significant prostate cancer with multi-parametric MRI followed by MR-guided and TRUS-guided biopsy in biopsy naïve men?

p 48

Chapter 5.0

Differentiation of prostatitis and prostate cancer by using diffusion-weighted MR imaging and MR-guided biopsy at 3T

p 64

Chapter 6.0

The accuracy and safety aspects of a novel robotic needle guide manipulator to perform transrectal prostate biopsies

p 82

Chapter 7.0

Evaluation of a robotic technique for transrectal MR-guided prostate biopsies

p 98

Chapter 8.0

Automated real-time needle-guide tracking for fast 3T MR-guided transrectal prostate biopsy: a feasibility study

p 112

Chapter 9.0

Summary and discussion

p 126

Samenvatting en conclusies

p 138

Dankwoord

p 144

Curriculum Vitae

p 147

Publications

p 148

CHAPTER 1.0 INTRODUCTION

Prostate cancer is the most commonly diagnosed form of cancer among male in Europe and the United States (1, 2). In the Netherlands prostate cancer was found in 21% of the total number of new cancer cases (Fig. 1) (3). Prostate cancer is not only frequently diagnosed it is also an important cause of death. In the Netherlands, prostate cancer is with 2535 men the second leading cause of death among men who die from cancer (11% of the total number of cancer deaths). In comparison, in the same year 3161 woman died from breast cancer (4).

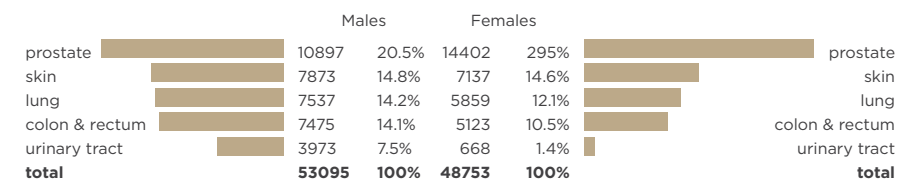


Figure 1: Incidence of most frequently diagnosed cancer locations in the Netherlands in 2013. With 10,897 new cases prostate cancer is the most frequently diagnosed cancer among men.

Current diagnosis of prostate cancer

In patients with an elevated prostate specific antigen (PSA) and/or abnormal digital rectal examination (DRE), random systematic transrectal ultrasound (TRUS)-guided biopsy is the standard of practice for prostate cancer diagnosis. However, this diagnostic pathway has limitations, because the PSA-test is highly sensitive but an unspecific marker and DRE and TRUS-guided biopsy are rather insensitive examinations for prostate cancer detection (5, 6).

With TRUS-guided biopsy an ultrasound probe is inserted in the rectum of the patient for biopsy guidance and 10 to 12 samples are obtained from the prostate according to a standardized scheme from the posterior peripheral zone. Due to sampling error more than 20% of the cancers are not detected in the first TRUS-guided biopsy session (7). With repeat TRUS-guided biopsies, prostate cancer detection rates decrease from 22% to 4% in four subsequent TRUS-guided biopsy sessions (7). Cancer detection rates of extensive saturation biopsy in men with 1, 2, and ≥ 3 prior negative TRUS biopsies were 56%, 42%, and 34%, respectively (8). Thus, a large number of patients with a persistently elevated or increasing PSA and one or more negative TRUS-guided biopsy sessions are subject to diagnostic insufficiency and uncertainty.

Besides the fact that, clinically significant tumours are missed with the current TRUS-guided biopsy protocol, clinically insignificant tumours are identified by chance. These tumours often remain dormant and clinically unimportant for decades. Consequently, early detection of prostate cancer, with the intent to diagnose this disease in a curable state, currently leads to over-diagnosis which in turn can result in over-treatment (9).

Furthermore, there is undergrading of tumour aggressiveness (represented by the Gleason score) when the less aggressive part of a tumour is sampled or the clinically significant lesion is missed. With the current clinical evaluation of PSA, DRE, and TRUS-guided biopsy it is not possible to accurately determine tumour characteristics and location since understaging (36%) and undergrading of the Gleason score (34-38%) is commonly seen (10-13). Understanding these limitations (Fig. 2) is of clinical importance because with these parameters, together with preference of the patient and physician, a decision is made for tailored treatment.

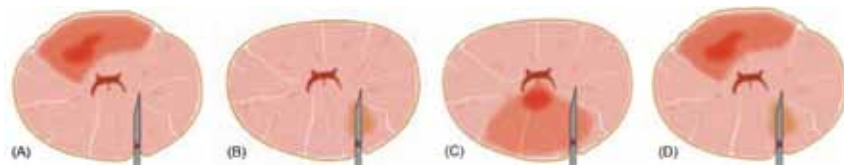


Figure 2: With the current TRUS-guided biopsy protocol clinically significant tumours are missed (A), furthermore clinically insignificant tumours are identified by chance (B), and there is undergrading of tumour aggressiveness (represented by the Gleason score) when the less aggressive part of a tumour is sampled (C) or the significant lesion is missed (D).

Furthermore, minimally invasive therapies are increasingly being investigated in localized prostate cancer (14-16). An important aspect is patient selection which relies on accurate tumour localization and risk stratification (17). Therefore, with the introduction of focal therapy the need for an adequate diagnostic tool has become even more important.

MR-guided prostate biopsy

With multi-parametric magnetic resonance imaging (MRI) techniques it is possible to obtain anatomical and functional information from prostatic tissue to identify cancerous lesions (18). Anatomical information can be obtained from T2-weighted MR imaging. However, T2-weighted imaging alone is sensitive but not specific for prostate cancer and should therefore be combined with functional imaging techniques (19). T1-weighted dynamic contrast enhanced (DCE) MRI following the administration of gadolinium-based contrast medium is the most common imaging method for evaluating tumour perfusion. Diffusion weighted imaging (DWI) is a measure for the mobility of water molecules. Differences in restricted diffusion are seen in tissues with a high cell density, such as prostate cancer. Apparent

diffusion coefficient (ADC)-values derived from DWI are related to prostate cancer aggressiveness (20). Functional MRI increases prostate cancer localization accuracy when added to anatomic T2-weighted MRI in a multi-parametric MRI exam (21, 22). Using the localization ability of multi-parametric MRI, it has recently become possible to target biopsies from cancer suspicious lesions with MR-guided biopsy rather than systematically sampling of the prostate with TRUS-guided biopsy. Besides the fact that less sampling cores are needed for diagnosis, this technique predominantly (44-87%) detects clinically significant prostate cancers in biopsy-naïve males and men with prior negative biopsies (18). Furthermore, the high negative predictive value (63 - 98%) of multi-parametric MRI can be used to rule out significant disease (18). These properties are promising regarding the current diagnostic dilemma since diagnosing insignificant tumours may cause unnecessary treatment of men who probably will not have clinical symptoms during their life (9). In this context it is important to keep in mind that most men will die with prostate cancer rather than die from it (23). Furthermore, multi-parametric MRI will play an important role in minimal invasive focal therapy regarding patient selection, treatment planning and monitoring and follow-up (14, 16, 24).

The question “which direction?” seems to be answered with MR-guided biopsy since it becomes possible to obtain biopsies from the most aggressive part of cancer suspicious lesions within the prostate seen on multi-parametric MRI. However, we are not there yet. Currently the only commercially available transrectal MR-guided prostate biopsy device is a manually adjustable device for needle guide positioning (25). After inserting a needle guide into the rectum (Fig. 3), MR images are acquired. Based on these MR images, the needle guide is manually positioned in the direction of the cancer suspicious lesion (Fig. 3).

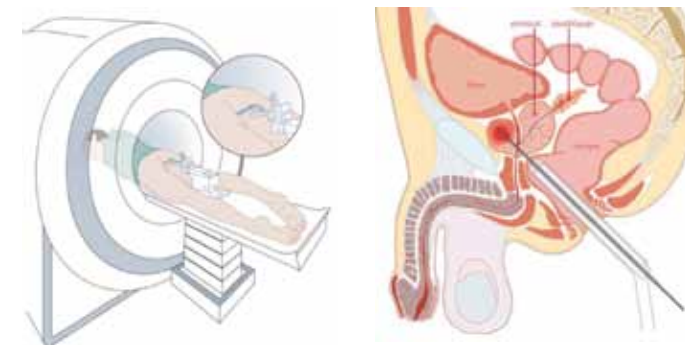


Figure 3: The patient is positioned in prone position with the needle guide inside the rectum (left image). The needle guide can be directed towards the cancer suspicious lesion by adjusting the biopsy device based on the acquired MR images (right image).

In order to manipulate needle guide direction the patient has to be moved out of the scanner bore and moved into the bore again for imaging. This is repeated many times until the needle is in the right position. Consequently, the physician needs to walk each time up and down between scanner room and control room to adjust needle guided direction and interpret needle guide direction on the MR-images. This procedure is unpleasant for the patient, time consuming and operator dependent. Furthermore, this increases the uncertainty of the exact needle position, due to potential movement of the patient during the procedure. In this thesis, we took the first step to solve these problems with the development of an MR-compatible robotic manipulator for real-time image guided positioning, which can be controlled at the operation console. In this way the patient does not need to be moved in and out of the magnet bore during needle guide positioning. The magnetic field used in MRI makes it a technically challenging area for robotics since metal and electricity cannot be applied within the scanner room. Specifically iron will be attracted by the magnetic field and other metals could disturb the homogeneity. Furthermore, radio frequency (RF) pulses required to create the MR signal can cause excessive heating in conducting materials by concentration of electrical currents (26).

Aim and outline of this thesis

In my thesis the symbiosis of imaging and robotics in MR-guided biopsy is investigated with the aim to improve prostate cancer diagnosis. The approach is described in the flowing chapters:

Chapter 2 reports on the detection rate of prostate cancer detected with MR-guided prostate biopsy in patients with an elevated PSA, one or more negative TRUS-guided biopsy sessions, and cancer suspicious lesions on 3T multi-parametric MRI. The aim is to proof the need for MR-guided biopsy. *Chapters 3* and *4* describe the location of prostate cancer in patients with repeated negative TRUS-guided biopsy sessions and biopsy naive patients respectively. Identifying prostate cancer locations and aggressiveness found with TRUS-guided biopsy and multi-parametric MRI followed by MR-guided biopsy provides insight in the diagnostic limitations of both techniques. In *chapter 5* we investigated whether it is possible to discriminate between prostatitis and prostate cancer based on apparent diffusion coefficient (ADC)-values derived from DWI. This imaging modality may help to reduce the number of false positive findings at prostate cancer MR imaging. Consequently, DWI may improve patient selection for MR-guided biopsy and therapy. *Chapter 6* is a phantom study where the feasibility of the in-house developed pneumatically actuated MR-compatible robotic manipulator is evaluated. Furthermore, safety aspects for patient care are evaluated. *Chapter 7* evaluates the accuracy and speed of the novel robotic technique compared to the manual biopsy method in patients. In *chapter 8* the feasibility of a real-time tracking sequence is demonstrated that can automatically align the image plane through the needle guide. This sequence has the potential to improve real-time imaging of the needle guide during manipulation with the robotic technique.

References

1. Ferlay J, Soerjomataram I, Dikshit R, Eser S, Mathers C, Rebelo M, et al. Cancer incidence and mortality worldwide: sources, methods and major patterns in GLOBOCAN 2012. *International journal of cancer Journal international du cancer*. 2015;136(5):E359-86.
2. Siegel RL, Miller KD, Jemal A. *Cancer statistics, 2015*. CA: a cancer journal for clinicians. 2015;65(1):5-29.
3. Integraal kankercentrum Nederland. Nederlandse Kankerregistratie Available from: <http://cijfersoverkanker.nl/>
4. Centraal Bureau voor de Statistiek. Doodsoorzaken. Available from: <http://statline.cbs.nl/>.
5. Schroder FH, Carter HB, Wolters T, van den Bergh RC, Gosselaar C, Bangma CH, et al. Early detection of prostate cancer in 2007. Part 1: PSA and PSA kinetics. *European urology*. 2008;53(3):468-77.
6. Schroder FH, van der Maas P, Beemsterboer P, Kruger AB, Hoedemaeker R, Rietbergen J, et al. Evaluation of the digital rectal examination as a screening test for prostate cancer. Rotterdam section of the European Randomized Study of Screening for Prostate Cancer. *Journal of the National Cancer Institute*. 1998;90(23):1817-23.
7. Djavan B, Ravery V, Zlotta A, Dobronski P, Dobrovits M, Fakhari M, et al. Prospective evaluation of prostate cancer detected on biopsies 1, 2, 3 and 4: when should we stop? *The Journal of urology*. 2001;166(5):1679-83.
8. Taira AV, Merrick GS, Galbreath RW, Andreini H, Taubenslag W, Curtis R, et al. Performance of transperineal template-guided mapping biopsy in detecting prostate cancer in the initial and repeat biopsy setting. *Prostate cancer and prostatic diseases*. 2010;13(1):71-7.
9. Loeb S, Bjurlin MA, Nicholson J, Tammela TL, Penson DF, Carter HB, et al. Overdiagnosis and overtreatment of prostate cancer. *European urology*. 2014;65(6):1046-55.
10. Berglund RK, Masterson TA, Vora KC, Eggener SE, Eastham JA, Guillonneau BD. Pathological upgrading and up staging with immediate repeat biopsy in patients eligible for active surveillance. *The Journal of urology*. 2008;180(5):1964-7; discussion 7-8.
11. Divrik RT, Eroglu A, Sahin A, Zorlu F, Ozen H. Increasing the number of biopsies increases the concordance of Gleason scores of needle biopsies and prostatectomy specimens. *Urologic oncology*. 2007;25(5):376-82.
12. Kvale R, Moller B, Wahlqvist R, Fossa SD, Berner A, Busch C, et al. Concordance between Gleason scores of needle biopsies and radical prostatectomy specimens: a population-based study. *BJU international*. 2009;103(12):1647-54.
13. Lattouf JB, Saad F. Gleason score on biopsy: is it reliable for predicting the final grade on pathology? *BJU international*. 2002;90(7):694-8.
14. Marshall S, Taneja S. Focal therapy for prostate cancer: The current status. *Prostate international*. 2015;3(2):35-41.
15. Sankineni S, Wood BJ, Rais-Bahrami S, Walton Diaz A, Hoang AN, Pinto PA, et al. Image-guided focal therapy for prostate cancer. *Diagnostic and interventional radiology*. 2014;20(6):492-7.
16. Bomers JG, Sedelaar JP, Barentsz JO, Futterer JJ. MRI-guided interventions for the treatment of prostate cancer. *AJR American journal of roentgenology*. 2012;199(4):714-20.
17. Kanthabalan A, Emberton M, Ahmed HU. Biopsy strategies for selecting patients for focal therapy for prostate cancer. *Current opinion in urology*. 2014;24(3):209-17.
18. Futterer JJ, Briganti A, De Visschere P, Emberton M, Giannarini G, Kirkham A, et al. Can Clinically Significant Prostate Cancer Be Detected with Multiparametric Magnetic Resonance Imaging? A Systematic Review of the Literature. *European urology*. 2015;68(6):1045-53.

19. Barentsz JO, Richenberg J, Clements R, Choyke P, Verma S, Villeirs G, et al. ESUR prostate MR guidelines 2012. *European radiology*. 2012;22(4):746-57.
20. Hambrock T, Somford DM, Huisman HJ, van Oort IM, Witjes JA, Hulsbergen-van de Kaa CA, et al. Relationship between apparent diffusion coefficients at 3.0-T MR imaging and Gleason grade in peripheral zone prostate cancer. *Radiology*. 2011;259(2):453-61.
21. Delongchamps NB, Rouanne M, Flam T, Beuvon F, Liberatore M, Zerbib M, et al. Multiparametric magnetic resonance imaging for the detection and localization of prostate cancer: combination of T2-weighted, dynamic contrast-enhanced and diffusion-weighted imaging. *BJU international*. 2011;107(9):1411-8.
22. Katahira K, Takahara T, Kwee TC, Oda S, Suzuki Y, Morishita S, et al. Ultra-high-b-value diffusion-weighted MR imaging for the detection of prostate cancer: evaluation in 201 cases with histopathological correlation. *European radiology*. 2011;21(1):188-96.
23. Delongchamps NB, Singh A, Haas GP. The role of prevalence in the diagnosis of prostate cancer. *Cancer control : journal of the Moffitt Cancer Center*. 2006;13(3):158-68.
24. Muller BG, van den Bos W, Pinto PA, de la Rosette JJ. Imaging modalities in focal therapy: patient selection, treatment guidance, and follow-up. *Current opinion in urology*. 2014;24(3):218-24.
25. Beyersdorff D, Winkel A, Hamm B, Lenk S, Loening SA, Taupitz M. MR imaging-guided prostate biopsy with a closed MR unit at 1.5 T: initial results. *Radiology*. 2005;234(2):576-81.
26. Woods TO. Standards for medical devices in MRI: present and future. *Journal of magnetic resonance imaging : JMRI*. 2007;26(5):1186-9.

CHAPTER 2.0 THREE-TESLA MAGNETIC RESONANCE (MR)-GUIDED PROSTATE BIOPSY IN MEN WITH INCREASED PROSTATE SPECIFIC ANTIGEN AND REPEATED, NEGATIVE, RANDOM, SYSTEMATIC, TRANSRECTAL ULTRASOUND BIOPSIES: DETECTION OF CLINICALLY SIGNIFICANT PROSTATE CANCERS

Caroline M.A. Hoeks, Martijn G. Schouten, Joyce G.R. Bomers,
Stefan P. Hoogendoorn, Christina A. Hulsbergen-van de Kaa,
Thomas Hambroek, Henk Vergunst, J.P. Michiel Sedelaar,
Jurgen J. Fütterer, Jelle O. Barentsz

European Urology 2012 Nov;62(5):902-9

Abstract

Background: Patients with elevated prostate-specific antigen (PSA) and one or more previous negative transrectal ultrasound (TRUS)-guided biopsy sessions are subject to diagnostic uncertainty due to TRUS-guided biopsy undersampling. Magnetic resonance (MR)-guided biopsy has shown high prostate cancer detection rates in studies with limited patient numbers.

Objective: Determine the detection rate of (clinically significant) prostate cancer for MR-guided biopsy of cancer suspicious lesions (CSLs) on 3T multi-parametric MR imaging in patients with elevated PSA and one or more negative TRUS-guided biopsy sessions.

Design, setting, and participants: Of 844 patients who underwent 3T multi-parametric MRI in our referral centre between March 2008 and February 2011, 438 consecutive patients with a PSA >4.0 ng/mL and one negative TRUS-guided biopsy session or more were included. MR-guided biopsy was performed in 265 patients. Exclusion criteria were existent prostate cancer, endorectal coil use, and multi-parametric MRI for indications other than cancer detection.

Intervention: Patients underwent MR-guided biopsy of multi-parametric MRI CSLs.

Measurements: (Clinically significant) MR-guided biopsy cancer-detection rates were determined. Clinically significant cancer was defined by accepted (i.e. Epstein and d'Amico) criteria based on PSA, Gleason score, stage, and tumour volume. Follow-up PSA and histopathology were collected. Sensitivity analysis was performed for patients with multi-parametric MRI CSLs without MR-guided biopsy.

Results and limitations: In a total of 117 patients, cancer was detected with MR-guided biopsy (n=108) or after negative MR-guided biopsy (n=9). Prostate cancer was detected in 108 of 438 patients (25%) and in 41% (108 of 265) of MR-guided biopsy patients. The majority of detected cancers (87%) were clinically significant. Clinically significant cancers were detected in seven of nine (78%) negative MR-guided biopsy patients in whom prostate cancer was detected during follow-up. Sensitivity analysis resulted in increased cancer detection (47-56%). Complications occurred in 0.2% of patients (5 of 265).

Conclusions: In patients with elevated PSA and one or more negative TRUS-guided biopsy sessions, MR-guided biopsy of multi-parametric MRI CSLs had a prostate cancer detection rate of 41%. The majority of detected cancers were clinically significant (87%).

Introduction

Prostate cancer is a major health care problem with 899 000 new cases and 258 000 deaths per year in Europe (1). In patients with elevated prostate-specific antigen (PSA) and/or abnormal digital rectal examination (DRE), random systematic transrectal ultrasound (TRUS)-guided biopsy is the most commonly used technique to further evaluate prostate cancer diagnosis. However, like PSA, which is an unspecific marker (specificity: 36%), and DRE, which is a rather insensitive examination (sensitivity: 37%) for prostate cancer detection, TRUS-guided biopsy also has its shortcomings (2, 3). Due to sampling error, >20% of cancers are not detected in the first TRUS-guided biopsy session (4). With repeat TRUS-guided biopsies, prostate cancer detection rates decreased from 22% to 4% in four subsequent TRUS-guided biopsy sessions (4). As a result of the mentioned issues, a large number of patients with a persistently elevated or increasing PSA and one or more negative TRUS-guided biopsy sessions are subject to diagnostic uncertainty.

Magnetic resonance (MR)-guided prostate biopsy of a detected cancer-suspicious lesion (CSL) on MR imaging (MRI) is a feasible diagnostic technique: prostate cancer detection rates with this method range from 37% to 59% (5-10). Moreover, the implementation of MR-guided biopsy has resulted in detection of predominantly (93%) clinically significant prostate cancer (8).

Functional MRI techniques increased prostate cancer localization accuracy (area under the curve (AUC): 0.84-0.91) when added to anatomic T2-weighted MRI (AUC: 0.69-0.81) in a multi-parametric MRI exam (11, 12). Using its localization strength, multi-parametric MRI of the prostate has increased opportunities for image-guided techniques like MR-guided biopsy. However, most MR-guided biopsy studies were performed with a low number of patients at a lower field strength of 1.5T.

Therefore, we aimed to determine the detection rate of (clinically significant) prostate cancer for MR-guided biopsy of CSLs detected on 3T multi-parametric MRI in patients with an elevated PSA and at least one previous negative TRUS-guided biopsy session in a large population.

Materials and methods

Patients

The need for informed consent for this retrospective study was waived by our institutional review board.

Between March 2008 and February 2011, 844 consecutive patients underwent multi-parametric MRI in our referral centre. Of these, 438 patients with PSA >4 ng/mL and at least one previous negative TRUS-guided biopsy session who had undergone multi-parametric MRI and/or MR-guided biopsy were included. Exclusion criteria were existent prostate cancer, use of an endorectal coil, and multi-parametric MRI for other indications than cancer detection. Patient selection is shown in a flow diagram in Figure 1.

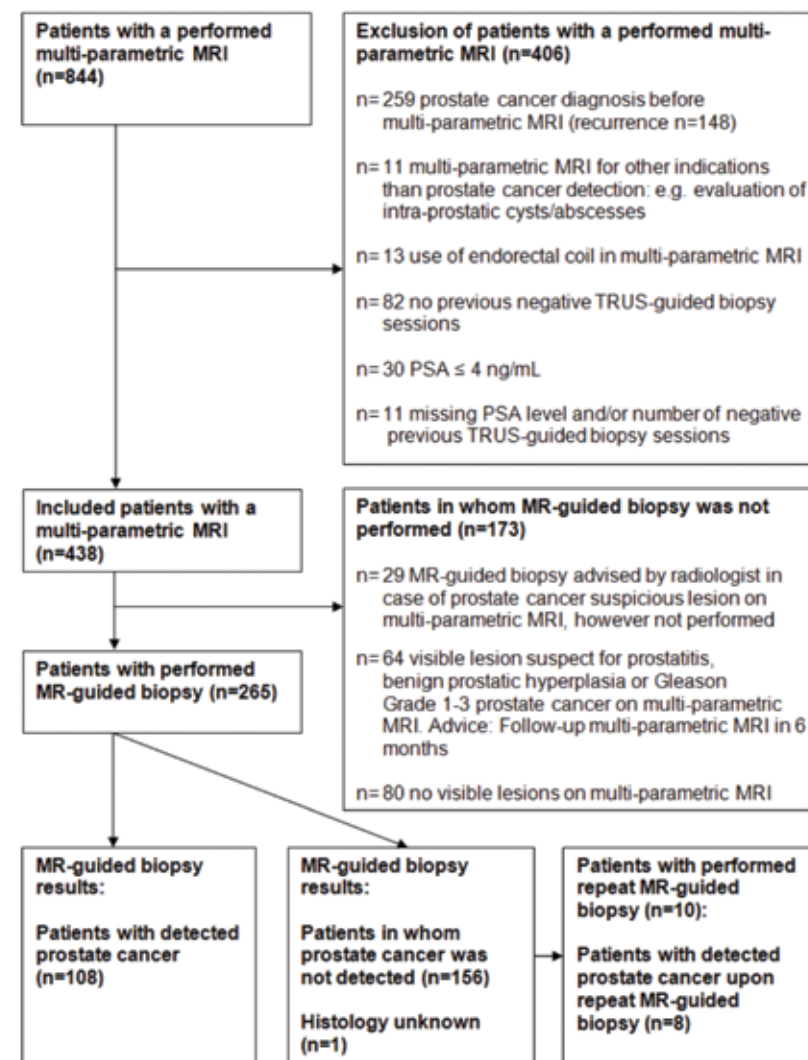


Figure 1: Study flow diagram. MRI = magnetic resonance imaging, PSA = prostate specific antigen, TRUS = transrectal ultrasound

Magnetic resonance imaging

Multi-parametric MRI and MR-guided biopsy were performed on two comparable 3T MR scanners (MAGNETOM Trio and MAGNETOM Skyra; Siemens Medical Solutions, Erlangen, Germany) using a combined spinal and pelvic-phased array coil. MRI parameters are presented in Table 1.

Magnetic resonance imaging interpretation

Two radiologists with 9 yr and 18 yr of experience in prostate MRI, respectively, evaluated the multi-parametric MRI examinations using in-house developed software (13). CSLs were defined on T2-weighted images in combination with diffusion-weighted MRI (DWI) and dynamic contrast-enhanced MRI as described

Protocol	Sequence	TR (ms)	TE (ms)	Flip angle (degrees)	Slice thickness (mm)	Field of view (mm x mm)	Matrix size	Voxel size (mm x mm x mm)	b-values (s/mm ²)	Temporal resolution (s)
Multi-parametric MRI of the prostate (MAGNETOM Trio)										
T2WI	axial and coronal TSE	4480	103	120	3.0	180 x 180	320 x 320	0. x 0.6 x 3.0	NA	NA
T2WI	Sagittal	4950	110	120	3.0	180 x 180	320 x 320	0.6 x 0.6 x 3.0	NA	NA
DWI	SSEPI axial	2500	64	NA	4.0	256 x 256	128 x 128	2.0 x 2.0 x 4.0	0/50/500/800	NA
DCE-MRI	GE axial 3D	800	1.47	8	4.0	230 x 230	180 x 180	1.8 x 1.8 x 4.0	NA	NA
DCE-MRI	Spoiled GE axial 3D	32	1.47	10	4.0	230 x 230	128 x 128	1.8 x 1.8 x 4.0	NA	2.5
Multi-parametric MRI of the prostate (MAGNETOM Skyra)										
T2WI	axial (TSE)	5180	101	160	3.0	192 x 192	320 x 320	0.6 x 0.6 x 3	NA	NA
T2WI	coronal (TSE)	4320	101	160	3.0	192 x 192	320 x 320	0.6 x 0.6 x 3	NA	NA
T2WI	sagittal (TSE)	4000	101	160	3.0	180 x 180	320 x 320	0.56 x 0.56 x 3	NA	NA
DWI	SSEPI axial	3000	64	NA	4.0	256 x 256	128 x 128	2 x 2 x 4	0/50/100/1200	NA
DCE-MRI	GE axial	800	1.53	14	3.0	192 x 192	128 x 128	1.5 x 1.5 x 3	NA	NA
DCE-MRI	GE axial	36	1.41	14	3.0	192 x 192	128 x 128	1.5 x 1.5 x 3	NA	3.5
MR-guided biopsy (MAGNETOM Trio)										
T2WI	TSE axial	3620	103	120	4.0	256 x 256	320 x 320	0.8 x 0.8 x 4.0	NA	NA
DWI	EPI axial	3300	60	NA	3.6	260 x 211	160 x 120	2.2 x 1.6 x 3.6	0/100/400/800	NA
SSFP	GE axial and sagittal	4.48	2.24	70	3.0	280 x 280	256 x 256	1.1 x 1.1 x 3.0	NA	NA
MR-guided biopsy (MAGNETOM Skyra)										
T2WI	TSE axial	3560	104	120	120	256 x 256	320 x 320	0.8 x 0.8 x 4	NA	NA
DWI	EPI axial	3000	64	NA	4.0	256 x 212	128 x 128	2.0 x 2.0 x 4.0	50/100/1600	NA
Balanced SSFP	GE axial and sagittal	4.56	2.28	70	3.0	280 x 280	256 x 256	1.1 x 1.1 x 3.0	NA	NA

Table 1: Imaging parameters. T2WI = T2-weighted MR imaging, DWI = diffusion weighted MR imaging, DCE-MRI = dynamic contrast enhanced MR imaging, SSFP = steady state free precession, TR = repetition time, TE = echo time, TSE = turbo spin echo, SSEPI = steady state echo planar imaging, GE = gradient echo, EPI = echo-planar imaging.

earlier (14). In addition to apparent diffusion coefficient (ADC) maps, DWI-calculated b1400 images were used to determine CSLs. A lesion was defined as a CSL on DWI in cases of focal restriction on the ADC map combined with an iso- to hypersignal intensity on the calculated b1400 image. Clinical data of all patients were available at MRI reading.

Magnetic resonance-guided prostate biopsy

MR-guided biopsy was performed in a separate session and every CSL was targeted. Two radiologists with 2 yr and two radiologists with 1 yr of MR-guided biopsy experience performed transrectal prostate MR-guided biopsy as described earlier (14). Axial T2-weighted images and DWI were acquired as baseline images for targeting.

Histopathology

Biopsy specimens were immediately fixed in formalin and subsequently underwent routine histopathologic evaluation by a urogenital histopathologist who had 18 yr of experience.

Prostate cancer: clinical significance

When prostatectomy was not performed, clinical significance of MR-guided biopsy detected prostate cancer was defined by: (1) a PSA >10 ng/mL and a PSA density >0.15 ng/mL per mL; (2) clinical stage \geq T2b; (3) a Gleason grade (GG) 4 or 5 within the biopsy specimen; or (4) a total cancer-core length (TCCL) \geq 10mm, where TCCL is the total cancer length in all MR-guided biopsy cores from one CSL (15-18). This definition was based on Epstein and d'Amico criteria (15, 18). In case of performed prostatectomy, prostate cancer was considered clinically significant when prostate cancer volume was \geq 0.5 mL or a stage \geq pT3 or a GG 4 or 5 (19, 20) was present.

Follow-up

Post MR-guided biopsy PSA measurements and histopathology results were collected until July 22, 2011, for all MR-guided biopsy patients.

Statistical analysis

Parametric continuous variables were reported as mean plus or minus the standard deviation; nonparametric continuous variables were reported as median and the interquartile range (IQR). The Pearson chi-square test was used to test for differences in proportions. In a multivariable logistic regression analysis, PSA, PSA density, and prostate volume were assessed as predictors for MR-guided biopsy prostate cancer detection. We used sensitivity analyses in which we assumed that, in all patients with visible MRI lesions, prostate cancer would have been detected if MR-guided biopsy would have been performed. A significance level of <0.05 was used for all analyses.

Results

Inclusion criteria were met in 438 of 844 consecutive men. MR-guided biopsy was performed in 265 of these 438 men (Fig. 1). MR-guided biopsy was not performed due to lack of visible lesions (n=80); advice for follow-up multi-parametric MRI in lesions suspicious for prostatitis, benign prostatic hyperplasia, or low-grade

cancer (n=64); or despite MR-guided biopsy advice (n=29). Patient characteristics are presented in Table 2. The last TRUS-guided biopsy had a median of nine cores (IQR: 9-10, available in 123 of 265 MR-guided biopsy patients) with transition zone (TZ) sampling in protocols of eight or more cores. The median MR-guided biopsy duration was 44 min (IQR: 35-51 min).

Characteristic	All patients (n=438)	Patients with detected prostate cancer on MR-guided biopsy (n=108)	Patients without detected prostate cancer on MR-guided biopsy (n=156)	p-value ¹ for patients with vs patients without detected prostate cancer
Median age in years (IQR)	66 (61-69)	65 (62-70)	64 (61-69)	0.29
PSA level in ng/mL (IQR)	11.4 (8.6-18.3)	18.0 (10.0-27.9)	12.0 (9.1-17.1)	< 0.001 ^{2,3}
Median prostate volume in mL (IQR)	67 (50-93)	53 (36-68)	70 (51-89)	< 0.001 ^{2,3}
Median number of previous negative TRUS biopsy sessions (IQR)	2 (2-3)	3 (2-3)	2 (2-3)	NA
Median interval between last TRUS biopsy and MR-guided biopsy in months (IQR)	12 (5-20)	13 (6-21)	11 (5-20)	0.16
Median interval between MR imaging and MR-guided biopsy in months (IQR)	2 (1-2)	1 (1-2)	2 (1-2)	0.002 ³
Median number of biopsied CSL (IQR)	1 (1-2)	1 (1-2)	2 (1-2)	NA
Median number of MR-guided biopsy cores for one CSL (IQR)	2 (2-3)	2 (2-3)	2 (2-3)	NA

Table 2: patients characteristics. MRI = magnetic resonance imaging, IQR = interquartile range, PSA = prostate-specific antigen, TRUS = transrectal ultrasound, CSL = cancer suspicious lesion, NA = not applicable.

¹ p-values were calculated using an independent t-test and a Mann-Whitney U test for nonparametric variables.

² Mann-Whitney U test.

³ p < 0.05 was considered statistically significant.

In a total of 117 patients, prostate cancer was detected with MR-guided biopsy (n=108) or during follow-up after negative MR-guided biopsy (n=9). Prostate cancer detection rates were 25% (108 of 438; 95% confidence interval (CI), 21-29%) in included patients and 41% (108 of 265; CI, 35-47%) in patients who underwent both multi-parametric MRI and MR-guided biopsy. The majority of detected cancers were clinically significant: a total of 87% (94 of 108) met the clinical criteria and 93% (26 of 28) met radical prostatectomy-specimen criteria. A total of 368 CRSs were indicated in the 265 MR-guided biopsy patients. With a median of two cores per CSL, prostate cancer was detected in 33% of CSLs (123 of 368; CI, 29-38%). The majority of CSLs (63% (78 of 123); CI, 55-71%) were detected in the TZ. Thirty-three percent (40 of 123; CI, 25-41%) of detected cancer CSLs were located in the peripheral zone (PZ). The remaining 4% (5 of 123; CI, 2-9%) were situated on the TZ-PZ border or in the seminal vesicles. Other predominant CSL diagnoses are shown in Table 3.

Histology in MR-guided biopsy cores of CSLs	Percentage of CSLs ¹
Prostate cancer	33 (123/368)
Prostatitis	30 (109/368)
Healthy intra-prostatic tissue	23 (85/368)
Atrophy	8 (31/368)
Material not representative for prostate tissue	5 (18/368)
HGPIN	4 (16/368)
Reactive atypia	2 (9/368)
AAH	2 (8/368)
Fibrosis	0.003 (1/368)
Total CSLs	100 (368/368)

Table 3: MR-guided biopsy histopathology results for cancer suspicious lesions. CSLs = cancer suspicious lesions, HGPIN = high-grade intraprostatic neoplasia; AAH = atypical adenomatous hyperplasia.

¹ Because some CSLs had more than one diagnosis, the sum of percentages is higher than 100%.

Significantly more prostate cancer was detected in patients with a prostate volume ≤ 50 mL (60%) versus >50 mL (36%; $p < 0.0001$) and in patients with PSA density >0.15 ng/mL per mL (52%) versus ≤ 0.15 ng/mL per mL (24%; $p < 0.0001$). Upon multivariable logistic regression analysis, PSA was not a predictor of MR-guided biopsy prostate cancer detection. After correction for PSA, only prostate volume ≤ 50 mL ($p = 0.008$) and PSA density >0.15 ng/mL per mL ($p < 0.0001$) were predictors of MR-guided biopsy prostate cancer detection in a final multivariable logistic regression model. These results are presented in Table 4.

	Percentage of patients with prostate cancer	CI	Total percentage of patients with prostate cancer upon MR-guided biopsy ²	Univariable analysis Chi-square test	Multi-variable logistic regression analysis, initial model OR	Multi-variable logistic regression analysis, final model OR
MRGB+	100 (108/108)	96-100	44 (117/264),	NA	NA	NA
MRGB-	6 (9/156)	3-11	CI: 38-50			
PSA ≤ 10 ng/mL						
MRGB+	100 (28/28)	86-100	36 (30/84),		(PSA $>10/ \leq 10$ ng/ml)	
MRGB-	5 (3/57)	1-15	CI: 26-46		OR = 1.13	
PSA > 10 ng/mL				0.09	CI: 0.53-2.40	NA
MRGB+	100 (80/80)	95-100	48 (86/179),		$p = 0.75$	
MRGB-	6 (6/99)	3-13	CI: 41-55			
Prostate volume ≤ 50 mL						
MRGB+	100 (47/47)	96-100	60 (52/86),		Prostate volume $\leq 50 / > 50$ mL	Prostate volume $\leq 50 / > 50$ mL
MRGB-	13 (6/40)	7-29	CI:50-70		OR = 2.28	OR = 2.21
Prostate volume >50 mL				$<0.0001^2$	CI:1.23-4.21	CI:1.23-3.97
MRGB+	100 (61/61)	93-100	36 (64/177),		$p=0.009^2$	$p=0.008^2$
MRGB-	3 (3/116)	1-8	CI:29-43			
PSA density ≤ 0.15 ng/mL/mL						
MRGB+	100 (15/15)	76-100	24 (17/71),		PSA density $> 0.15 / \leq 0.15$	PSA density $> 0.15 / \leq 0.15$
MRGB-	5 (3/57)	1-15	CI: 15-35		OR=3.50	OR=3.76
PSA density > 0.15 ng/mL/mL				$<0.0001^2$	CI: 1.52-8.05	CI: 1.84-7.68
MRGB+	100 (93/93)	95-100	52 (99/192),		$P=0.003^2$	$p<0.0001^2$
MRGB-	6 (6/99)	3-13	CI: 45-59			

Table 4: Univariable and multivariable analysis of dichotomized PSA, prostate volume and PSA density related to MR-guided prostate cancer detection in patients with initial positive MR-guided biopsy and initial negative MR-guided biopsy results¹. CI = 95% confidence interval, PSA = prostate-specific antigen, MRGB+ = patients with prostate cancer on initial MR-guided biopsy, MRGB- = patients without prostate cancer on initial MR-guided biopsy, DR = detection rate, OR = odds ratio, Chi-square = Pearson Chi-squared test, NA = not applicable.

¹ The final multivariable logistic regression model consisted of two independent variables (PSA density and prostate volume (as dichotomized categorical covariates)) and one dependent variable (prostate cancer detection on MR-guided biopsy).

² Statistically significant difference at a threshold of $p < 0.05$.

³ One patient with initial negative MR-guided biopsy had prostate cancer detected upon TRUS biopsy. This patient is not added to the totals in the fourth column.

In sensitivity analysis, prostate cancer detection rates would have increased to 47% (137 of 294; CI, 41-52%) if MR-guided biopsy would have been performed and prostate cancer would have been detected in patients with a multi-parametric MRI CSL who were advised to undergo MR-guided biopsy (n=29). Detection rates would have increased even further to 56% (201 of 358; CI, 51-56%) if MR-guided biopsy would have been performed and prostate cancer would also have been detected in patients with a multi-parametric MRI suspicious for prostatitis, benign prostatic hyperplasia, or low-grade cancer, and in whom repeat multi-parametric MRI was advised (n=64). A patient example of multi-parametric MRI and MR-guided biopsy is shown in Figure 2.

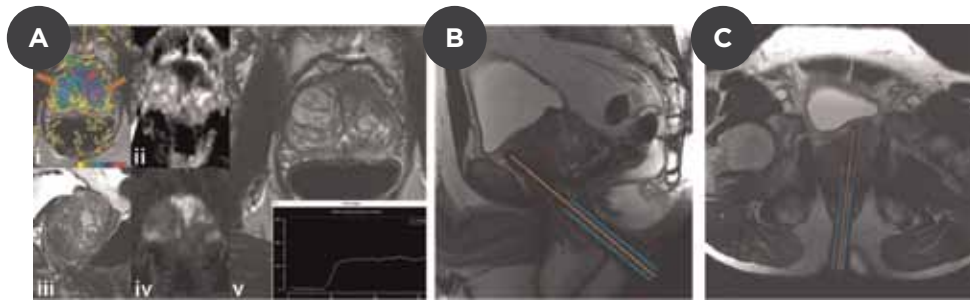


Figure 2: A 76-yr-old patient with a prostate-specific antigen level of 32 ng/mL and density of 0.46 ng/mL per mL, clinical stage T1c, and one previous negative TRUS-guided biopsy session underwent multi-parametric MRI for a clinical indication of prostate cancer detection. (A) A ventral transition zone cancer is visible (demarcated regions). A focal lenticular-shaped homogeneous low-signal intensity (blue demarcation) in the ventral prostate is visible on (iii) sagittal and (v) axial T2-weighted MRI. A focal (ii) low apparent diffusion-coefficient value (blue demarcation) and (iv) high signal intensity (blue demarcation) on the calculated b1600 image are visible in the same area on diffusion-weighted MRI. The K^{trans} overlay on T2-weighted images can be appreciated (i). Dynamic contrast-enhanced MRI shows asymmetric increased enhancement (black demarcation) matching the other functional images and T2-weighted (i). Benign prostate hyperplasia nodules are also enhanced (orange arrows). (B) Sagittal and (C) transverse balanced gradient echo images were made to confirm the needle positions. Needle artefacts (orange lines) and needle guides (blue lines with white-dotted top) are visible. In this magnetic resonance-guided biopsy specimen, a Gleason score 4 + 5 prostate cancer was found in the ventral transition zone.

Follow-up

Reported MR-guided biopsy complications were sepsis with hospitalization in one patient and a vasovagal reaction in four other patients. Only in 51 of 156 negative MR-guided biopsy patients was a follow-up of 5 months, including two PSA measurements or histopathology, available. In 6% (9 of 156; CI, 3-6%) of negative- MR-guided biopsy patients, prostate

cancer was detected during this mean follow-up of 5 months. Detected cancers were clinically significant in 78% (seven of nine patients) based on clinical criteria and in 100% (four of four) based on radical prostatectomy-specimen criteria. Follow-up results of patients who underwent multi-parametric MRI for suspicion of prostate cancer are presented in Figure 3.

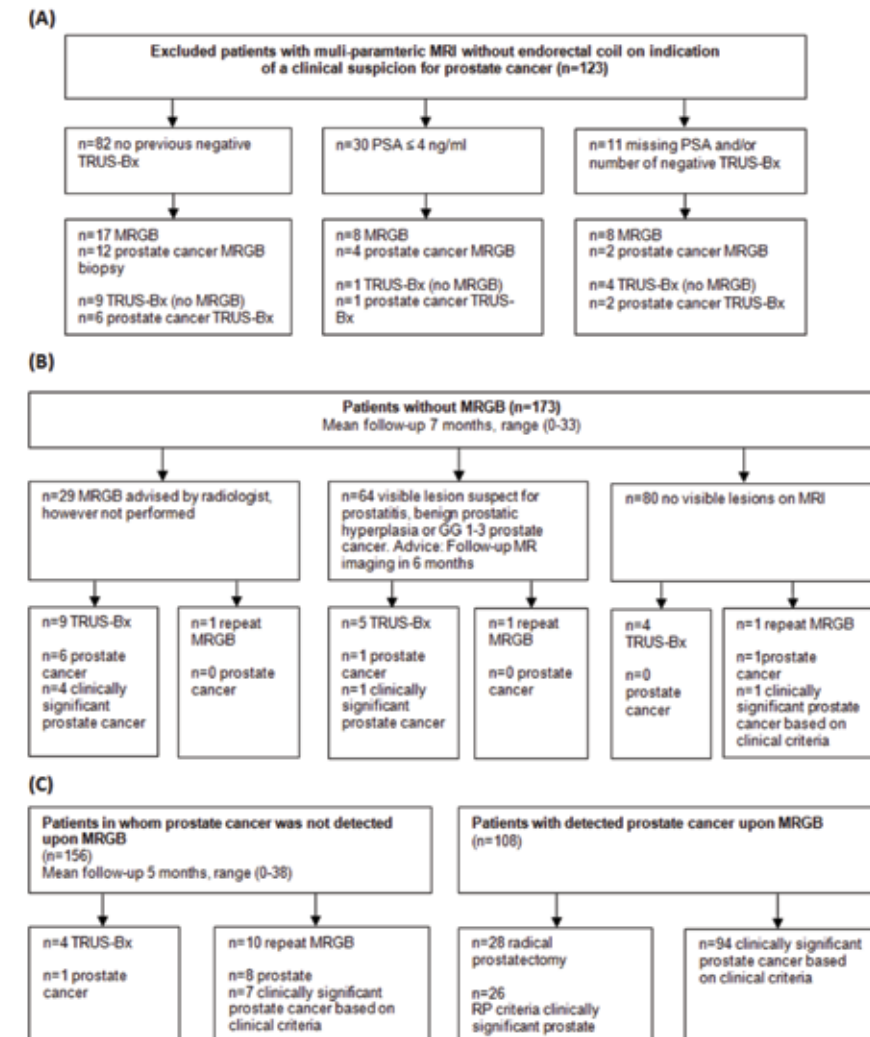


Figure 3: Follow-up histopathology results in patients with multi-parametric MRI: (A) excluded patients with multi-parametric MRI, (B) included multi-parametric MRI patients without MR-guided biopsy, (C) patients with multi-parametric MRI and MR-guided biopsy. GG = Gleason grade, MRGB = magnetic resonance-guided prostate biopsy, TRUS-Bx biopsy = transrectal ultrasound-guided biopsy.

Discussion

In patients with one or more negative TRUS-guided biopsy sessions, MR-guided biopsy of 3T multi-parametric MRI-detected CSLs resulted in a prostate cancer detection rate of 41%. In our study, MR-guided biopsy detected more cancers than repeated TRUS-guided biopsy ($\leq 18\%$) (21, 22). Furthermore, our number of detected clinically significant cancers (87%) is high compared to an estimated 56% of clinically significant cancers for repeat TRUS-guided biopsy in screening (23). We detected more clinically significant cancers because our referred patient population probably contained more cancers of higher Gleason score than a screening population. Another reason for detecting many clinically significant cancers may be higher MRI detection rates for higher Gleason score cancers (24). Furthermore, MR-guided biopsy has higher GG concordance with prostatectomy specimens compared to systematic TRUS-guided biopsy and, therefore, less undergrading may have occurred (25).

Our detection rate of 41% is in agreement with some MR-guided biopsy publications (37-39%) (6, 10). However, our detection rate is lower compared to other MR-guided biopsy studies (52-59%) (5, 8, 9). This may be explained by the fact that in our study, as opposed to these last studies, not all patients underwent MR-guided biopsy. Finally, for clinically significant cancers, our detection rate (87%) approaches that of Hambrook et al. (93%) (25). The detection rate of clinically significant cancers of Roethke et al. was lower than ours (81%) (5). This may be explained by the fact that they did not add multi-parametric MRI to T2-weighted images in the first 52 of their 100 patients.

Our relatively high detection rates of prostate cancer in the TZ (63%) agree with results of Hambrook et al. (57% in TZ) (8). However, in other reports, TZ cancer-detection rates (47% and 35%, respectively) were lower than PZ cancer-detection rates (respectively, 53% and 64%) (5, 6). Heterogeneity of patient populations due to differences in the number of previous TRUS-guided biopsy sessions, the TRUS-guided biopsy protocol, and in the number of cores in TRUS-guided biopsies makes it difficult to compare results of reported predominant prostate cancer locations.

Clinical alternatives to MR-guided biopsy are limited to saturation biopsy protocols (including transperineal template biopsies). Saturation biopsies have the disadvantages of possibly requiring anaesthesia and a high number of cores. Detection rates of protocols including 20-38 cores ranged from 14% to 41% without significantly increasing the likelihood of detecting clinically significant cancers (26). In MR-guided biopsy, only a limited number of cores (median two cores per CSL) are needed to detect a high percentage (86%) of clinically significant cancers. Furthermore, in MR-guided biopsy, no general anaesthesia is required. Clinical use of MR-guided biopsy is currently restricted by its limited availability and its rather long procedure times (median: 44min). However, application of MR-ultrasound fusion techniques (using registration), needle-guide tracking sequences, and implementation of robotics may improve these drawbacks in the near future (27-29). When these issues are solved, multi-parametric MRI and MR-

guided biopsy could be applied on a larger scale for prostate cancer detection in patients with an elevated PSA and one or more negative TRUS-guided biopsy sessions. However, prostate cancer detection rates for random systematic TRUS-guided biopsy versus targeted MR-guided biopsy should be prospectively compared in patients stratified for previously performed similar TRUS-guided biopsy protocols.

Our study has several limitations. First, our follow-up is limited to two or fewer PSA measurements within 1 yr without histopathology examinations in most patients. Inferring conclusions from false-negative MR-guided biopsy results remains difficult based on this limited follow-up. However, regardless of follow-up duration, differentiation of a patient with small-volume cancer missed by MR-guided biopsy from a patient without prostate cancer remains problematic without availability of radical prostatectomy specimens directly after MR-guided biopsy. Second, as our work was performed in a referral centre, interpatient variation in the number and the protocols of previous negative TRUS-guided biopsy sessions is present. Furthermore, inpatient variation exists due to time differences between protocols of different TRUS-guided biopsy sessions in a single patient. Furthermore, in some patients, bias may have been caused by the relatively low number of TRUS-guided biopsy cores for the sampled prostate-cancer volume. Third, MR-guided biopsy was performed by four radiologists who did not perform consensus image reading. Possible differences in image interpretation between reading radiologists and MR-guided biopsy radiologists may have biased our results. Finally, a TCCL ≥ 10 mm, recently defined to predict a radical prostatectomy specimen tumour volume ≥ 0.5 mL using TRUS-guided (5 mm grid) template biopsy simulations (17), was used as a criterion for clinically significant prostate cancer in MR-guided biopsy specimens. As MR-guided biopsy is targeted precisely to a lesion and is not taken every 5 mm according to a grid, our TCCL criterion may have overestimated MR-guided biopsy results for clinically significant cancers. However, as no results on MR-guided biopsy TCCL for prediction of tumour volume exist currently, we incorporated this ultrasound criterion for estimation of tumour volume based on MR-guided biopsy specimens. In conclusion, in patients with an elevated PSA level and one or more previous negative TRUS-guided guided prostate biopsy sessions MR-guided biopsy of 3T multi-parametric MRI detected CSLs has a detection rate of 41% for predominantly clinically significant prostate cancer (87%).

References

1. Ferlay J, Parkin DM, Steliarova-Foucher E. Estimates of cancer incidence and mortality in Europe in 2008. *Eur J Cancer*. 2010;46(4):765-81.
2. Schroder FH, Carter HB, Wolters T, et al. Early detection of prostate cancer in 2007. Part 1: PSA and PSA kinetics. *Eur Urol*. 2008;53(3):468-77.
3. Schroder FH, van der Maas P, Beemsterboer P, et al. Evaluation of the digital rectal examination as a screening test for prostate cancer. Rotterdam section of the European Randomized Study of Screening for Prostate Cancer. *J Natl Cancer Inst*. 1998;90(23):1817-23.
4. Djavan B, Ravery V, Zlotta A, et al. Prospective evaluation of prostate cancer detected on biopsies 1, 2, 3 and 4: when should we stop? *J Urol*. 2001;166(5):1679-83.
5. Roethke M, Anastasiadis AG, Lichy M, et al. MRI-guided prostate biopsy detects clinically significant cancer: analysis of a cohort of 100 patients after previous negative TRUS biopsy. *World J Urol*. 2012;30(2):213-8.
6. Franiel T, Stephan C, Erbersdobler A, et al. Areas suspicious for prostate cancer: MR-guided biopsy in patients with at least one transrectal US-guided biopsy with a negative finding—multi-parametric MR imaging for detection and biopsy planning. *Radiology*. 2011;259(1):162-72.
7. Beyersdorff D, Winkel A, Hamm B, et al. MR imaging-guided prostate biopsy with a closed MR unit at 1.5 T: initial results. *Radiology*. 2005;234(2):576-81.
8. Hambrock T, Somford DM, Hoeks C, et al. Magnetic resonance imaging guided prostate biopsy in men with repeat negative biopsies and increased prostate specific antigen. *J Urol*. 2010;183(2):520-7.
9. Anastasiadis AG, Lichy MP, Nagele U, et al. MRI-guided biopsy of the prostate increases diagnostic performance in men with elevated or increasing PSA levels after previous negative TRUS biopsies. *Eur Urol*. 2006;50(4):738-48; discussion 48-9.
10. Engelhard K, Hollenbach HP, Kiefer B, et al. Prostate biopsy in the supine position in a standard 1.5-T scanner under real time MR-imaging control using a MR-compatible endorectal biopsy device. *Eur Radiol*. 2006;16(6):1237-43.
11. Katahira K, Takahara T, Kwee TC, et al. Ultra-high-b-value diffusion-weighted MR imaging for the detection of prostate cancer: evaluation in 201 cases with histopathological correlation. *Eur Radiol*. 2011;21(1):188-96.
12. Delongchamps NB, Rouanne M, Flam T, et al. Multiparametric magnetic resonance imaging for the detection and localization of prostate cancer: combination of T2-weighted, dynamic contrast-enhanced and diffusion-weighted imaging. *BJU Int*. 2011;107(9):1411-8.
13. Vos PC, Hambrock T, Barenstz JO, et al. Computer-assisted analysis of peripheral zone prostate lesions using T2-weighted and dynamic contrast enhanced T1-weighted MRI. *Phys Med Biol*. 2010;55(6):1719-34.
14. Hambrock T, Futterer JJ, Huisman HJ, et al. Thirty-two-channel coil 3T magnetic resonance-guided biopsies of prostate tumor suspicious regions identified on multimodality 3T magnetic resonance imaging: technique and feasibility. *Invest Radiol*. 2008;43(10):686-94.
15. Bastian PJ, Mangold LA, Epstein JI, et al. Characteristics of insignificant clinical T1c prostate tumors. A contemporary analysis. *Cancer*. 2004;101(9):2001-5.
16. Partin AW, Yoo J, Carter HB, et al. The use of prostate specific antigen, clinical stage and Gleason score to predict pathological stage in men with localized prostate cancer. *J Urol*. 1993;150(1):110-4.
17. Ahmed HU, Hu Y, Carter T, et al. Characterizing clinically significant prostate cancer using template prostate mapping biopsy. *J Urol*. 2011;186(2):458-64.
18. D'Amico AV, Whittington R, Malkowicz SB, et al. Biochemical outcome after radical prostatectomy or external beam radiation therapy for patients with clinically localized prostate carcinoma in the prostate specific antigen era. *Cancer*. 2002;95(2):281-6.
19. Stamey TA, Freiha FS, McNeal JE, et al. Localized prostate cancer. Relationship of tumor volume to clinical significance for treatment of prostate cancer. *Cancer*. 1993;71(3 Suppl):933-8.
20. Gleason DF, Mellinger GT. Prediction of prognosis for prostatic adenocarcinoma by combined histological grading and clinical staging. *J Urol*. 1974;111(1):58-64.
21. Roehl KA, Antenor JA, Catalona WJ. Serial biopsy results in prostate cancer screening study. *J Urol*. 2002;167(6):2435-9.
22. Campos-Fernandes JL, Bastien L, Nicolaiew N, et al. Prostate cancer detection rate in patients with repeated extended 21-sample needle biopsy. *Eur Urol*. 2009;55(3):600-6.
23. Roemeling S, Roobol MJ, Kattan MW, et al. Nomogram use for the prediction of indolent prostate cancer: impact on screen-detected populations. *Cancer*. 2007;110(10):2218-21.
24. Ikonen S, Karkkainen P, Kivisaari L, et al. Magnetic resonance imaging of prostatic cancer: does detection vary between high and low gleason score tumors? *Prostate*. 2000;43(1):43-8.
25. Hambrock T, Hoeks C, Hulsbergen-van de Kaa C, et al. Prospective assessment of prostate cancer aggressiveness using 3T diffusion-weighted magnetic resonance imaging-guided biopsies versus a systematic 10-core transrectal ultrasound prostate biopsy cohort. *Eur Urol*. 2012;61(1):177-84.
26. Scattoni V, Zlotta A, Montironi R, et al. Extended and saturation prostatic biopsy in the diagnosis and characterisation of prostate cancer: a critical analysis of the literature. *Eur Urol*. 2007;52(5):1309-22.
27. Schouten MG, Bomers JG, Yakar D, et al. Evaluation of a robotic technique for transrectal MRI-guided prostate biopsies. *Eur Radiol*. 2012;22(2):476-83.
28. de Oliveira A, Rauschenberg J, Beyersdorff D, et al. Automatic passive tracking of an endorectal prostate biopsy device using phase-only cross-correlation. *Magn Reson Med*. 2008;59(5):1043-50.
29. Pinto PA, Chung PH, Rastinehad AR, et al. Magnetic resonance imaging/ultrasound fusion guided prostate biopsy improves cancer detection following transrectal ultrasound biopsy and correlates with multiparametric magnetic resonance imaging. *J Urol*. 2011;186(4):1281-5.

CHAPTER 3.0 LOCATION OF PROSTATE CANCERS DETERMINED BY MULTI-PARAMETRIC AND MR-GUIDED BIOPSY IN PATIENTS WITH ELEVATED PROSTATE SPECIFIC ANTIGEN LEVEL AND AT LEAST ONE NEGATIVE TRANSRECTAL ULTRASOUND-GUIDED BIOPSY

*Martijn G. Schouten, Caroline M.A. Hoeks, Joyce G.R. Bomers,
Christina A. Hulsbergen-van de Kaa, J. Alfred Witjes,
Les C. Thompson, Maroeska M. Rovers, Jelle O. Barentsz,
Jurgen J. Fütterer*

American Journal of Roentgenology 2015 Jul;205(1):57-63

Abstract

Objective: The purpose of this article is to identify histopathologically proven prostate cancer locations using MRI followed by MR-guided biopsy in patients with elevated prostate-specific antigen (PSA) levels and at least one negative transrectal ultrasound (TRUS)-guided biopsy session. Our hypothesis is that in this patient group most cancers are located in the anterior portion of the prostate. This may have implications for the biopsy strategy regarding the location of sampling.

Materials and methods: This retrospective study consisted of 872 consecutive men who had undergone MR-guided prostate biopsy. Inclusion criteria were PSA level greater than or equal to 4 ng/mL, one or more negative TRUS-guided biopsy session, the presence of suspicious lesions on previous multi-parametric MRI, and prostate cancer histopathologically proven by MR-guided biopsy. Thereafter, the location of intermediate- or high-risk cancers and cancers with a maximum cancer core length of 6 mm or longer were determined. The proportion of cancer locations was compared using a chi-square test. One-way ANOVA analyses were performed to compare patient characteristics.

Results: Results were presented on both a patient and lesion basis because a single patient can have multiple lesions. In total, 176 of 872 patients met the inclusion criteria. Prostate cancer was detected in 202 of 277 (73%) suspicious lesions. In total, 76% of patients had cancer of the transition zone and anterior fibromuscular stroma. Peripheral zone cancers were found in 30% of the patients, and 6% had cancers in both zones. In 70% of cases (141/202; 95% CI; 63-76%), lesions were located anteriorly; this included 75% (132/176; 95% CI; 69-81%) of patients. Intermediate- or high-risk prostate cancer was found in 93% (128/138; 95% CI; 88-96%) of patients. Of these patients, 73% (94/128; 95% CI; 66-81%) had anterior involvement. Cancers with a maximum cancer core length of 6 mm or more were more likely to be located in the anterior part of the prostate than were cancers with a core length of less than 6 mm (66% vs 6%). Most cancers 58% (102/176; 95% CI; 51-65%) were found in the mid prostate. Anterior involvement of prostate cancer detected by MR-guided biopsy was statistically significantly ($p = 0.04$) higher in patients with two or more negative TRUS-guided biopsy sessions (79%) than in those with one negative TRUS-guided biopsy session (55%).

Conclusion: Anterior involvement was high (75%) in patients with an elevated PSA level and one or more negative TRUS-guided biopsy session, and the majority of these cancers (93%) were intermediate or high risk.

Introduction

Transrectal ultrasound (TRUS)-guided biopsy protocols primarily sample the peripheral zone (PZ), because most prostate cancers are located in this zone at initial biopsy (1). In routine autopsy studies, most cancer foci (83-85%) were found in the PZ (2, 3).

In patients who underwent cystoprostatectomy for bladder cancer treatment, 75% of the prostate cancers were located in the PZ (4). In patients with increasing prostate-specific antigen (PSA) levels and repeated negative TRUS-guided biopsy sessions, the diagnosis of intermediate- or high-risk cancers is often delayed (1). With repeated TRUS-guided biopsies, prostate cancer detection rates decreased from 22% to 4% in four subsequent TRUS-guided biopsy sessions (5). Transperineal saturation biopsies are considered as a good alternative for patients with repeated negative TRUS-guided biopsy sessions, because higher cancer detection rates (37-53%) are reported (6-8). With the use of this technique, 37-54% of patients with one or more negative TRUS-guided biopsy sessions had cancers in the PZ (8, 9) and 18-77% had transition zone (TZ) involvement. Anterior involvement (i.e., the anterolateral horn of the PZ, anterior fibromuscular stroma, and TZ) was seen in 44-83% of patients (6, 8-12).

The use of MR-guided prostate biopsy increased prostate cancer detection rates (38-52%) in patients with an elevated PSA level and one or more negative TRUS-guided biopsy sessions. Furthermore, the TZ was the predominant location of these detected cancers, which is similar to the findings of saturation biopsies (13-16). Therefore, identifying the location of prostate cancer found with MR-guided biopsy may provide insight to cancers missed with standard TRUS-guided biopsy schemes. This may have implications for the biopsy strategy regarding the location of sampling in this particular patient group. The purpose of our study was to identify the location of prostate cancer diagnosed with MR-guided biopsy in patients with an elevated PSA level and at least one negative TRUS-guided biopsy session.

Materials and methods

Patient selection

This retrospective study consisted of a cohort of 872 consecutive men who had undergone MR-guided prostate biopsy between March 2008 and March 2012 in our referral center. Inclusion criteria were PSA level 4 ng/mL or higher, one or more negative TRUS-guided biopsy session, the presence of suspicious lesions on previous multi-parametric MRI, and prostate cancer histopathologically proven by MR-guided biopsy. Exclusion criteria were an unknown number of previous TRUS-guided biopsy sessions, interval between last TRUS-guided biopsy and MR-guided biopsy longer than 2 years, and previous prostate cancer diagnosis, including a suspicion of recurrent prostate cancer or seminal vesicle involvement. The flowchart in Figure 1 describes reasons for inclusion and exclusion.

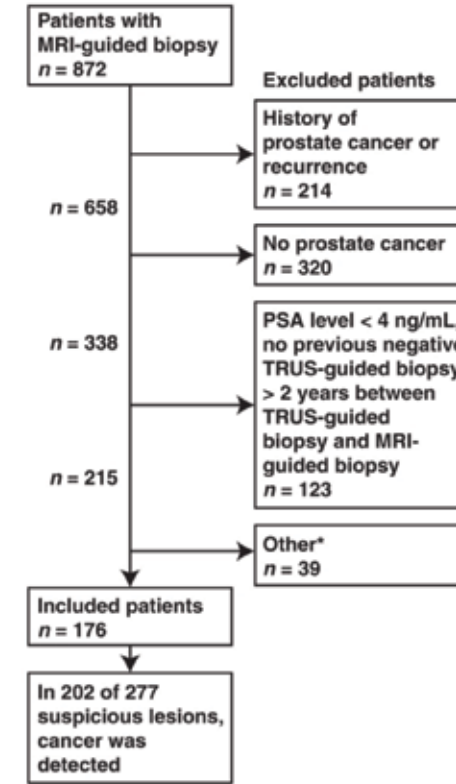


Figure 1: Flowchart describing patient selection and reasons for exclusion. In total, 176 patients were included; 277 suspicious lesions were biopsied, and cancer was detected in 202 (73%) of them. *Other category included patients with unknown number of previous negative transrectal ultrasound (TRUS)-guided biopsies, unknown prostate-specific antigen (PSA) level or pathologic findings, and seminal vesicle involvement. In total, 696 patients were excluded.

Diagnostic MRI Protocol

Multi-parametric prostate MRI and MR-guided biopsy were performed on a 3T MRI scanner (Magnetom Trio and Magnetom Skyra, both from Siemens Healthcare) using a spinal and pelvic phased-array coil. The image parameters were applied according to the European Society of Urogenital Radiology guidelines (14, 17). Two radiologists with 9 and 18 years of experience in reading prostate MRI examinations evaluated the multi-parametric MRI data using in-house developed software (18). Lesions suspicious for cancer were defined on T2-weighted imaging in combination with diffusion-weighted imaging and dynamic contrast-enhanced MRI (19). Clinical data of all patients were available during MR image interpretation. Prostate volume (mL) was estimated on the MR images using an ellipsoid formula: length x width x height x 1/6 x π .

MR-guided biopsy

Transrectal MR-guided prostate biopsy was performed in a separate session with the same MRI systems used for the diagnostic images (19). Axial T2-weighted images and diffusion-weighted images were acquired to relocate the suspicious lesion described on the diagnostic multi-parametric MRI. During the MR-guided biopsy procedure, two confirmation scans (each in a different plane, with the needle left in situ) were acquired to verify the location of the biopsy needle. In this study, a fully automatic 18-gauge titanium double shot biopsy gun with needle length of 175 mm and tissue core sampling length of 17 mm was used.

Location of prostate cancer

Two readers with 2 and 4 years of experience in MR-guided prostate biopsy determined in consensus the location of histopathologically proven prostate cancer according to the position of the needle on the MRI confirmation scans. The biopsy location was determined using biplanar MRI confirmation scans (sagittal and transversal) with the needle left in situ (Fig. 2). The location was reported according to an adapted scheme as described by Dickinson et al. (20). In this adapted scheme, the prostate was divided into 36 different segments (Fig. 3). One segment was assigned to each lesion, even when the cancer involved more segments on the multi-parametric MRI. When the sampling core was located in two segments, the segment with the lowest apparent diffusion coefficient value on the MR images was chosen, because a low apparent diffusion coefficient value is associated with more aggressive prostate cancer (21). Furthermore, 5 mm or more of the sampling core had to be located in the assigned segment.

In our study, the anterior portion of the prostate was defined as the area 17 mm anterior from the posterior prostatic surface irrespective of prostate size. This definition was chosen because during a standard TRUS-guided biopsy the physician obtains samples from the prostate by firing a needle with a 17 mm notch from the posterior prostate surface (20).

In some patients, more than one cancer-positive lesion was detected. Therefore, the results were presented in two ways: on a lesion basis and on a patient basis.

Intermediate- or high-risk cancer and maximum cancer core length

Intermediate- or high-risk prostate cancer lesion was defined as follows: a Gleason grade component of 4 or 5 within the biopsy specimen, or a maximum cancer core length in one MR-guided biopsy core 6 mm or longer, for which the longest maximum cancer core length (cancer volume percentage x length of biopsy core) was taken for every patient. With a maximum cancer core length 6 mm or longer, cancer volumes of 0.5 mL or greater can be predicted with a sensitivity of 95% or greater (22). Both aggression and maximum cancer core length were correlated with prostate cancer location.

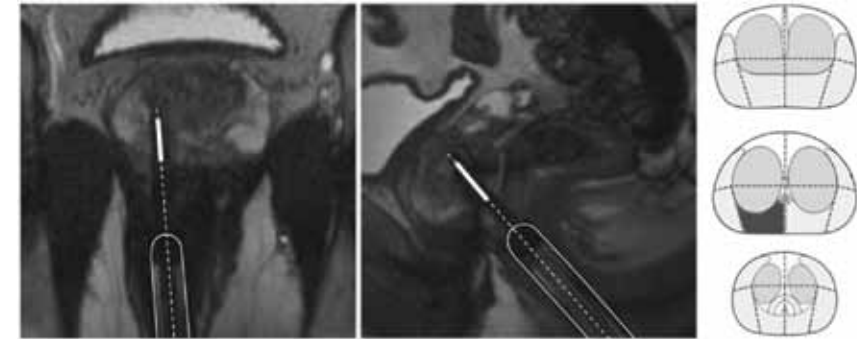


Figure 2: Axial (left) and sagittal (middle) balanced gradient-echo images of prostate with biopsy needle (dashed line) and biopsy core (thick solid line) inserted (needle guide is also delineated with solid line). Corresponding segment was annotated (right) as right medial peripheral zone in mid prostate (dark gray segment, middle).

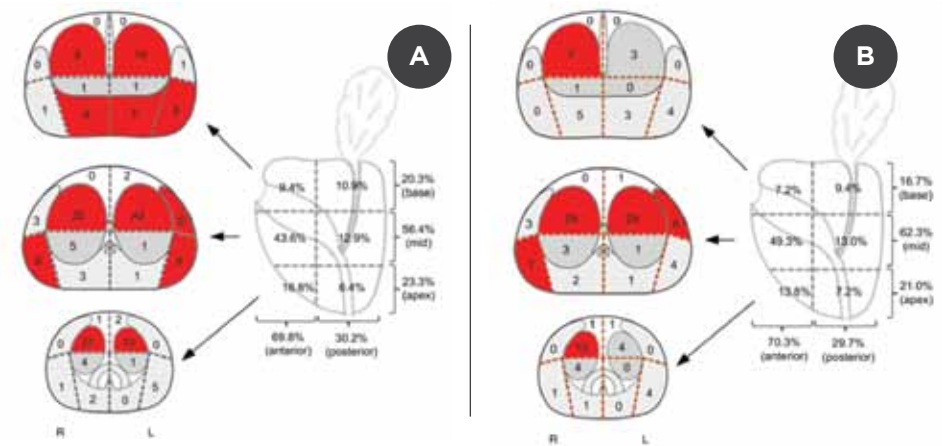


Figure 3: Schematic axial and sagittal views of prostate. Diagrams show all cancer locations (A) and intermediate- or high-risk cancer locations (B). Horizontal dashed lines (17 mm) in axial views (left) separate anterior and posterior part of prostate. Peripheral zone (light gray), transition zone (dark gray), and anterior fibromuscular stroma (white) are shown on right (R) and left (L) sides. Numbers shown in axial view are numbers of histologically proven prostate cancer lesions found in MR-guided biopsy specimen for that specific segment. Segments with more than five positive lesions are colored red. In total, 202 (138 intermediate- or high-risk) lesions with prostate cancer were detected in 176 (128 intermediate- or high-risk) patients. In schematic sagittal views of prostate (right), distribution of histopathologically proven prostate cancer locations after MR-guided biopsy is shown as percentage of all lesions (A) and intermediate- or high-risk lesions (B). Adapted with permission from Dickinson et al. (20).

Statistical analysis

The proportion of patients with cancer in each prostate location was compared using a chi-square test. The corresponding 95% CIs were calculated using the modified Wald method. One-way ANOVA analyses were performed to compare the means of age, PSA level, prostate volume, and PSA density between the different negative TRUS-guided biopsy session groups. All analyses were performed with SPSS software (version 20.0, IBM).

Results

Patient selection and suspicious lesions

In total, 176 of the 872 patients were included; reasons for exclusion are described in Figure 1. In these patients, 277 suspicious lesions were biopsied, and cancer was detected in 202 lesions (73%). Patient characteristics are shown in Table 1. The median time between the last TRUS-guided biopsy and MR-guided biopsy was 8 months (range, 0-23 months).

All patients							Patients with significant PCa						
Number of previous negative TRUS biopsy sessions	1	2	3	≥4	Total	<i>p</i>	1	2	3	≥4	Total	<i>p</i>	
Mean age (years)	63	64	66	66	65	0.09	64	65	66	68	66	0.08	
Mean PSA (ng/mL)	11	21	23	29	22	<0.01	12	21	25	33	24	0.01	
Mean prostate volume (mL)	51	50	52	56	52	0.66	42	49	53	57	51	0.19	
Mean PSA density (ng/mL/cc)	0.3	0.5	0.5	0.6	0.5	0.06	0.4	0.6	0.5	0.6	0.5	0.40	
Median number of cores during last biopsy session	10	10	10	10	10		10	10	10	10	10		
Patients with PCa (%(n))	17.6 (31)	28.4 (50)	28.9 (51)	25.0 (44)	176		14.1 (18)	29.7 (38)	30.5 (39)	25.8 (33)	128		
Lesions with PCa	16.8 (34)	27.7 (56)	28.2 (57)	26.1 (55)	202		13.8 (19)	30.4 (42)	29.7 (41)	26.1 (36)	138		
Gleason score													
5	2	1	4	4	11		0	1	1	4	6		
6	18	21	15	21	75		7	8	5	10	30		
7	9	28	24	16	77		9	28	24	16	77		
8	4	5	11	10	30		4	5	11	10	30		
9	0	1	3	3	7		0	1	3	3	7		
10	1	0	0	1	2		1	0	0	1	2		
≥8	5	6	14	14	39		5	6	14	14	39		
Patients with involvement of (% (n))													
Transition zone or anterior fibromuscular stroma	61.3 (19)	74.0 (37)	84.3 (43)	79.5 (35)	76.1 (134)	0.11	55.6 (10)	71.1 (27)	84.6 (33)	78.8 (26)	75.0 (96)	0.11	
Peripheral zone	38.7 (12)	34.0 (17)	21.6 (11)	27.3 (12)	29.5 (52)	0.34	44.4 (8)	36.8 (14)	20.5 (8)	30.3 (10)	31.3 (40)	0.25	
Anterior portion	54.8 (17)	78.0 (39)	82.4 (42)	77.3 (34)	75.0 (132)	0.04	50.0 (9)	76.3 (29)	79.5 (31)	75.8 (25)	73.4 (94)	0.11	
Posterior portion	48.4 (15)	26.0 (13)	21.6 (11)	29.5 (13)	29.5 (52)	0.07	55.6 (10)	26.3 (10)	25.6 (10)	33.3 (11)	32.0 (41)	0.12	
Base	29.0 (9)	12.0 (6)	25.5 (13)	31.8 (14)	23.9 (42)	0.12	27.8 (5)	7.9 (3)	25.6 (10)	30.3 (10)	21.9 (28)	0.09	
Mid	45.2 (14)	60.0 (30)	58.8 (30)	63.6 (28)	58.0 (102)	0.43	38.9 (7)	65.8 (25)	64.1 (25)	69.7 (23)	62.5 (80)	0.16	
Apex	29.0 (9)	30.0 (15)	25.5 (13)	22.7 (10)	26.7 (47)	0.86	38.9 (7)	28.9 (11)	23.1 (9)	24.2 (8)	27.3 (35)	0.62	

Table 1: Patient Characteristics and Zonal Distribution Stratified by the Number of Negative Transrectal Ultrasound (TRUS) Biopsy Sessions.

Note: Patients with an anterior or peripheral zone prostate cancer can have a posterior, transition zone, or anterior fibromuscular stroma cancer as well. The p-values shown are the results for the one-way ANOVA analyses (age, prostate-specific antigen (PSA) level, prostate volume, and PSA density) and the chi-square analyses to compare proportions of patients with certain prostate cancer (PCa) locations for different parameters including the number of previous negative TRUS-guided biopsy sessions.

Prostate cancer locations detected with MR-guided biopsy

Lesion basis: The distribution of lesions with histologically proven prostate cancer for each segment is shown in Figure 3. Lesions were located anteriorly in 70% of cases (141/202; 95% CI, 63-76%).

Patient basis: In 75% (132/176; 95% CI, 69-81%) of patients, there was involvement of the anterior part of the prostate. Anterior involvement of prostate cancer detected by MR-guided biopsy was statistically significantly ($p = 0.04$) higher in patients with two or more negative TRUS-guided biopsy sessions 79% (115/145; 95% CI, 74-85%) compared with those with one negative TRUS-guided biopsy session 55% (17/31; 95% CI, 39-71%) (Fig. 4).

In total, 76% (134/176; 95% CI, 70-83%) of the patients had cancer involvement of the TZ and anterior fibromuscular stroma. PZ cancers were found in 30% (52/176; 95% CI, 23-37%), and 6% of patients (11/176; 95% CI, 3-10%) had cancer in both zones. In 60% (123/202; 95% CI, 54-67%) of cases, cancer was detected in the TZ and anterior fibromuscular stroma only. The same numbers were found for solitary anterior cancers. Most cancers were found in the mid prostate 58% (102/176; 95% CI, 51-65%) followed by the apex 27% (47/176; 95% CI, 21-34%) and base 24% (42/176; 95% CI, 18-30%). No statistically significant differences were found among the base, mid, or apex and the number of negative TRUS-guided biopsy sessions (Table 1).

In patients with a high PSA level or high PSA density, more cancers were located anteriorly compared with patients with a lower PSA or lower PSA density ($p < 0.0001$). Most cancers with a Gleason score of 5 were found in the anterior part of the prostate (Fig. 4). However, anterior involvement was not statistically significantly different ($p = 0.30$) between different Gleason scores.

Prostate cancer location of intermediate- or high-risk cancers

Lesion basis: For 115 of 202 lesions (57%), the maximum cancer core length could be obtained from the pathology report. Most (66%; 76/115) had a maximum cancer core length greater than or equal to 6 mm. The relationship between maximum cancer core length and the location of prostate cancer is shown in Table 2. In 66% of cases (50/76; 95% CI, 55-76%), lesions with a maximum cancer core length of greater than or equal to 6 mm were located in the anterior portion, whereas 56% (22/39; 95% CI, 41-72%) of lesions with a maximum cancer core length less than 6 mm were located in the anterior portion; the difference was not statistically significant.

	MCCL <6 mm (n=39)	MCCL ≥6 mm (n=76)
Anterior	22 (56.4) [41-72]	50 (65.8) [55-76]
Peripheral zone	16 (41.0) [26-56]	25 (32.9) [22-43]
Transition zone and anterior fibromuscular stroma	23 (59.0) [44-74]	51 (67.1) [57-78]

Table 2: Correlation between maximum cancer core length (MCCL) and location of prostate cancer per lesion. The MCCL could be determined from the pathology report from 115 lesions. Data are number (%) of lesions [95% CI].

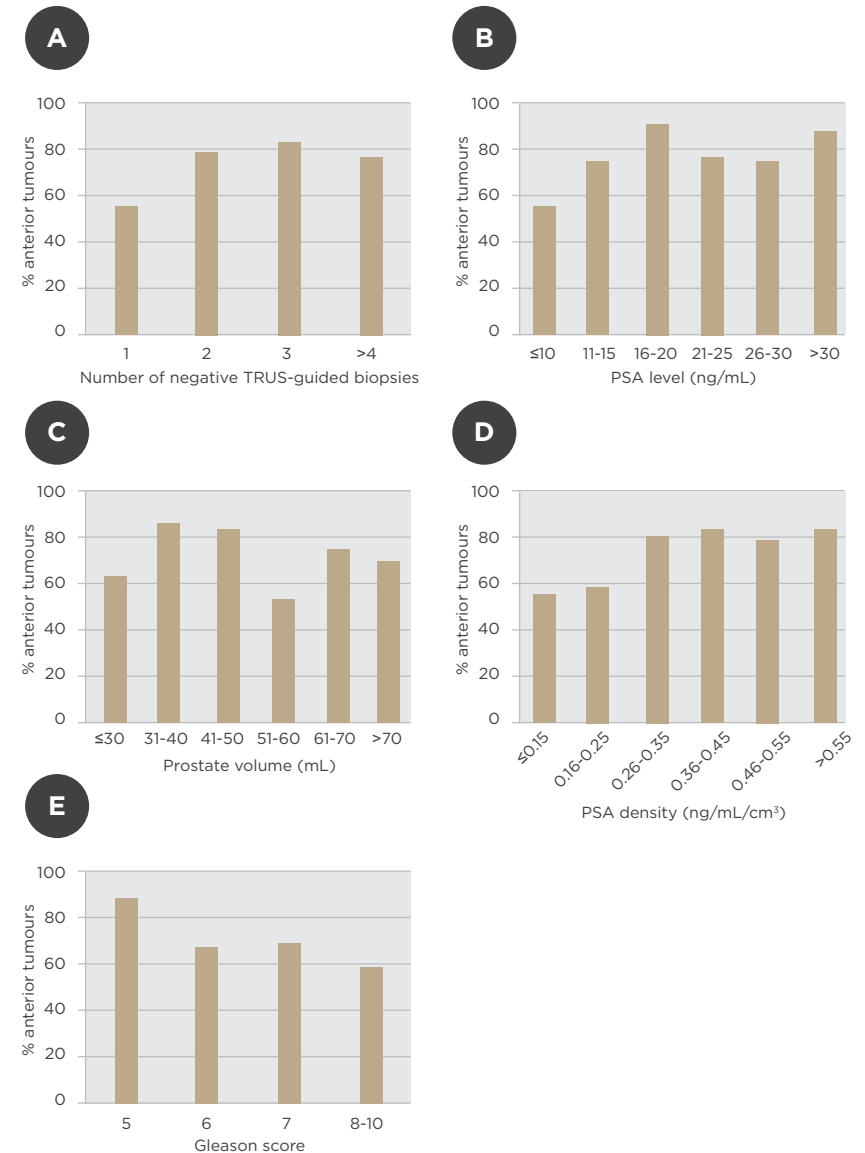


Figure 4: Percentage of anterior prostate cancers (A-E). Graphs show percentage of anterior prostate cancers with respect to number of negative transrectal ultrasound (TRUS)-guided biopsy sessions (A), prostate-specific antigen (PSA) level (B), prostate volume (C), PSA density (D), and Gleason score (E). In patients with higher PSA level, higher PSA density, and larger prostate volume, more cancers were located anteriorly compared with patients with lower PSA level, PSA density ($p < 0.0001$). There were no statistically significant differences between Gleason score and cancer location ($p = 0.30$). Data in A-D are presented on per-patient basis and those in E are presented on per-lesion basis. Patients with anterior or peripheral zone cancer can have posterior and transition zone cancer as well.

Patient basis: For 138 patients it was possible to determine whether intermediate- or high-risk prostate cancer was present; in 38 patients with a highest Gleason grade of 3, the maximum cancer core length was not described in the pathology report. Intermediate- or high-risk prostate cancer was found in 93% of patients (128/138; 95% CI, 88-96%). Of these patients, 73% (94/128; 95% CI, 66-81%) had anterior involvement. Among all patients with cancer, 65% (114/176; 95% CI, 58-72%) had a Gleason grade of 4 or higher.

Discussion

In patients with prostate cancer initially missed with TRUS-guided biopsy, multi-parametric MRI followed by MR-guided biopsy detected cancer in the anterior part in 75% of cases. In particular, patients with repeated negative TRUS-guided biopsy sessions more often received a diagnosis of anterior prostate cancer (79%). Intermediate- or high-risk prostate cancer was found in 93% of cases. Of these patients, 73% had anterior involvement. In 66% of cases, the lesions with a maximum cancer core length of greater than or equal to 6 mm were located in the anterior portion, which was a higher proportion than the lesions with a maximum cancer core length less than 6 mm (56%). These results confirm our hypothesis that in patients with an elevated PSA level and one or more negative TRUS-guided biopsy session, more cancers are located in the anterior portion of the prostate. This is most likely the result of undersampling of the anterior part using standardized TRUS-guided biopsy schemes.

Comparison with other biopsy strategies

Another method to sample the prostate in cases of negative TRUS-guided biopsies and elevated PSA levels is transperineal saturation biopsies. In the literature, higher detection rates were reported for this method in this patient group when compared with standard TRUS-guided biopsy schemes. Furthermore, most of these patients also had anterior involvement (77%); TZ and PZ involvement was seen in 45-77% and 37-54% of patients, respectively (6, 8-10). The higher PZ involvement found with transperineal template TRUS-guided biopsy compared with MR-guided biopsy may be explained by the fact that it is difficult to target and determine the exact needle location with transperineal biopsy. With MR-guided biopsy, a biplanar confirmation scan was made with the needle left in situ. In these images, the TZ and PZ can easily be discriminated. This is not possible on TRUS images because no confirmation scans are made with the needle left in situ.

Intermediate- or high-risk prostate cancer was found in 93% of patients, which is higher than the detection rate with transperineal template TRUS-guided biopsy (60-89%) (6, 7, 23). However, the criteria for intermediate- or high-risk prostate cancer differ (i.e., maximum cancer core length, total cancer core length, and number of positive cores) among studies. Furthermore, the criteria used for template TRUS-guided biopsy are not applicable to MR-guided biopsy because

these criteria also use the number of positive cores. Among the patients in our study who received a diagnosis of cancer, 65% had a Gleason grade of 4 or higher, which is comparable to the results found in transperineal template TRUS-guided biopsy studies (34-72%) (6, 10, 24).

Although systematic transperineal template TRUS-guided biopsy improves the detection rate of prostate cancer, the procedure is more expensive and invasive than standard TRUS-guided biopsy (25). Extended TRUS-biopsy schemes have been investigated in which TZ sampling was added to the standard PZ biopsies in patients with previous negative TRUS-guided biopsy sessions and persistently elevated PSA level. Solitary TZ cancers were found in 8-31% of the patients (26,27). In our study, 60% of the patients had a solitary TZ cancer. This is of important clinical value because these cancers were missed with TRUS-guided biopsy. Nevertheless, the detection rate of TRUS-guided biopsy with additional TZ biopsies is lower (17-28%) than that of transperineal template TRUS-guided biopsy (27-30).

MR-guided biopsy is a relatively new technique in the detection of prostate cancer and has shown superior results compared with TRUS-guided biopsy (17). The fusion of MR images with TRUS images is another new technique that combines the localization strength of MRI and real-time ultrasound imaging. Only a limited number of studies are available in patients with an elevated PSA level and at least one negative TRUS-guided biopsy session. Those studies found an increase in the detection rate and more intermediate- or high-risk cancers were found compared with standard TRUS-guided biopsy schemes (31-33). Studies that compare MR-guided biopsy and fusion of MR images with TRUS images regarding detection rate, number of intermediate- or high-risk prostate cancers, and prostate cancer location and cancer size are necessary to determine which technique is beneficial in which patient (28).

The high number of lesions with prostate cancer found in the TZ (69%) is comparable to earlier published results in small patient populations who underwent MR-guided biopsy (63-70%) and saturation biopsy (45-77%) (13-15). To our knowledge, this is the first study to describe the location of prostate cancer detected with MR-guided biopsy in relation to the number of negative TRUS-guided biopsies in a large population. This is of clinical importance because it will help both radiologists and urologists to focus on areas with targeted biopsy areas where cancers are most likely to be. Furthermore, these results have implications for diagnosis because physicians might pay extra attention to locations that are likely to contain prostate cancer.

Limitations

Some limitations of our study should be discussed. First, only patients with positive biopsy results were included. Similar to systematic transperineal template TRUS-guided biopsy, prostate cancer may be missed with multi-parametric MRI and MR-guided biopsy. Inevitably, this introduced a patient selection bias because we have currently no information about the patients with negative findings. Thus far, there is no reference standard in this patient group.

Second, in this study, the anterior portion was defined as the area ventral to a fixed distance of 17 mm from the posterior prostatic surface. Therefore, the fraction between anterior and posterior volume was not equal in all prostates and depended on prostate volume. However, in this study, the number of anterior lesions did not increase with larger prostate volumes, which is in agreement with the hypothesis that the posterior 17 mm of the prostate is sampled with TRUS-guided biopsy. Furthermore, in patients with a small prostate, an anteriorly located lesion could be classified as a posterior lesion because the whole prostate was within the 17 mm line.

Third, only one segment was assigned to each lesion to prevent a large cancer on MRI accounting for two lesions. When the sampling core was located in two segments, the segment with the highest suspicion for prostate cancer (i.e., the lowest apparent diffusion coefficient value) on the MRI was chosen. Therefore, cancers may extend beyond the assigned segment.

Fourth, our study had a retrospective design without randomization and comparison with other biopsy approaches; therefore, it may inherently contain another bias regarding patient selection. However, this is a well-defined series of consecutive patients, which strengthens its applicability in daily clinical practice. Fifth, the maximum cancer core length could be obtained in 57% of the lesions because the cancer volume percentage or biopsy core length could not be obtained from the pathology report. With the defined criteria for intermediate- or high-risk prostate cancer, it was possible to determine in only 138 of the patients whether intermediate- or high-risk prostate cancer was present because in 38 patients with a highest Gleason grade of 3, the maximum cancer core length was unknown.

Conclusion

The aim of this study was to identify the location of histopathologically proven prostate cancer using multi-parametric MRI followed by MR-guided biopsy. The results presented in this article confirm our hypothesis that anterior involvement is high (75%) in patients with an elevated PSA level and at least one negative TRUS-guided biopsy session. Furthermore, most (93%) of these cancers are intermediate- or high-risk.

References

1. Chun FK, Epstein JI, Ficarra V, et al. Optimizing performance and interpretation of prostate biopsy: a critical analysis of the literature. *Eur Urol*. 2010;58(6):851-64.
2. Sanchez-Chapado M, Olmedilla G, Cabeza M, et al. Prevalence of prostate cancer and prostatic intraepithelial neoplasia in Caucasian Mediterranean males: an autopsy study. *Prostate*. 2003;54(3):238-47.
3. Soos G, Tsakiris I, Szanto J, et al. The prevalence of prostate carcinoma and its precursor in Hungary: an autopsy study. *Eur Urol*. 2005;48(5):739-44.
4. Nevoux P, Ouzzane A, Ahmed HU, et al. Quantitative tissue analyses of prostate cancer foci in an unselected cystoprostatectomy series. *BJU Int*. 2012;110(4):517-23.
5. Djavan B, Ravery V, Zlotta A, et al. Prospective evaluation of prostate cancer detected on biopsies 1, 2, 3 and 4: when should we stop? *J Urol*. 2001;166(5):1679-83.
6. Patel V, Merrick GS, Allen ZA, et al. The incidence of transition zone prostate cancer diagnosed by transperineal template-guided mapping biopsy: implications for treatment planning. *Urology*. 2011;77(5):1148-52.
7. Taira AV, Merrick GS, Galbreath RW, et al. Performance of transperineal template-guided mapping biopsy in detecting prostate cancer in the initial and repeat biopsy setting. *Prostate Cancer Prostatic Dis*. 2010;13(1):71-7.
8. Pinkstaff DM, Igel TC, Petrou SP, et al. Systematic transperineal ultrasound-guided template biopsy of the prostate: three-year experience. *Urology*. 2005;65(4):735-9.
9. Igel TC, Knight MK, Young PR, et al. Systematic transperineal ultrasound guided template biopsy of the prostate in patients at high risk. *J Urol*. 2001;165(5):1575-9.
10. Merrick GS, Gutman S, Andreini H, et al. Prostate cancer distribution in patients diagnosed by transperineal template-guided saturation biopsy. *Eur Urol*. 2007;52(3):715-23.
11. Pal RP, Elmussareh M, Chanawani M, et al. The role of a standardized 36 core template-assisted transperineal prostate biopsy technique in patients with previously negative transrectal ultrasonography-guided prostate biopsies. *BJU Int*. 2012;109(3):367-71.
12. Gershman B, Zietman AL, Feldman AS, et al. Transperineal template-guided prostate biopsy for patients with persistently elevated PSA and multiple prior negative biopsies. *Urol Oncol*. 2012.
13. Roethke M, Anastasiadis AG, Lichy M, et al. MRI-guided prostate biopsy detects clinically significant cancer: analysis of a cohort of 100 patients after previous negative TRUS biopsy. *World J Urol*. 2012;30(2):213-8.
14. Hoeks CM, Schouten MG, Bomers JG, et al. Three-Tesla magnetic resonance-guided prostate biopsy in men with increased prostate-specific antigen and repeated, negative, random, systematic, transrectal ultrasound biopsies: detection of clinically significant prostate cancers. *Eur Urol*. 2012;62(5):902-9.
15. Hambrock T, Somford DM, Hoeks C, et al. Magnetic resonance imaging guided prostate biopsy in men with repeat negative biopsies and increased prostate specific antigen. *J Urol*. 2010;183(2):520-7.
16. Franiel T, Stephan C, Erbersdobler A, et al. Areas suspicious for prostate cancer: MR-guided biopsy in patients with at least one transrectal US-guided biopsy with a negative finding--multiparametric MR imaging for detection and biopsy planning. *Radiology*. 2011;259(1):162-72.
17. Barentsz JO, Richenberg J, Clements R, et al. ESUR prostate MR guidelines 2012. *Eur Radiol*. 2012;22(4):746-57.
18. Vos PC, Hambrock T, Barentsz JO, et al. Computer-assisted analysis of peripheral zone prostate lesions using T2-weighted and dynamic contrast enhanced T1-weighted MRI. *Phys Med Biol*. 2010;55(6):1719-34.
19. Hambrock T, Futterer JJ, Huisman HJ, et al. Thirty-two-channel coil 3T magnetic resonance-guided biopsies of prostate tumor suspicious regions identified on multimodality 3T magnetic resonance imaging: technique and feasibility. *Invest Radiol*. 2008;43(10):686-94.

20. Dickinson L, Ahmed HU, Allen C, et al. Scoring systems used for the interpretation and reporting of multiparametric MRI for prostate cancer detection, localization, and characterization: could standardization lead to improved utilization of imaging within the diagnostic pathway? *J Magn Reson Imaging*. 2013;37(1):48-58.
21. Thoeny HC, Forstner R, De Keyzer F. Genitourinary applications of diffusion-weighted MR imaging in the pelvis. *Radiology*. 2012;263(2):326-42.
22. Ahmed HU, Hu Y, Carter T, et al. Characterizing clinically significant prostate cancer using template prostate mapping biopsy. *J Urol*. 2011;186(2):458-64.
23. Zaytoun OM, Moussa AS, Gao T, et al. Office based transrectal saturation biopsy improves prostate cancer detection compared to extended biopsy in the repeat biopsy population. *J Urol*. 2011;186(3):850-4.
24. Ahyai SA, Isbarn H, Karakiewicz PI, et al. The presence of prostate cancer on saturation biopsy can be accurately predicted. *BJU Int*. 2010;105(5):636-41.
25. Merrick GS, Taubenslag W, Andreini H, et al. The morbidity of transperineal template-guided prostate mapping biopsy. *BJU Int*. 2008;101(12):1524-9.
26. Liu IJ, Macy M, Lai YH, et al. Critical evaluation of the current indications for transition zone biopsies. *Urology*. 2001;57(6):1117-20.
27. Ishizuka O, Mimura Y, Oguchi T, et al. Importance of transition zone prostate biopsies in patients with gray-zone PSA levels undergoing the ultrasound-guided systematic ten-biopsy regimen for the first time. *Urol Int*. 2005;74(1):23-6.
28. Babaian RJ, Toi A, Kamoi K, et al. A comparative analysis of sextant and an extended 11-core multisite directed biopsy strategy. *J Urol*. 2000;163(1):152-7.
29. Abdel-Khalek M, Sheir KZ, El-Baz M, et al. Is transition zone biopsy valuable in benign prostatic hyperplasia patients with serum prostate-specific antigen >10 ng/ml and prior negative peripheral zone biopsy? *Scand J Urol Nephrol*. 2005;39(1):49-55.
30. Abdel-Khalek M, El-Baz M, Ibrahim el H. Is extended 11-core biopsy valuable in benign prostatic hyperplasia patients with intermediate serum prostate-specific antigen (4.1-10 ng/ml) and prior negative sextant biopsy? *Scand J Urol Nephrol*. 2004;38(4):315-20.
31. Kuru TH, Roethke MC, Seidenader J, et al. Critical evaluation of magnetic resonance imaging targeted, transrectal ultrasound guided transperineal fusion biopsy for detection of prostate cancer. *J Urol* 2013; 190:1380-1386
32. Sonn GA, Chang E, Natarajan S, et al. Value of targeted prostate biopsy using magnetic resonance-ultrasound fusion in men with prior negative biopsy and elevated prostate-specific antigen. *Eur Urol* 2014; 65:809-815
33. Miyagawa T, Ishikawa S, Kimura T, et al. Realtime virtual sonography for navigation during targeted prostate biopsy using magnetic resonance imaging data. *Int J Urol* 2010; 17:85-860

CHAPTER 4.0 WHY AND WHERE DO WE MISS SIGNIFICANT PROSTATE CANCER WITH MULTI-PARAMETRIC MRI FOLLOWED BY MR-GUIDED AND TRUS-GUIDED BIOPSY IN BIOPSY NAIVE MEN?

*Martijn G. Schouten, Marloes van der Leest, Morgan R. Pokorny,
Martijn Hoogenboom, Jelle O. Barentsz, Les C. Thompson,
Jurgen J. Fütterer*

European Urology 2017 Jun;71(6):896-903

Abstract

Background: Knowledge of significant prostate cancer locations being missed with magnetic resonance (MR)- and transrectal ultrasound (TRUS)-guided biopsy may help to improve these techniques.

Objective: To identify the location of significant prostate cancer lesions being missed with MR- and TRUS-guided biopsy.

Design, Setting, and Participants: In a referral center 223 consecutive biopsy-naive men with elevated prostate specific antigen level and/or abnormal digital rectal examination were included. Histopathologically proven cancer locations, Gleason score and tumor length were determined.

Intervention: All subjects underwent multi-parametric MRI and 12-core systematic TRUS-guided biopsy. MR-guided biopsy was performed in all patients with suspicion of prostate cancer on multi-parametric MRI (n=142).

Outcome Measurements and Statistical Analysis: Cancer locations were compared between MR- and TRUS-guided biopsy. Proportions were expressed as percentages, and the corresponding 95% CIs were calculated.

Results and limitations: In total 191 lesions were found in 108 patients with significant prostate cancer. From these lesion 74% (141/191) were defined as significant prostate cancer on either MR- or TRUS-guided biopsy. MR-guided biopsy detected 74% (105/141) of these lesions, this was 61% (86/141) with TRUS-guided biopsy. TRUS-guided biopsy detected more lesions compared to MR-guided biopsy (140 vs 109). However, these lesions were often low-risk (39%). Significant lesions missed with MR-guided biopsy had most often involvement of dorsolateral (58%) and apical (37%) segments and missed segments with TRUS-guided biopsy were located anteriorly (79%), anterior mid prostate (50%) and anterior apex (23%).

Conclusions: Both techniques have difficulties in detecting apical lesions. MR-guided biopsy most often missed cancer with involvement of the dorsolateral part (58%) and TRUS-guided biopsy with involvement of the anterior part (79%).

Patient summary: Both biopsy techniques do miss cancer in specific locations within the prostate. Identification of these lesions may help to improve these techniques.

Introduction

Early detection of prostate cancer, with the intent to diagnose this disease in a curable state, currently leads to over-diagnosis which in turn can result in over-treatment (1). Over-diagnosis is the main disadvantage of the present clinical standard where men with elevated serum prostate specific antigen (PSA) levels and/or abnormal digital rectal examination (DRE) undergo random systematic 10 to 12-core prostate transrectal ultrasound (TRUS)-guided biopsy. Other limitations of TRUS-guided biopsy are under-detection and under-grading of clinically significant prostate cancer (2). The number of cores and location for systematic sampling is a topic of debate (2-4). In biopsy naïve patients, generally accepted schemes for systematic sampling with TRUS-guided biopsy are limited to the posterior peripheral zone since most cancers are located in this region (2, 4). In the repeat biopsy setting most cancers are located in the anterior apex of the prostate (2, 4, 5).

Multi-parametric MRI can be used to reduce over-diagnosis and subsequent over-treatment (6). multi-parametric MRI is able to detect significant prostate cancer (44-87%) in biopsy-naïve males and men with prior negative biopsies. Furthermore, the high negative predictive value (63-98%) of multi-parametric MRI can be used to rule out significant prostate cancer (7-9).

Although multi-parametric MRI is a promising technique, significant prostate cancer may be missed (10). The interpretation of multi-parametric MRI can sometimes be difficult (11, 12). Current research has not focused on the location of cancers missed with multi-parametric MRI followed by MR-guided biopsy. Knowledge of lesions being missed with MR- and TRUS-guided biopsy is of clinical importance for diagnosis and treatment.

The purpose of this study is to identify the location of significant prostate cancer lesions being missed with MR-guided biopsy and systematic TRUS-guided biopsy in biopsy naïve patients at risk for prostate cancer.

Materials and methods

Patient selection and imaging

This study was a retrospective analysis of stored MR-images of biopsy-naïve consecutive subjects with an elevated PSA level and/or abnormal DRE. All subject enrolled by referral from urologists from July 2012 through January 2013 and were included in a previous prospectively study. However, no detailed data were published on the location of prostate cancer (13).

All subjects underwent multi-parametric MRI performed at 3T (Magnetom Skyra, Siemens) according to the ESUR prostate MR-guidelines (14). multi-parametric MRI scans were scored independently by three readers (1, 1, and 19 years of experience, respectively) using the Prostate Imaging Reporting and Data System version 1.0 (PI-RADS): from 1 (low) to 5 (high) according to the likelihood of significant prostate cancer being present (14). Disagreements in PI-RADS were resolved by consensus.

Prostate biopsy

Both MR- and TRUS-guided biopsy were performed in a second visit Figure 1. The standard diagnostic pathway consisted of systematic TRUS-guided biopsy only for men who had a PI-RADS 1 or 2 reported on multi-parametric MRI. MR-guided biopsy was performed in all patients with a PI-RADS 3-5 lesion on multi-parametric MRI, followed by systematic TRUS-guided biopsy as well (15). Each PI-RADS 3-5 lesions on multi-parametric MRI was biopsied using two to three cores. Seminal vesicles were sampled if suspicious for tumor invasion.

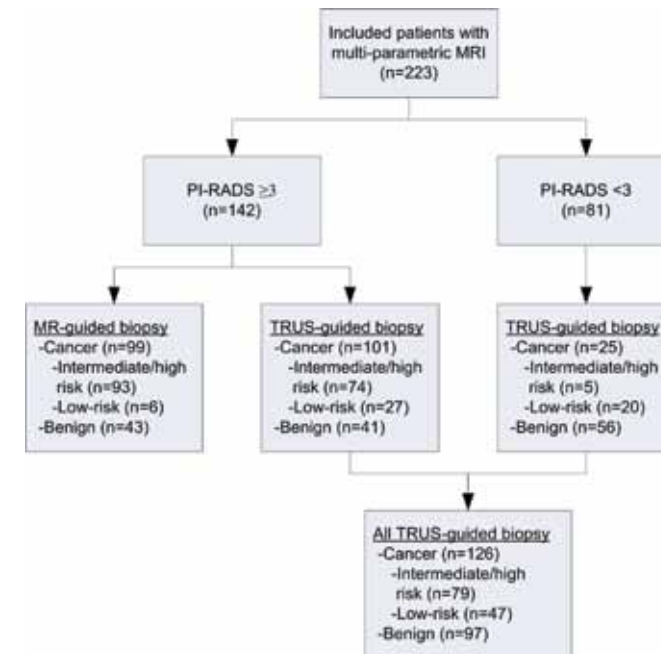


Figure 1: Flowchart describing the diagnostic pathways. All patients underwent both multi-parametric MRI and TRUS-guided biopsy. Patients with a PI-RADS ≥ 3 on multi-parametric MRI received MR-guided biopsy in addition to TRUS-guided biopsy. PI-RADS = Prostate Imaging Reporting and Data System

During the MR-guided biopsy session an axial diffusion weighted image (DWI) was acquired to relocate the cancer suspicious lesions (CSL) described on the diagnostic multi-parametric MRI. After needle insertion with MR-guided biopsy two confirmation scans were acquired to verify the biopsy location. TRUS-guided biopsy was performed within 30 minutes after MR-guided biopsy by an urologist blinded to the multi-parametric MRI and MR-guided biopsy procedure. Any lesions seen on TRUS were targeted using the core for the relevant prostate zone.

Histopathology and risk stratification

All biopsy specimens underwent evaluation by a urogenital-histopathologist blinded to the biopsy strategy. Low-risk prostate cancer was defined as either low- volumes Gleason score (GS) 3+3 or 3+4 (9). Significant prostate cancer (=intermediate- and/or high-risk prostate cancer) on MR- and TRUS-guided biopsy was defined as a GS $\geq 4+3$ or GS 3+4 (>4mm, or >1 positive core), or a GS 3+3 with a core length >6mm. Furthermore, a GS 3+3 was defined as significant prostate cancer when more than 1 or 2 cores were positive on MR- and TRUS-guided biopsy, respectively (13). Thus, for lesions with a GS 3+3 the number of cores was modality specific.

Biopsy outcome

Results were described on a segment, lesion and patient level.

1. *Segment:* Cancer locations were reported according to an adapted scheme as described by Barentsz et al. (16) (Fig. 2). Two readers (MS and ML), both with 2 years of experience in multi-parametric MRI of the prostate, determined in consensus the involved segments of the earlier defined CSL on multi-parametric MRI. Segments with suspicion on multi-parametric MRI (PI-RADS 3-5) were labeled as cancer when histopathologically proven with MR-guided biopsy. With TRUS-guided biopsy, 6 lateral and 6 medial samples from the posterior base, mid and apex were obtained according to a standard scheme for initial biopsy (2). A positive biopsy core was assigned to the corresponding segment(s). Segments of significant prostate cancer lesions (defined below) that were cancer positive on only one modality were considered as locations missed with the other modality. It should be noted that “missed with MR-guided biopsy” can be the results of not identifying a CSL on multi-parametric MRI, or incorrect needle positioning during the MR-guided biopsy procedure.
2. *Lesion:*
 - a TRUS-guided biopsy: All cancer positive segments (Fig. 2) that had a direct connection (neighbouring segments in the anterior-posterior, left-right or superior-inferior direction) were labelled as a single lesion.
 - b MR-guided biopsy: All cancer suspicious segments seen on the diagnostic multi-parametric MRI that had a direct connection were labelled as a single lesion when cancer was proven in at least one of these segments with MR-guided biopsy. Lesions with ≥ 1 matching segment on MR- and TRUS-guided biopsy were defined as the same lesion. To determine whether a lesions contained significant prostate cancer each lesion was evaluated separately by using the same criteria applied on a patient level. The maximum cancer core length (MCCL) and total cancer core length (TCCL) were determined to evaluate tumour volume.
3. *Patient:* Three groups were defined: patients with significant prostate cancer detected with MR-guided biopsy alone (group 1) or TRUS-guided biopsy alone (group 2) and with both techniques (group 3).

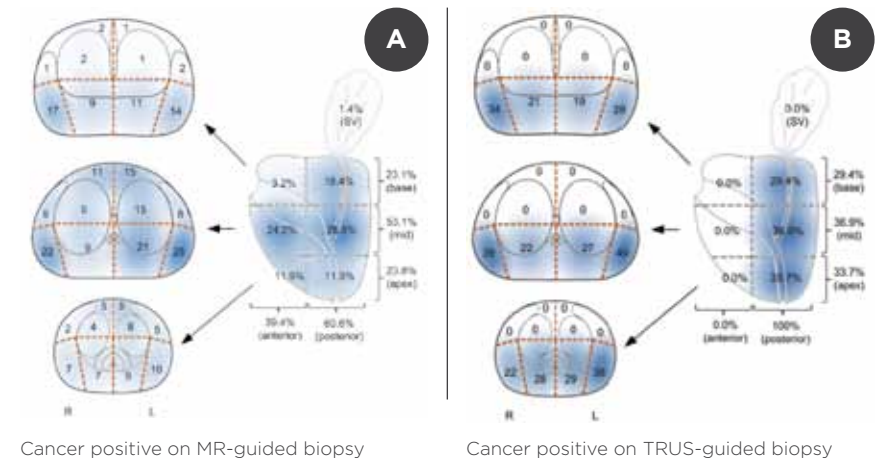


Figure 2: Distribution maps of cancer positive segments in patients with significant prostate cancer on MR-guided biopsy (left) and TRUS-guided biopsy (right). The anterior portion of the prostate was defined by a hypothetical line drawn 17mm anterior from the posterior prostatic surface irrespective of prostate size, which represents the core length commonly used during TRUS-guided biopsy (17).
SV = seminal vesicles.

The highest GS was determined on a patient and lesions level by combining histopathology from MR- and TRUS-guided biopsy.

Statistics

One-way ANOVA was performed to determine significant differences in age, PSA or prostate volume. The proportions of cancer positive segments were expressed as percentages, and the corresponding 95% CIs were calculated. The Fisher's exact test was performed to determine significant differences between groups. The Wilcoxon-signed rank test was used to determine significant differences between the MCCL and TCCL found with MR- and TRUS-guided biopsy. Since patients served as their own control we used the McNemar's test to detect a significant difference between the association of MR- and MR-guided biopsy and outcome. A significant difference was considered when the p-value was <0.05. The Standards for Reporting of Diagnostic Accuracy Studies (STARD) guidelines were followed to report the results. All analyses were performed with SPSS software (version 20.0, IBM).

Results

Patient characteristics and histopathological outcome of the 223 included patients are shown in Tables 1 and 2 and reported before (13).

Patient basis

Combined histopathology from MR- and TRUS-guided biopsy revealed prostate cancer in 64% of the patients (142/223, 95% CI; 57-70%) and 48% (108/223, 95% CI; 42-55%) of the cases showed significant prostate cancer. MR- and TRUS-guided biopsy detected significant prostate cancer in 42% (93/223) and 35% (79/223) of the patients, respectively and this was statistically significant different ($p < 0.0001$). Low-risk cancer was significantly ($p < 0.0001$) more often detected with TRUS-guided biopsy (21%, 47/223) compared to MR-guided biopsy (3%, 6/223). In patients diagnosed with significant prostate cancer on MR- and TRUS-guided biopsy upgrading of the GS was seen in 32% (35/108) with MR-guided biopsy and in 22% (24/108) with TRUS-guided biopsy, this was statistically significant different ($p < 0.001$).

	All patients		Significant PCa detected with:			p-value
	Included patients	Negative on MR- and TRUS-guided biopsy	MR-guided biopsy only (group 1)	TRUS-guided biopsy only (group 2)	Both modalities positive (group 3)	
Number of patients (%)	223 (100)	81 (36.3)	29 (13.0)	15 (6.7)	64 (28.7)	NA
Mean age (SD) years	62.4 (7.4)	59.6 (7.2)	63.5 (7.0)	62.7 (5.8)	65.5 (6.7)	0.2
Mean PSA (SD) ng/ml	5.9 (3.1)	5.1 (2.2)	6.7 (4.5)	4.9 (1.0)	7.1 (3.5)	0.1
Mean prostate volume (SD) cc	46.8 (22.6)	56.2 (24.4)	40.0 (17.1)	40.0 (10.1)	39.0 (19.9)	1.0

Table 1: Patient characteristics of all included patients in whom cancer was not detected, and patients in which prostate cancer was detected with MR-guided biopsy only (group 1), TRUS-guided biopsy only (group 2) and both modalities (group 3). The p-value of one way ANOVA is given for the comparison between groups 1-3.

PSA = Prostate specific antigen. PCa = prostate cancer. SD = standard deviation

In 15 patients significant prostate cancer was detected with TRUS-guided biopsy only (3 PI-RADS 3, 7 PI-RADS 4-5, and in 5 patients no CSLs were seen on multi-parametric MRI). Retrospectively, in 6/10 patients with a PI-RADS ≥ 3 the MR-guided biopsy needle was not in the correct position and in 1 patient the images of the MR-guided biopsy were not stored and thus not available for re-evaluation. Anterior tumor involvement was seen in 41% (44/108, 95% CI; 31-50%) of the patients with significant prostate cancer.

		TRUS-guided biopsy					totals		
		no cancer	Low-risk PCa		Significant PCa				
			Gleason 3+3 low volume	Gleason 3+4 low volume	Gleason 3+3 high volume	Gleason 3+4 High volume		Gleason $\geq 4+3$	
MR-guided biopsy	no cancer	81	23	8	3	4	5	124	
	Low-risk PCa	Gleason 3+3 low volume	0	1	1	1	1	1	5
		Gleason 3+4 low volume	0	1	0	0	0	0	1
	Significant PCa	Gleason 3+3 high volume	3	2	2	1	2	0	10
		Gleason 3+4 High volume	8	4	3	2	16	7	40
		Gleason $\geq 4+3$	5	0	2	0	4	32	43
totals		97	31	16	7	27	45	223	

Table 2: Histopathological biopsy outcome on a per patient level for MR- and TRUS-guided biopsy for the total cohort of 223 men. Green shading indicates patients where MR-guided biopsy upgraded the Gleason score in relation to TRUS-guided biopsy. Analogous blue shading indicates patients where TRUS-guided biopsy upgraded the Gleason score in relation to MR-guided biopsy. A dark color represents a larger discrepancy between the two modalities. PCa = prostate cancer.

Lesion basis

In total 191 lesions were found in 108 patients with significant prostate cancer (Table 3). From these lesions 74% (141/191, 95% CI; 68-80%) were defined as significant prostate cancer on either MR- or TRUS-guided biopsy. MR-guided biopsy detected 74% (105/141) of these lesions, and this was 61% (86/141) with TRUS-guided biopsy (13% difference, 95% CI; 8-19%). In 37% (64/175, 95% CI; 30-44%) of the CSLs seen on multi-parametric MRI no prostate cancer was found with MR-guided biopsy. Reasons for failure of MRI to identify cancer lesions are shown in table 4.

		TRUS-guided biopsy						totals	
		no cancer	Low-risk PCa		Significant PCa				
			Gleason 3+3 low volume	Gleason 3+4 low volume	Gleason 3+3 high volume	Gleason 3+4 High volume	Gleason ≥ 4+3		
MR-guided biopsy	no cancer		36	12	5	14	15	82	
	Low-risk PCa	Gleason 3+3 low volume	1	0	0	1	0	1	3
		Gleason 3+4 low volume	1	0	0	0	0	0	1
	Significant PCa	Gleason 3+3 high volume	7	1	1	0	4	0	13
		Gleason 3+4 High volume	24	3	1	1	9	9	47
		Gleason ≥ 4+3	18	0	0	0	2	25	45
totals		51	40	14	7	29	50	191	

Table 3: Highest Gleason score for all lesions (n=191) detected with MR- and TRUS-guided biopsy in patients with significant cancer (n=108). Green shading indicates patients where MR-guided biopsy upgraded the Gleason score in relation to TRUS-guided biopsy. Analogous blue shading indicates patients where TRUS-guided biopsy upgraded the Gleason score in relation to MR-guided biopsy. A dark color represents a larger discrepancy between the two modalities. PCa = prostate cancer.

Situation	Low-risk	Significant PCa	All lesions
Lesions detected with TRUS-guided biopsy in all patients	93	86	179
Lesions detected with MR-guided biopsy in all patients	10	105	115
Negative multi-parametric MRI but positive TRUS-guided biopsy (likely reading failure)	81	33	114
Positive multi-parametric MRI but negative MR-guided biopsy and negative TRUS-guided biopsy (likely reading failure)	0	0	56
Positive multi-parametric MRI and positive TRUS-guided biopsy but negative MR-guided biopsy (likely sampling failure)	5	3	8

Table 4: Reasons for failure of MRI to identify cancer lesions. PCa = prostate cancer.

In 15 patients in which significant prostate cancer was detected with TRUS-guided biopsy only, 26 lesions were detected of which 50% (13/26, 95% CI; 31-69%) contained significant prostate cancer. In retrospect (with knowledge of the cancer locations from MR-guided biopsy) 8 lesions could be defined as significant on multi-parametric MRI. In 3 of these significant prostate cancer lesions, low-risk cancer was diagnosed with MR-guided biopsy and 5 significant prostate cancer lesions were not seen on the initial detection MRI.

TRUS-guided biopsy detected more lesions (73%, 140/191) compared to MR-guided biopsy (57%, 109/191) (16% difference, 95% CI; 12-21%). However, more lesions were low-risk prostate cancer (28%, 54/191) compared to MR-guided biopsy (2%, 4/191) (26% difference, 95% CI; 20-32%).

The MCCL and TCCL of lesions solitary detected with TRUS-guided biopsy were significantly (p<0.0001) smaller than MR-guided biopsy lesions (Table 5 - page 58). In patients diagnosed with significant prostate cancer on MR- and/or TRUS-guided biopsy upgrading of the GS was seen in 41% (58/141) with MR-guided biopsy and in 35% (49/141) with TRUS-guided biopsy (6% difference, 95% CI; 3-11%).

Anterior tumor involvement was seen in 31% (44/140, 95% CI; 24-39%) of the significant prostate cancer.

Segment basis

MR- and TRUS-guided biopsy identified 277 and 347 cancer positive segments respectively in patients with significant prostate cancer. The distribution of these segments is shown in Figure 2. With MR- and TRUS-guided biopsy, most cancer positive segments were located in the mid prostate; 53% (147/277, 95% CI; 47-59%) and 37% (128/347, 95% CI; 32-42%) respectively. In total, 39% (109/277, 95% CI; 34-45%) of MR-guided positive segments were located in the anterior part of the prostate.

Situation	MR-guided biopsy	TRUS-guided biopsy	p-value (MR-guided biopsy vs TRUS-guided biopsy)
All lesions	109	140	NA
Number of missed lesions	82	51	NA
Number of missed significant lesions	34	49	NA
Mean MCCL (mm) of lesions detected with both modalities (SD):	10.0 (4.6)	9.5 (4.7)	0.64
Mean TCCL (mm) of lesions detected with both modalities (SD):	19.6 (12.3)	24.2 (21.1)	0.17
Mean MCCL (mm) of missed lesions and thus solitary detected with the other modality (SD):	3.4 (3.4)	8.6 (4.2)	<0.0001
Mean TCCL (mm) of missed lesions and thus solitary detected with the other modality (SD)	6.6 (8.6)	16.9 (10.2)	<0.0001

Table 5: Differences between mean maximum cancer core length (MCCL) and total cancer core length (TCCL) in patients with significant cancer. The p-value of the Wilcoxon-signed rank test is provided.

In lesions with significant prostate cancer, MR- and TRUS-guided biopsy missed 97 and 111 segments respectively (Fig. 3). Lesions missed with MR-guided biopsy, which had significant prostate cancer detected with TRUS-guided biopsy, appear to be located in the apex (37%, 36/97, 95% CI; 28-47%) and dorsolateral segments (58%, 56/97, 95% CI; 47-67%). Missed significant prostate cancer lesions on TRUS-guided biopsy had most often involvement of anterior segments (79%, 88/111, 95% CI; 71-86%). Specifically: anterior mid prostate (50%, 56/111, 95% CI; 41-60%) and anterior apex (23%, 25/111, 95% CI; 15-31%).

Discussion

This paper extrapolates on a previously published study, but focuses on lesions missed with MR- and TRUS-guided biopsy. Significant prostate cancer lesions missed with MR-guided biopsy most often had involvement of the dorsolateral (58%) and apical (37%) segments. With TRUS-guided biopsy, missed significant prostate cancer lesions had involvement of segments located anteriorly (79%), anterior mid prostate (50%) and anterior apex (23%). Anterior tumor involvement was seen in 41% of the patients, which is consistent with the literature (18). Lesions localized in the apical region were difficult to detect with both modalities, which is also concordant with the literature (18-21).

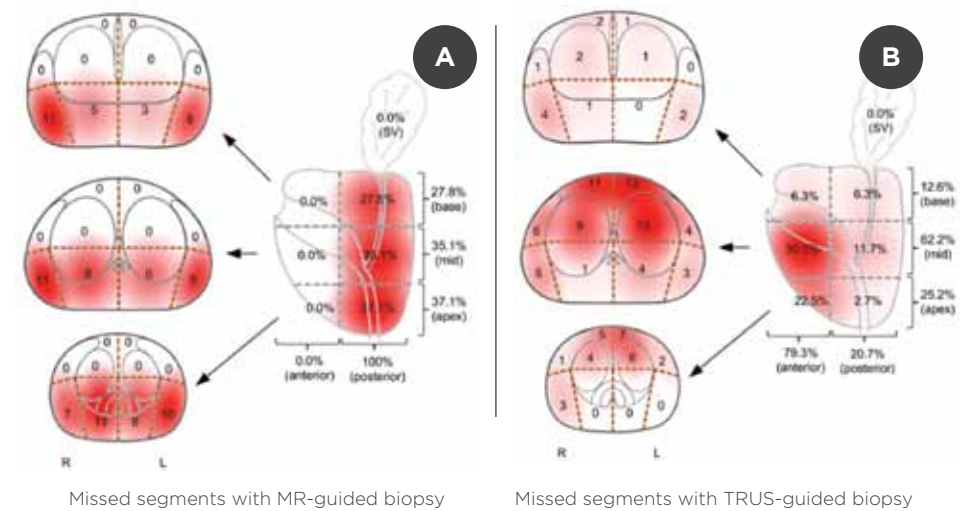


Figure 3: Distribution maps of the segments of significant prostate cancer lesions that were missed with MR-guided biopsy (left) and TRUS-guided biopsy (right). SV = seminal vesicles.

significant prostate cancer is associated with increased age, PSA level and a small prostate volume (22). Although not statistically significant the patient characteristics in our study (Table 1) confirm these relations, but the PSA levels in patients with significant prostate cancer detected with TRUS-guided biopsy (group 2) did not confirm this relation.

Multi-parametric MRI evaluation can be difficult in the apex given the small size of this region and its location at the margin of the prostate (12). Also, some focal lesions might be unnoticed on standard DWI protocols due to signal received from surrounding benign prostatic tissue which overshadows the lesion (11). This may be overcome by using high b-values (1400-2000 s/mm²) (11, 16). In our diagnostic protocol we used a calculated b-value of 1400 s/mm² which may not be sufficient. Furthermore, from the 67 lesions seen on multi-parametric MRI which were negative on MR-guided biopsy only 3 lesions contained significant prostate cancer on TRUS-guided biopsy, which suggests these CSLs were false-positive on multi-parametric MRI rather than being missed with MR-guided biopsy.

The relatively high involvement of dorsolateral segments in significant prostate cancer lesions missed with MR-guided biopsy might be explained by subcapsular tumours (12). Critical evaluation of small areas with abnormal signal intensity on DWI and dynamic contrast enhanced (DCE) images in the absence of a readily apparent mass abutting the capsule is recommended (12). Furthermore, since the exact needle location is not known with TRUS-guided biopsy some lateral biopsy samples can be false-positive. This may occur in case the biopsy core was located in both the medial and lateral segments but the tumor is confined within the medial segment.

Ukimura et al. recommends sampling according to a medial sextant pattern with ≥ 4 cores from the lateral peripheral zone. Furthermore, this review advises obtaining samples from the anterior apex, anterior lateral horn and anterior transition zone in the repeat biopsy setting (2). The results found in our study confirm these recommendations.

To our knowledge this is the first study which describes the differences between MR- and TRUS-guided biopsy regarding cancer location in biopsy naïve men at risk for prostate cancer. The results have clinical implications for both radiologists and urologists. For example, to optimize biopsy sites for TRUS-guided biopsy and systematic sampling with MRI targeted TRUS-biopsy (23). Based on our observation it is reasonable to obtain additional samples at initial TRUS-guided biopsy from the anterior apex and anterior mid prostate since these are the most common sites where cancer is missed. Adding cores in the extreme anterior apex has been shown to be beneficial (24). Similarly, it might be reasonable to obtain additional random biopsies from dorsolateral and apical regions during multi-parametric MRI targeted TRUS-guided biopsy to improve detection of significant prostate cancer without the need for systematic 12-core biopsy (25).

Regarding costs and patients comfort TRUS-MRI fusion is an interesting alternative for MR-guided biopsy (26). Although there is no study comparing multi-parametric MRI targeted TRUS-guided biopsy and in-bore MR-guided biopsy, the visual feedback regarding the accuracy of needle placement makes the in-bore MR-guided biopsy, to our opinion, more accurate.

In our study only 18% of the patients with a PI-RADS 3 lesion on multi-parametric MRI had significant prostate cancer. This figure was 89% in patients with a PI-RADS 4,5 lesion. Although considerable efforts have been undertaken to determine the optimal threshold for biopsy, this is still a topic of debate (27). Based on the findings from our study it might be interesting to investigate a region-dependent threshold for biopsy. For example, a threshold of PI-RADS 3 for lesions in the apical and dorsolateral regions and a threshold of PI-RADS 4,5 for lesions elsewhere in the prostate.

Some limitations of this study should be addressed. Firstly, there is no universally accepted and validated definition for significant prostate cancer (28). The modality-specific definition used in our study make the results difficult to compare with other studies. Furthermore, in the case in which a patient has multiple low-risk lesions, this definition can diagnose a patient as having significant prostate cancer without having a discrete significant prostate cancer lesion. However, this definition was created to allow comparison of two to four MR-guided biopsy cores with 12-cores obtained with TRUS-guided biopsy.

Secondly, whole mount prostatectomy would be the most reliable tool for histopathologic evaluation but is ethically impossible in patients with no proven cancer on biopsy. An alternative approach is to use 5mm transperineal template prostate mapping (4). The need for general anesthesia and increased complication rate makes this a highly invasive technique and presents challenges in recruiting patients for clinical trials when less invasive alternatives are available (4).

Third, a sub-analysis of patients who underwent prostatectomy would provide an excellent reference standard, however this may have introduced selection bias. By comparing the biopsy results between MR- and TRUS-guided biopsy we were able to directly compare differences between these modalities in a large patient group.

Conclusions

Both MR- and TRUS-guided biopsy have difficulties in detecting apical lesions. MR-guided biopsy most often missed cancer with involvement of the dorsolateral part (58%) and TRUS-guided biopsy missed lesions with involvement of the anterior part (79%).

References

1. Loeb S, Bjurlin MA, Nicholson J, Tammela TL, Penson DF, Carter HB, et al. Overdiagnosis and overtreatment of prostate cancer. *European urology*. 2014;65:1046-55.
2. Ukimura O, Coleman JA, de la Taille A, Emberton M, Epstein JI, Freedland SJ, et al. Contemporary role of systematic prostate biopsies: indications, techniques, and implications for patient care. *European urology*. 2013;63:214-30.
3. Scattoni V, Maccagnano C, Capitanio U, Gallina A, Briganti A, Montorsi F. Random biopsy: when, how many and where to take the cores? *World journal of urology*. 2014;32:859-69.
4. Sivaraman A, Sanchez-Salas R, Barret E, Ahallal Y, Rozet F, Galiano M, et al. Transperineal template-guided mapping biopsy of the prostate. *International journal of urology : official journal of the Japanese Urological Association*. 2015;22:146-51.
5. Bittner N, Merrick GS, Butler WM, Bennett A, Galbreath RW. Incidence and pathological features of prostate cancer detected on transperineal template guided mapping biopsy after negative transrectal ultrasound guided biopsy. *The Journal of urology*. 2013;190:509-14.
6. Rosenkrantz AB, Taneja SS. Prostate MRI can reduce overdiagnosis and overtreatment of prostate cancer. *Academic radiology*. 2015;22:1000-6.
7. Futterer JJ, Briganti A, De Visschere P, Emberton M, Giannarini G, Kirkham A, et al. Can Clinically Significant Prostate Cancer Be Detected with Multiparametric Magnetic Resonance Imaging? A Systematic Review of the Literature. *European urology*. 2015.
8. Thompson JE, van Leeuwen PJ, Moses D, Shnier R, Brenner P, Delprado W, et al. The Diagnostic Performance of Multiparametric Magnetic Resonance Imaging to Detect Significant Prostate Cancer. *The Journal of urology*. 2015.
9. Abd-Alazeez M, Kirkham A, Ahmed HU, Arya M, Anastasiadis E, Charman SC, et al. Performance of multiparametric MRI in men at risk of prostate cancer before the first biopsy: a paired validating cohort study using template prostate mapping biopsies as the reference standard. *Prostate cancer and prostatic diseases*. 2014;17:40-6.
10. Sivaraman A, Sanchez-Salas R, Ahmed HU, Barret E, Cathala N, Mombet A, et al. Clinical utility of transperineal template-guided mapping biopsy of the prostate after negative magnetic resonance imaging-guided transrectal biopsy. *Urologic oncology*. 2015;33:329 e7-11.
11. Rosenkrantz AB, Taneja SS. Radiologist, be aware: ten pitfalls that confound the interpretation of multiparametric prostate MRI. *AJR American journal of roentgenology*. 2014;202:109-20.
12. Rosenkrantz AB, Verma S, Turkbey B. Prostate cancer: top places where tumors hide on multiparametric MRI. *AJR American journal of roentgenology*. 2015;204:W449-56.
13. Pokorny MR, de Rooij M, Duncan E, Schroder FH, Parkinson R, Barentsz JO, et al. Prospective study of diagnostic accuracy comparing prostate cancer detection by transrectal ultrasound-guided biopsy versus magnetic resonance (MR) imaging with subsequent MR-guided biopsy in men without previous prostate biopsies. *European urology*. 2014;66:22-9.
14. Barentsz JO, Richenberg J, Clements R, Choyke P, Verma S, Villeirs G, et al. ESUR prostate MR guidelines 2012. *European radiology*. 2012;22:746-57.
15. Hambrock T, Futterer JJ, Huisman HJ, Hulsbergen-vandeKaa C, van Basten JP, van Oort I, et al. Thirty-two-channel coil 3T magnetic resonance-guided biopsies of prostate tumor suspicious regions identified on multimodality 3T magnetic resonance imaging: technique and feasibility. *Investigative radiology*. 2008;43:686-94.
16. Barentsz JO, Weinreb JC, Verma S, Thoeny HC, Tempny CM, Shtern F, et al. Synopsis of the PI-RADS v2 Guidelines for Multiparametric Prostate Magnetic Resonance Imaging and Recommendations for Use. *European urology*. 2015.
17. Dickinson L, Ahmed HU, Allen C, Barentsz JO, Carey B, Futterer JJ, et al. Magnetic resonance imaging for the detection, localisation, and characterisation of prostate cancer: recommendations from a European consensus meeting. *European urology*. 2011;59:477-94.
18. Abdelsayed GA, Danial T, Kaswick JA, Finley DS. Tumors of the Anterior Prostate: Implications for Diagnosis and Treatment. *Urology*. 2015;85:1224-8.
19. Mai Z, Yan W, Zhou Y, Zhou Z, Chen J, Xiao Y, et al. Transperineal template-guided prostate biopsy: 10 years of experience. *BJU international*. 2014.
20. Iremashvili V, Pelaez L, Jorda M, Manoharan M, Arianayagam M, Rosenberg DL, et al. Prostate sampling by 12-core biopsy: comparison of the biopsy results with tumor location in prostatectomy specimens. *Urology*. 2012;79:37-42.
21. Tan N, Margolis DJ, Lu DY, King KG, Huang J, Reiter RE, et al. Characteristics of Detected and Missed Prostate Cancer Foci on 3-T Multiparametric MRI Using an Endorectal Coil Correlated With Whole-Mount Thin-Section Histopathology. *AJR American journal of roentgenology*. 2015;205:87-92.
22. Zhu X, Albertsen PC, Andriole GL, Roobol MJ, Schroder FH, Vickers AJ. Risk-based prostate cancer screening. *European urology*. 2012;61:652-61.
23. Salami SS, Ben-Levi E, Yaskiv O, Ryniker L, Turkbey B, Kavoussi LR, et al. In patients with a previous negative prostate biopsy and a suspicious lesion on magnetic resonance imaging, is a 12-core biopsy still necessary in addition to a targeted biopsy? *BJU international*. 2015;115:562-70.
24. Moussa AS, Meshref A, Schoenfield L, Masoud A, Abdel-Rahman S, Li J, et al. Importance of additional "extreme" anterior apical needle biopsies in the initial detection of prostate cancer. *Urology*. 2010;75:1034-9.
25. Schoots IG, Roobol MJ, Nieboer D, Bangma CH, Steyerberg EW, Hunink MG. Magnetic resonance imaging-targeted biopsy may enhance the diagnostic accuracy of significant prostate cancer detection compared to standard transrectal ultrasound-guided biopsy: a systematic review and meta-analysis. *European urology*. 2015;68:438-50.
26. Bjurlin MA, Mendhiratta N, Wysock JS, Taneja SS. Multiparametric MRI and targeted prostate biopsy: Improvements in cancer detection, localization, and risk assessment. *Central European journal of urology*. 2016;69:9-18.
27. Hamoen EH, de Rooij M, Witjes JA, Barentsz JO, Rovers MM. Use of the Prostate Imaging Reporting and Data System (PI-RADS) for Prostate Cancer Detection with Multiparametric Magnetic Resonance Imaging: A Diagnostic Meta-analysis. *European urology*. 2015;67:1112-21.
28. Ploussard G, Epstein JI, Montironi R, Carroll PR, Wirth M, Grimm MO, et al. The contemporary concept of significant versus insignificant prostate cancer. *European urology*. 2011;60:291-303.

CHAPTER 5.0 DIFFERENTIATION OF PROSTATITIS AND PROSTATE CANCER BY USING DIFFUSION- WEIGHTED MR IMAGING AND MR-GUIDED BIOPSY AT 3T

*Klaas N.A. Nagel, Martijn G. Schouten, Thomas Hambroek,
Geert J.S. Litjens, Caroline M.A. Hoeks, Bennie ten Haken,
Jelle O. Barentsz, Jurgen J. Fütterer*

Radiology 2013 Apr;267(1):164-72

Abstract

Purpose: To determine if prostatitis and prostate cancer can be distinguished by using apparent diffusion coefficients (ADCs) on magnetic resonance (MR) images, with specimens obtained at MR-guided biopsy as the standard of reference.

Materials and Methods: The need for institutional review board approval and informed consent was waived. MR-guided biopsies were performed in 130 consecutive patients with cancer-suspicious regions (CSLs) on multi-parametric MR images obtained at 3T. In this retrospective study, 88 patients met the inclusion criteria. During the biopsy procedure, an axial diffusion-weighted sequence was performed and ADC maps were generated (repetition time ms/echo time ms, 2000/67; section thickness, 4 mm; in-plane resolution, 1.8 x 1.8 mm; and b-values of 0, 100, 500, and 800 s/mm²). Subsequently, a confirmation image with the needle left in situ was acquired and projected on the ADC map. The corresponding ADCs at the biopsy location were compared with the histopathologic outcomes of the biopsy specimens. Linear mixed-model regression analyses were used to test for ADC differences between the histopathologic groups.

Results: The study included 116 biopsy specimens. Median ADCs of normal prostate tissue, prostatitis, low-grade prostate cancer (Gleason grade components 2 or 3), and high-grade prostate cancer (Gleason grade components 4 or 5) were 1.22 x 10⁻³ mm²/s (standard deviation, ± 0.21), 1.08 x 10⁻³ mm²/s (± 0.18), 0.88 x 10⁻³ mm²/s (± 0.15), and 0.88 x 10⁻³ mm²/s (± 0.13), respectively. Although the median ADCs of biopsy specimens with prostatitis were significantly higher compared with low- and high-grade prostate cancer (P < 0.001), there is a considerable overlap between the tissue types.

Conclusion: Diffusion-weighted imaging is a non invasive technique that shows differences between prostatitis and prostate cancer in both the peripheral zone and central gland, although its usability in clinical practice is limited as a result of significant overlap in ADC values.

Introduction

Urologists often face the dilemma of treating a patient in whom there is a high suspicion for prostate cancer based on an elevated prostate-specific antigen (PSA) level (1-3). Benign prostatic hyperplasia can also lead to elevated PSA levels and is not always associated with clinical symptoms. Therefore, differentiation between prostate cancer and benign prostatic hyperplasia in the central gland (CG) is a major challenge for the urologist and also for the radiologist. Prostatitis is normally a diffuse disease, whereas benign prostatic hyperplasia and tumour normally present as focal disease. Prostatitis can be a cause of an elevated PSA level; however, this is clinically a difficult diagnosis. As a consequence, prostatitis patients will undergo transrectal ultrasonography (TRUS)-guided biopsy sessions. Moreover, prostate cancer can still be present in patients with biopsy-proved prostatitis. This illustrates the need for a non-invasive diagnostic test that can be used to differentiate between prostate cancer and prostatitis (4).

Magnetic resonance (MR) imaging of the prostate is the imaging modality of choice in prostate cancer detection, localization, and staging (5-8). The diagnostic value of anatomic T2-weighted MR imaging in discriminating prostate cancer from benign prostate tissue is limited. The interpretation of these images can be affected by false-positive findings such as prostatitis, post biopsy haemorrhage, and fibrosis (9-11). To improve the diagnostic accuracy of prostate MR imaging, functional imaging techniques have been applied, such as dynamic contrast-enhanced MR imaging (12-14), proton MR spectroscopic imaging (15-17), and diffusion-weighted (DW) MR imaging (18-21), with limited success to date.

DW imaging has been shown to aid in distinguishing between malignant and benign prostate tissue based on relatively lower apparent diffusion coefficients (ADCs) of cancer tissue (22-35). The correlation between the ADC and tissue is usually done by using TRUS-guided biopsy and step-section specimens after prostatectomy as a standard of reference (31-35). Even using improved correlation methods (35) there is still an uncertainty whether the correct tissue is sampled and correlated with imaging.

MR-guided biopsy may overcome the latter limitations. A confirmation MR image can be acquired with the needle left in situ. This allows for an accurate verification of the biopsy location in the cancer suspicious lesion (CSL) and correlation with the ADC map. Therefore, the purpose of our study was to determine if prostatitis and prostate cancer can be distinguished by using ADCs on MR images, with specimens obtained at MR-guided biopsy as the standard of reference.

Materials and methods

Patients

Institutional review board approval was not required, and the need for informed consent was waived.

Between October 2008 and March 2010, 130 consecutive patients underwent MR-guided prostate biopsy of CSLs seen on previous diagnostic 3T MR prostate images and were eligible for inclusion in this retrospective study. MR-guided biopsy was performed in male patients with (a) an elevated PSA level (>4 ng/mL), (b) family history of prostate cancer, (c) suspicion for prostate cancer based on diagnostic MR examination of the pelvis, and (d) at least one negative TRUS-guided biopsy. Inclusion criterion for this study was that a DW sequence was performed at both the diagnostic MR examination and the MR-guided biopsy examination (Fig. 1). Exclusion criteria for this study were patients with suspicion of recurrent prostate cancer after therapy (prostatectomy, radiation therapy, chemotherapy, cryosurgery, or high-intensity focused ultrasound therapy), and biopsy specimens that could not be categorized within the following histopathologic groups: normal prostate tissue, prostatitis, low-grade prostate cancer (Gleason grade components 2 or 3) and high-grade prostate cancer (Gleason grade components 4 or 5). Eighty-eight patients met the inclusion criteria and were included for further analysis.

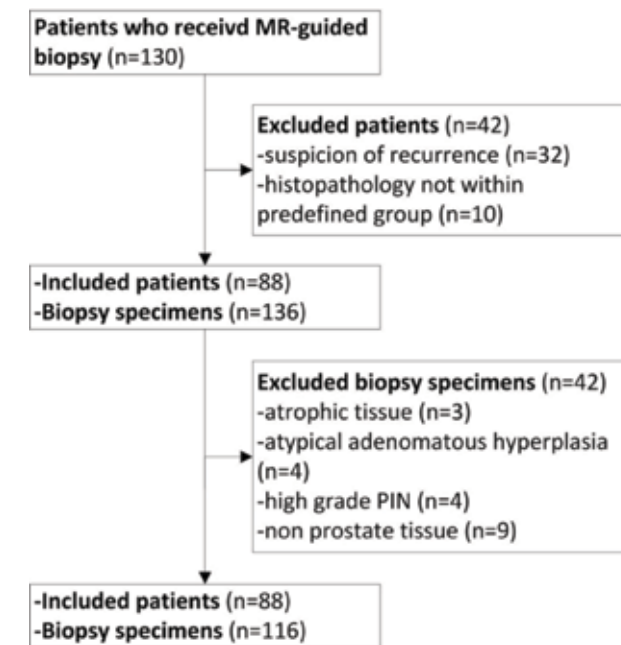


Figure 1: Study flow diagram.

Diagnostic MR imaging

Before the biopsy procedure, a diagnostic MR examination was performed with a 3T MR imager (Trio Tim; Siemens, Erlangen, Germany). This multi-parametric detection and localization examination consisted of T2-weighted imaging, DW imaging, and dynamic contrast-enhanced MR imaging (36). Peristalsis was suppressed with an intramuscular administration of 20 mg butylscopolaminebromide (Buscopan; Boehringer-Ingelheim, Ingelheim, Germany) and 1 mg of glucagon (Glucagen; Nordisk, Gentofte, Denmark).

The imaging protocol included the following sequences (Table 1): First, a T2-weighted turbo spin-echo sequence was performed in three planes. Second, a single-shot echo-planar imaging sequence with diffusion modules and fat suppression pulses was performed. The imager software automatically calculated ADC maps. Third, three-dimensional T1-weighted spoiled gradient-echo images were acquired during an intravenous bolus injection of a paramagnetic gadolinium chelate, 0.1 mmol of gadopentetate dimeglumine (Dotarem; Guerbet, Paris, France) per kilogram of body weight, which was administered with a power injector (Spectris Medrad, Warrendale) at 2.5 mL/s and followed by a 15 mL saline flush. With this sequence, a three-dimensional volume covering the entire prostate was acquired every 2.5 s during 210 s, with the same positioning angle and centre as the transverse T2-weighted sequence. Before contrast material injection, the same transverse three-dimensional T1-weighted gradient-echo sequence (with the exception of repetition time ms/echo time ms, 800/1.6, and flip angle of 8°) was used to obtain proton-density images, with identical positioning to allow calculation of the relative gadolinium chelate concentration curves.

Diagnostic MR image interpretation

The diagnostic MR images were analyzed with an in-house developed analytical software workstation that calculated the dynamic contrast-enhanced MR imaging parameters and projected these parameters as colour overlay maps over the T2-weighted images (37, 38). Images of all patients were read by two radiologists in consensus with 15 years (J.O.B.) and 7 years (J.J.F.) of experience in prostate MR imaging. The high-spatial-resolution, axial T2-weighted images were used as basis for evaluation of the prostate, and all other functional imaging modalities were interpreted in relation to these. On T2-weighted images, the generally known prostate cancer detection criteria were used to determine CSLs. These included low-signal-intensity areas in the peripheral zone (PZ) and/or a homogeneous low T2 signal intensity area with ill-defined margins or a lenticular shape within the CG (39). After identification of CSLs on T2-weighted images, the ADC maps and multi-parametric dynamic contrast-enhanced MR imaging colour maps transfer constant (K^{trans}), extravascular extracellular volume (v_e), rate constant (K_{ep}), and washout were analyzed in a colour overlay mode on the T2-weighted images. The generally known features of prostate cancer on dynamic contrast-enhanced MR images (13, 40) (high v_e , K^{trans} , K_{ep} , and negative washout) and areas of restriction on ADC maps (especially in the PZ and CG) were used to identify CSLs qualitatively (38). Additionally, after the functional data from

Imaging Protocol	Sequence	Repetitions time (ms)	Echo time (ms)	Flip angle (degree)	Voxel size (mm ³)	b-values (s/mm ²)	Temporal resolution (s)
Diagnostic MR imaging session							
T2WI	Axial turbo spin-echo	3620	116	180	0.4 x 0.4 x 3.0	NA	NA
DW	Single-shot echo-planar with diffusion modules and fat suppression pulses	2500	91		1.5 x 1.5 x 3.0	0, 50, 500, and 800	NA
DCE	3D T1-weighted spoiled gradient echo	34	1.6	14	1.5 x 1.5 x 4.0	NA	2.5
Proton density	3D T1-weighted spoiled gradient echo	800	1.6	8	1.5 x 1.5 x 4.0	NA	NA
MR-guided biopsy session							
True FISP	True FISP	4.48	2.24	70	1.1 x 1.1 x 3.0	NA	NA
DW	Single-shot echo-planar with diffusion modules and fat suppression pulses	2000	67		1.8 x 1.8 x 4.0	0, 100, 500, and 800	NA
T2WI	Axial turbo spin-echo	3620	104	120	0.8 x 0.8 x 4.0	NA	NA

Table 1: Imaging parameters. DCE = dynamic contrast enhanced, NA = not applicable, 3D = three dimensional, T2-weighted MR imaging

DW and dynamic contrast-enhanced MR imaging were evaluated in relation to the CSL findings on the T2-weighted images, the DW and dynamic contrast-enhanced MR images were viewed separately and in combination to determine additional CSLs not evident on T2-weighted images. Finally, the information from all the imaging modalities were combined and used to determine the CSLs within the PZ and CG of the prostate (38).

MR-guided biopsy protocol

In a second session, prostate biopsies were performed in the same MR imager with a dedicated MR-compatible biopsy device (Invivo, Schwerin, Germany) (38, 41-43). As previously described, the patient was placed in a prone position and the rectally inserted needle sleeve was attached to the arm of the MR-compatible biopsy device. A pelvic phased-array coil was used for signal reception (36, 38). Identification of the CSL, determined during the initial MR examination, was achieved by using the following MR sequences (Table 1): First, an axial T2-weighted turbo spin-echo sequence was performed. Second, an axial DW

sequence was performed with a single-shot echo-planar imaging sequence with diffusion modules and fat suppression pulses. Water diffusion in three directions was measured by using four b-values. Finally, the imager software calculated ADC maps automatically (Fig. 2).

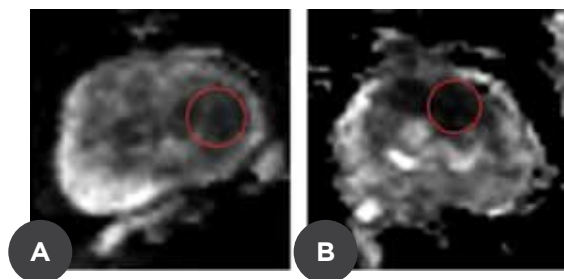


Figure 2: ADC maps calculated from a single-shot echo-planar DW image in three orthogonal diffusion gradients (2000/67; b = 0, 100, 500, and 800 s/mm²) in the axial plane in two men with a CSL in the CG. (A) Image in a 72-year-old man (PSA = 22.1 ng/mL) shows a CSL (red circle) with a median ADC of 0.97×10^{-3} mm²/s. Histopathologic examination of the corresponding biopsy specimens revealed prostatitis. (B) Image in a 65-year-old man (PSA = 30.0 ng/mL) shows a suspicious region (red circle) with a median ADC of 0.83×10^{-3} mm²/s. Histopathologic examination of this biopsy specimen revealed low-grade prostate cancer (Gleason grade 3 + 3).

After identification of the CSLs, adjustments were applied to the biopsy device to move the needle sleeve exactly toward a CSL (41, 42). To control needle sleeve direction, T2-weighted true fast imaging with steady precession (FISP) images were acquired in the axial and sagittal direction. Biopsy was performed in all determined CSLs on the diagnostic MR images, even if they were not visible on the T2-weighted anatomic MR images obtained at the time of biopsy. In these cases, the DW MR images were used to move the needle sleeve toward the CSL. After fixation of the needle sleeve in the correct position, one or more tissue samples were taken at the region with lowest ADCs in each CSL with an 18-gauge, fully automatic, core needle, double-shot biopsy gun (Invivo) with a needle length of 150 or 175 mm and tissue sampling core length of 17 mm. After obtaining a biopsy specimen, fast T2-weighted axial and sagittal true-FISP images were obtained with the needle left in situ.

MR image correlation

During the biopsy session, at least one biopsy specimen was obtained from each CSL. The biopsy specimen that was located in the most diffusion-restricted area of each CSL was selected for image analysis. This was performed by using the true-FISP confirmation image and the corresponding ADC map obtained during the biopsy session. Some patients had multiple CSLs. The CSLs of all patients were analyzed without knowledge of the histopathologic outcomes. MR images of the biopsy specimens were analyzed with an in-house developed analytical software workstation (37). The calculated ADC maps were projected on the post

biopsy T2-weighted true-FISP images (confirmation image with the needle left in situ) to determine the biopsy location. By using this location, a region of interest was drawn manually with the size and extent of the most diffusion-restricted region on the ADC map, representing the biopsied CSL (Fig. 3). In case of the absence of restricted diffusion on the ADC maps, a low-signal-intensity area on T2-weighted images was used to draw the region of interest. All regions of interest were annotated in consensus by two radiologists (T.H., J.J.F.). Of each region of interest, the median and standard deviation of the ADC values were calculated (median size, 51; range 8-335 voxels). Multiple regions of interest were obtained in case a patient had multiple CSLs.

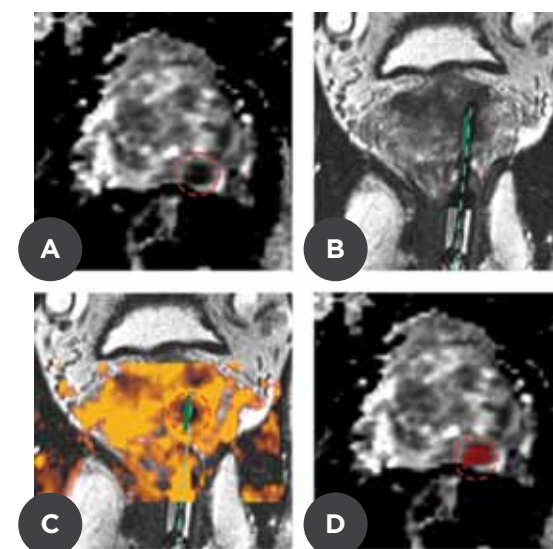


Figure 3: Images obtained in a 66-year-old man (PSA = 21.6 ng/mL) with a CSL in the PZ. Biopsy revealed a Gleason grade 3 + 3 prostate cancer. (A) The CSL (red circle) at pre biopsy MR imaging is visible on the ADC map, calculated from an axial single-shot echo-planar DW image by using three orthogonal diffusion gradients (2000/67; b = 0, 100, 500, and 800 s/mm²). (B) Control T2-weighted true-FISP image (4.48/2.24) obtained during biopsy in axial and sagittal plane shows the position of the biopsy needle (dashed blue line) with a sampling core length of 17 mm (green line). (C) After projection of the ADC map on the true-FISP image, (D) a region of interest was drawn manually with the size and extent of the restricted diffusion region on the ADC map.

Histopathologic evaluation

Biopsy specimens were processed by means of a routine fixation in formaldehyde, embedded in paraffin, and stained with hematoxylin-eosin before being evaluated by a pathologist for the presence of prostate cancer or other benign pathologic lesions. Biopsy specimens with prostate cancer were graded according to the 2005 ISUP Modified Gleason Grading System (44).

Statistical Analysis

A Mann-Whitney U test was performed to determine how ADC operates as a discriminatory test between prostatitis and CSLs. We have studied data summaries by region in addition to histopathologic grouping. The analyses were conducted by using linear mixed-effects regression models without autoregressive time-component, because in some patient multiple regions of interest were drawn. The significance level was set at a P value of less than 0.05. All analyses were performed with statistical software (SPSS, version 18.0.0; SPSS, Chicago, Ill).

Results

In our study, 88 of the 130 consecutive patients with CSLs on diagnostic MR images met the inclusion criteria and were included in our study (Table 2).

Reason for exclusion	Number excluded
Excluded patients	42
Prostate treatment (prostatectomy, radiation therapy, chemotherapy, cryosurgery, or HIFU therapy)	32
Deviating biopsy specimens	10
Atrophic tissue	4
Atypical adenomatous	1
High-grade PIN	3
Nonprostate tissue	2
Excluded biopsy specimens of included patients	20
Atrophic tissue	3
Atypical adenomatous hyperplasia	4
High-grade PIN	4
Nonprostate tissue	9

Table 2: Biopsy findings excluded from analysis. Data are numbers of patients excluded or numbers of biopsy specimens excluded (among included patients). HIFU = high-intensity focused ultrasound, PIN = prostate intraepithelial neoplasia.

These patients had one (n=62), two (n=24) or three CSLs (n=2). A total of 136 MR-guided prostate biopsy specimens were obtained. Twenty biopsy specimens could not be categorized within the defined histopathologic groups (Table 2) and were excluded from further analysis. Consequently, 116 biopsy specimens were included and divided in four histopathologic classified groups: normal prostate tissue (32), prostatitis (42), low-grade prostate cancer (25), and high-grade prostate cancer (17). The 42 cancer-positive biopsy specimens were obtained from 39 patients. Patient and biopsy characteristics of these groups are shown in Table 3. In six cases, the determined CSLs on the initial diagnostic MR images

Characteristic	All patients	Normal tissue	Prostatitis	Low-grade PCa	High-grade PCa	Excluded tissue
No. of included patients	88					
No. of included biopsy specimens	116	32	42	25	17	
No. of excluded biopsy specimens	20					20
Median no. of previous negative TRUS-guided biopsy sessions	2 (0-6)	2 (0-6)	2 (1-5)	2 (0-5)	3 (1-4)	
Mean age (y)	63 (44-76)	62 (52-76)	63 (50-73)	63 (44-72)	67 (56-73)	
Median PSA (ng/mL)	11.0 (0.1-58.0)	11.1 (0.8-36.0)	10.9 (0.1-30.2)	10.0 (1.2-51.0)	15.0 (18.0-51.0)	
Median prostate volume (mL)	49 (18-263)	79 (20-108)	55 (30-263)	40 (18-107)	42 (25-98)	
Median time between MR-guided biopsy and initial diagnostic MR examination (wk)	8.9 (0.0-31.7)	8.7 (2.3-21.0)	8.7 (0.0-31.7)	10.0 (2.1-31.4)	8.3 (3.1-16.4)	

Location of CSLs

PZ	69	23	27	14	5
CG	47	9	15	11	12

No. of excluded biopsy specimens among the included patients

Atrophic tissue					3
Atypical adenomatous hyperplasia					4
High-grade PIN					4
Nonprostate tissue					9

Low-grade PCa Gleason score

2+3				2	
3+2				1	
3+3				22	

High-grade PCa Gleason score

3+4					12
3+5					1
4+3					3
4+5					1

Table 3: Patient and biopsy characteristics. Data are numbers of patients or biopsy specimens, and numbers in parentheses are the range. PIN = prostate intraepithelial neoplasia, PCa = prostate cancer

were not visible on the MR images obtained at biopsy (hereafter, the “biopsy MR images”). Although not visible, the suspected area was biopsied. Furthermore, no new CSLs were seen on the biopsy MR images. Therefore, the numbers of CSLs on the diagnostic and biopsy MR images were equal. During the image analysis, 12 CSLs showed a low-signal-intensity area on T2-weighted images and no restricted diffusion on the ADC maps, and 15 CSLs had an area of restricted diffusion without abnormality on the T2-weighted images. Discrepancies between the CSLs on the diagnostic MR images and the corresponding CSLs on the biopsy MR images were found in 5% (six of 116) of the biopsy specimens. Biopsy specimens with normal prostate tissue, prostatitis, low-grade prostate cancer, and high-grade prostate cancer had a mean ADC of $1.22 \times 10^{-3} \text{ mm}^2/\text{s} \pm 0.21$ (standard deviation), $1.08 \times 10^{-3} \text{ mm}^2/\text{s} \pm 0.18$, $0.88 \times 10^{-3} \text{ mm}^2/\text{s} \pm 0.15$, and $0.88 \times 10^{-3} \text{ mm}^2/\text{s} \pm 0.13$, respectively (Fig. 4, Table 4). The linear mixed-model analyses revealed significant differences between mean ADCs of the groups with normal prostate tissue and prostatitis ($P = 0.002$), the groups with prostatitis and low-grade prostate cancer ($P < 0.001$), and the groups with prostatitis and high-grade prostate cancer ($P < 0.001$). The difference between the mean ADCs of the groups with low-grade and high-grade prostate cancer was not significant ($P = 0.76$).

Also, differences in mean ADCs between the three classified groups were analyzed for the PZ and CG. A total of 69 and 47 biopsy specimens were obtained from the PZ and CG, respectively. Median ADCs of the classified groups and regions are shown in Table 4. The linear mixed-model analyses showed a significant difference between the mean ADCs of the biopsy specimens with normal prostate tissue and prostatitis in the PZ ($P = 0.012$). This statistical analysis was not performed for the CG, because the number of biopsy specimens with normal prostate tissue in the CG was too low ($n=9$). In both PZ and CG, however, significant differences in mean ADCs were found between the groups with prostatitis and low-grade prostate cancer (PZ: $P = 0.01$, CG: $P < 0.001$). Furthermore, a significant difference was revealed between the groups with prostatitis and high-grade prostate cancer in the PZ ($P = 0.016$). The difference between the mean ADCs of the groups with low-grade prostate cancer and high-grade prostate cancer in PZ was not significant ($P = 0.84$). Again, the numbers in the group with high-grade prostate cancer in the CG was too low ($n=5$) to use for statistical analyses.

Discussion

In our study cohort, we found differences between mean ADCs of biopsy specimens with prostatitis and low- and high-grade prostate cancer ($P < 0.001$), even though there was a high degree of overlap. It is questionable whether differences in mean ADCs of $0.14 \times 10^{-3} \text{ mm}^2/\text{s}$ between the groups with prostate cancer and prostatitis, although statistically significant, are also clinically useful. The overlap of ADCs between these two histopathologic groups hinders a reliable differentiation between prostatitis and prostate cancer in routine clinical practice. Nevertheless, a CSL with a mean ADC of less than $0.75 \times 10^{-3} \text{ mm}^2/\text{s}$ appears suspicious for prostate

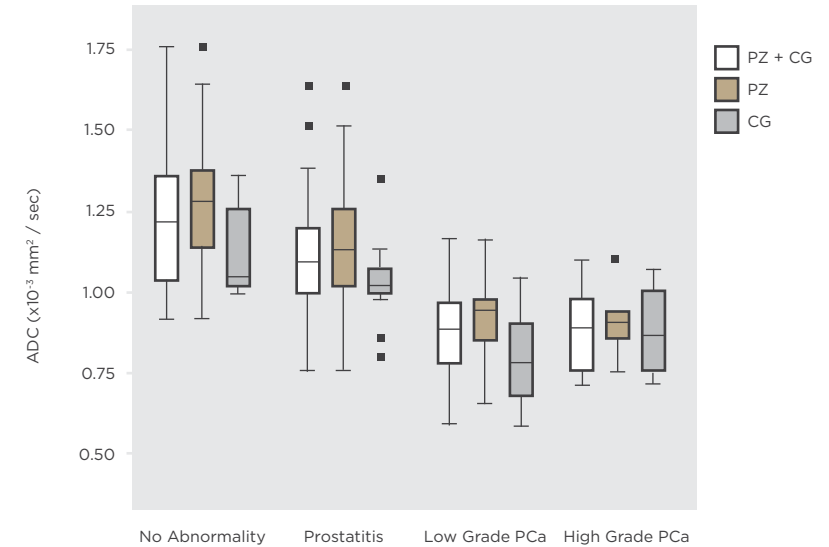


Figure 4: Box-and-whisker plots for the DW imaging of the suspicious areas according to histologic diagnosis of normal prostate, prostatitis, and low- and high-grade prostate cancer in the PZ, CG, and combined PZ and CG. Centre horizontal line = median, bottom and top edges of box = 25th and 75th percentiles, vertical line = range of data. PZ = peripheral zone, CG = central gland

Group	PZ		CG	
	Mean ADC \pm standard deviation ¹	No. of specimens	Mean ADC \pm standard deviation ¹	No. of specimens
Normal tissue	1.28 ± 0.22^2	23	1.03 ± 0.15^3	9
Prostatitis	1.13 ± 0.20	27	1.02 ± 0.13	15
Low-grade PCa	0.94 ± 0.13^2	14	0.78 ± 0.15^2	11
High-grade PCa	0.90 ± 0.13^3	5	0.86 ± 0.13^2	12

Table 4: Mean ADCs of the histopathologic groups

¹ unit of measure is $10^{-3} \text{ mm}^2/\text{s}$.

² Mean in this histopathologic group is significantly different from that of the reference group, prostatitis ($P < 0.05$).

³ Number of biopsy specimens of this group is too low for reliable statistical analysis.

PCa = prostate cancer, PZ = peripheral zone, CG = central gland, ADC = apparent diffusion coefficient.

cancer (Fig. 4) and a biopsy procedure might be recommended. Future studies will be needed that focus on the combined approach of functional imaging techniques to reduce the diagnostic overlap between prostatitis and prostate cancer.

In recent years, several studies have demonstrated significant differences between the ADCs of malignant and benign prostate tissue by using TRUS-guided biopsy (22-27) or step-section specimens after prostatectomy as reference standard (31-34). In these previously described studies, mean ADCs for malignant and benign prostate tissue varied over a relatively broad range from $0.93 \times 10^{-3} \text{ mm}^2/\text{s}$ to $1.38 \times 10^{-3} \text{ mm}^2/\text{s}$ and from $1.34 \times 10^{-3} \text{ mm}^2/\text{s}$ to $1.96 \times 10^{-3} \text{ mm}^2/\text{s}$, respectively. However, in our study, mean ADCs were lower for both malignant (range, 0.78 to $0.90 \times 10^{-3} \text{ mm}^2/\text{s}$) and benign (range, 0.99 to $1.13 \times 10^{-3} \text{ mm}^2/\text{s}$) biopsy specimens. This may be explained by the fact that the biopsy specimens with normal prostate tissue were CSLs based on multi-parametric MR imaging. The regions of interest of the previously described studies were annotated without abnormalities on multi-parametric MR images. This could have resulted in relatively higher ADCs compared with our study.

The prostate cancer detection rate of our study (44%) is lower compared with previous reports (52%-59%) (41, 43, 45). This could be explained by inclusion of one patient with a low PSA level (0.1 ng/mL) and patients with a positive family history of prostate cancer.

A limited number of studies have assessed the histopathologic findings of CSLs on ADC maps with step-section specimens after prostatectomy (31-34). It is difficult to correlate the ADC maps with the corresponding histologic slices, since deformation and shrinkage of the prostate may occur after prostatectomy. Furthermore, all these studies have annotated the CSLs on ADC maps according to step-section specimens of the prostate.

In our study, the time interval between the initial diagnostic MR examination and the biopsy session ranged from 0 to 32 weeks. Discrepancies between the CSLs on the diagnostic MR images and the corresponding CSLs on the biopsy MR images were found in 5% (six of 116) of the biopsy specimens. However, all determined CSLs on the diagnostic MR images underwent biopsy, even if they were not visible on the biopsy MR images. The image analyses were not negatively affected by large time intervals, because the biopsy MR images were used to determine the ADCs of the CSLs, instead of the diagnostic MR images. These biopsy MR images were obtained on the same day of the biopsy session. Therefore, growth or shrinkage of the CSL was minimized.

Our study had a number of limitations. First, during manipulation of the needle sleeve, the prostate may have moved (i.e. due to patient motion, peristaltic movement, and/or bladder filling). It is therefore imaginable that the ADC map, obtained before the needle sleeve manipulation, does not exactly match with the confirmation image on which the needle is left in situ. During the image analyses, these movements were corrected manually by using anatomic landmarks such as cysts, calcifications, and femoral head and pelvic bones around the prostate. Advanced registration software using anatomic landmarks may help to overcome these discrepancies (46).

Second, the spatial resolution of DW imaging was limited (1.8 x 1.8 mm). This may result in missing CSLs with a diameter smaller than approximately 4-5 mm. Conversely, the diameter of an 18-gauge biopsy needle, and the corresponding biopsy specimen, was approximately 1.0 mm. However, this titanium needle causes image artefacts on post biopsy true-FISP images with a diameter of approximately 6 mm. Even if the spatial resolution of DW imaging can be improved in future, the accuracy of the determination of the position of the biopsy needle will likely remain limited due to these needle artefacts. In the future these may be overcome by using novel material for needle manufacture.

In biopsy specimens obtained in patients with prostate cancer, the entire specimen may not contain prostate cancer. In our study, we did not include tumour biopsy volumetry. Because the histopathologic reports did not describe the localization of the cancerous components in the biopsy specimen, we have disregarded the volume percentage. However, this limitation could have influenced the accuracy of the measurements. The change in the diagnostic MR imaging protocol during the study period and the differences between the diagnostic and biopsy protocol may have influenced lesion detection.

In conclusion, DW imaging is a non invasive technique that demonstrates a difference in mean ADC between prostatitis and prostate cancer by using MR-guided biopsy specimens as standard of reference, although its usability in clinical practice is limited due to a high degree of overlap.

References

1. Hochreiter WW. The issue of prostate cancer evaluation in men with elevated prostate-specific antigen and chronic prostatitis. *Andrologia* 2008;40(2):130-133.
2. Battikhi MN, Hussein I. Age-specific reference ranges for prostate specific antigen total and free in patients with prostatitis symptoms and patients at risk. *Int Urol Nephrol* 2006;38(3-4):559-564.
3. Ozden C, Ozdal OL, Guzel O, et al. The correlation between serum prostate specific antigen levels and asymptomatic inflammatory prostatitis. *Int Urol Nephrol* 2007;39(3):859-863.
4. Collins MM, Stafford RS, O'Leary MP, et al. How common is prostatitis? A national survey of physician visits. *J Urol* 1998; 159(4):1224-1228.
5. Yu KK, Hricak H. Imaging prostate cancer. *Radiol Clin North Am* 2000;38(1):59-85.
6. Fütterer JJ. MR imaging in local staging of prostate cancer. *Eur J Radiol* 2007; 63(3):328-334.
7. Engelbrecht MR, Jager GJ, Laheij RJ, et al. Local staging of prostate cancer using magnetic resonance imaging: a meta-analysis. *Eur Radiol* 2002;12(9):2294-2302.
8. Scheidler J, Hricak H, Vigneron DB, et al. Prostate cancer: localization with threedimensional proton MR spectroscopic imaging- clinicopathologic study. *Radiology* 1999;213(2):473-480.
9. Quint LE, Van Erp JS, Bland PH, et al. Prostate cancer: correlation of MR images with tissue optical density at pathologic examination. *Radiology* 1991;179(3):837-842.
10. Lovett K, Rifkin MD, McCue PA, et al. MR imaging characteristics of noncancerous lesions of the prostate. *J Magn Reson Imaging* 1992;2(1):35-39.
11. Schiebler ML, Tomaszewski JE, Bezzi M, et al. Prostatic carcinoma and benign prostatic hyperplasia: correlation of high-resolution MR and histopathologic findings. *Radiology* 1989;172(1):131-137.
12. Kim CK, Park BK, Kim B. Localization of prostate cancer using 3T MRI: comparison of T2-weighted and dynamic contrast-enhanced imaging. *J Comput Assist Tomogr* 2006;30(1):7-11.
13. Engelbrecht MR, Huisman HJ, Laheij RJ, et al. Discrimination of prostate cancer from normal peripheral zone and central gland tissue by using dynamic contrast-enhanced MR imaging. *Radiology* 2003;229(1): 248-254.
14. Yakar D, Hambrock T, Huisman H, et al. Feasibility of 3T dynamic contrast-enhanced magnetic resonance-guided biopsy in localizing local recurrence of prostate cancer after external beam radiation therapy. *Invest Radiol* 2010;45(3):121-125.
15. Heijmink SW, Scheenen TW, Fütterer JJ, et al. Prostate and lymph node proton magnetic resonance (MR) spectroscopic imaging with external array coils at 3 T to detect recurrent prostate cancer after radiation therapy. *Invest Radiol* 2007;42(6):420-427.
16. Wang L, Hricak H, Kattan MW, et al. Prediction of organ-confined prostate cancer: incremental value of MR imaging and MR spectroscopic imaging to staging nomograms. *Radiology* 2006;238(2):597-603.
17. Kurhanewicz J, Vigneron DB, Hricak H, et al. Threedimensional H-1 MR spectroscopic imaging of the in situ human prostate with high (0.24-0.7-cm³) spatial resolution. *Radiology* 1996;198(3):795-805.
18. Gibbs P, Tozer DJ, Liney GP, et al. Comparison of quantitative T2 mapping and diffusion-weighted imaging in the normal and pathologic prostate. *Magn Reson Med* 2001;46(6):1054-1058.
19. Issa B. In vivo measurement of the apparent diffusion coefficient in normal and malignant prostatic tissues using echo-planar imaging. *J Magn Reson Imaging* 2002;16(2):196-200.
20. Chan I, Wells W 3rd, Mulkern RV, et al. Detection of prostate cancer by integration of line-scan diffusion, T2-mapping and T2-weighted magnetic resonance imaging; a multichannel statistical classifier. *Med Phys* 2003;30(9):2390-2398.
21. Miao H, Fukatsu H, Ishigaki T. Prostate cancer detection with 3-T MRI: comparison of diffusion-weighted and T2-weighted imaging. *Eur J Radiol* 2007;61(2):297-302.
22. Pickles MD, Gibbs P, Sreenivas M, et al. Diffusion-weighted imaging of normal and malignant prostate tissue at 3.0T. *J Magn Reson Imaging* 2006;23(2): 130-134.
23. Tanimoto A, Nakashima J, Kohno H, et al. Prostate cancer screening: the clinical value of diffusion weighted imaging and dynamic MR imaging in combination with T2-weighted imaging. *J Magn Reson Imaging* 2007;25(1): 146-152.
24. Shimofusa R, Fujimoto H, Akamata H, et al. Diffusion-weighted imaging of prostate cancer. *J Comput Assist Tomogr* 2005;29(2): 149-153.
25. Hosseinzadeh K, Schwarz SD. Endorectal diffusion-weighted imaging in prostate cancer to differentiate malignant and benign peripheral zone tissue. *J Magn Reson Imaging* 2004;20(4):654-661.
26. Sato C, Naganawa S, Nakamura T, et al. Differentiation of noncancerous tissue and cancer lesions by apparent diffusion coefficient values in transition and peripheral zones of the prostate. *J Magn Reson Imaging* 2005;21(3):258-262.
27. Tamada T, Sone T, Jo Y, et al. Apparent diffusion coefficient values in peripheral and transition zones of the prostate: comparison between normal and malignant prostatic tissues and correlation with histologic grade. *J Magn Reson Imaging* 2008;28(3): 720-726.
28. Stewart CS, Leibovich BC, Weaver AL, et al. Prostate cancer diagnosis using a saturation needle biopsy technique after previous negative sextant biopsies. *J Urol* 2001;166(1):86-91;
29. Salomon L, Colombel M, Patard JJ, et al. Value of ultrasound-guided systematic sextant biopsies in prostate tumor mapping. *Eur Urol* 1999;35(4):289-293.
30. Amsellem-Ouazana D, Younes P, Conquy S, et al. Negative prostatic biopsies in patients with a high risk of prostate cancer. Is the combination of endorectal MRI and magnetic resonance spectroscopy imaging (MRSI) a useful tool? A preliminary study. *Eur Urol* 2005;47(5):582-586.
31. Yoshimitsu K, Kiyoshima K, Irie H, et al. Usefulness of apparent diffusion coefficient map in diagnosing prostate carcinoma: correlation with stepwise histopathology. *J Magn Reson Imaging* 2008;27(1): 132-139.
32. Kim CK, Park BK, Lee HM, et al. Value of diffusion-weighted imaging for the prediction of prostate cancer location at 3T using a phased-array coil: preliminary results. *Invest Radiol* 2007;42(12): 842-847.
33. Van As N, Charles-Edwards E, Jackson A, et al. Correlation of diffusion-weighted MRI with whole mount radical prostatectomy specimens. *Br J Radiol* 2008;81(966): 456-462.
34. Hambrock T, Somford DM, Huisman HJ, et al. Relationship between apparent diffusion coefficients at 3.0-T MR imaging and Gleason grade in peripheral zone prostate cancer. *Radiology* 2011;259(2):453-461.
35. Drew B, Jones EC, Reinsberg S, et al. Device for sectioning prostatectomy specimens to facilitate comparison between histology and in vivo MRI. *J Magn Reson Imaging* 2010; 32(4):992-996.
36. Yakar D, Hambrock T, Hoeks C, et al. Magnetic resonance-guided biopsy of the prostate: feasibility, technique, and clinical applications. *Top Magn Reson Imaging* 2008;19(6):291-295.
37. Vos PC, Hambrock T, Hulsbergen-van de Kaa CA, et al. Computerized analysis of prostate lesions in the peripheral zone using dynamic contrast enhanced MRI. *Med Phys* 2008;35(3):888-899.
38. Hambrock T, Fütterer JJ, Huisman HJ, et al. Thirty-two-channel coil 3T magnetic resonance-guided biopsies of prostate tumor suspicious regions identified on multimodality 3T magnetic resonance imaging: technique and feasibility. *Invest Radiol* 2008; 43(10):686-694.
39. Akin O, Sala E, Moskowitz CS, et al. Transition zone prostate cancers: features, detection, localization, and staging at endorectal MR imaging. *Radiology* 2006;239(3):784-792.
40. Fütterer JJ, Heijmink SW, Scheenen TW, et al. Prostate cancer localization with dynamic contrast-enhanced MR imaging and proton MR spectroscopic imaging. *Radiology* 2006;241(2):449-458.

41. Anastasiadis AG, Lichy MP, Nagele U, et al. MRI-guided biopsy of the prostate increases diagnostic performance in men with elevated or increasing PSA levels after previous negative TRUS biopsies. *Eur Urol* 2006;50(4):738-748
42. Beyersdorff D, Winkel A, Hamm B, et al. MR imaging guided prostate biopsy with a closed MR unit at 1.5 T: initial results. *Radiology* 2005; 234(2):576-581.
43. Hambrock T, Somford DM, Hoeks C, et al. Magnetic resonance imaging guided prostate biopsy in men with repeat negative biopsies and increased prostate specific antigen. *J Urol* 2010;183(2):520-527.
44. Epstein JI, Allsbrook WC Jr, Amin MB, et al. ISUP Grading Committee. The 2005 International Society of Urological Pathology (ISUP) consensus conference on Gleason grading of prostatic carcinoma. *Am J Surg Pathol* 2005;29(9): 1228-1242.
45. Roethke M, Anastasiadis AG, Lichy M, et al. MRI-guided prostate biopsy detects clinically significant cancer: analysis of a cohort of 100 patients after previous negative TRUS biopsy. *World J Urol* 2012;30(2):213-218.
46. Ukimura O, Hirahara N, Fujihara A, et al. Technique for a hybrid system of realtime transrectal ultrasound with preoperative magnetic resonance imaging in the guidance of targeted prostate biopsy. *Int J Urol* 2010;17(10):890-893.

CHAPTER 6.0 THE ACCURACY AND SAFETY ASPECTS OF A NOVEL ROBOTIC NEEDLE GUIDE MANIPULATOR TO PERFORM TRANSRECTAL PROSTATE BIOPSIES

*Martijn G. Schouten, Janneke Ansems, W. Klaas Jan Renema,
Dennis G.H. Bosboom, Tom W.J. Scheenen, and Jurgen J. Fütterer*

Medical Physics 2010 Sep;37(9):4744-50

Abstract

Purpose: To introduce a new in-house developed pneumatically controlled magnetic field compatible manipulator as an aid to perform magnetic resonance (MR)-guided biopsies of the prostate.

Methods: A pneumatic controlled manipulator with five degrees of freedom constructed of plastic to achieve magnetic field compatibility was developed to guide biopsies. A risk analysis, mechanical tests, and RF safety tests with respect to needle tip heating were performed to assure future patient safety and to meet standard safety requirements for the use in a medical environment. The accuracy of needle positioning with the needle guide manipulator to sample a predefined target was measured in agar phantoms on a 3T whole body MR system. The in-plane error was used to evaluate the accuracy, which is defined as the orthogonal distance between target and biopsy needle. The time for each step in the biopsy procedure was recorded to evaluate the procedure time. The influence of the insertion angle with respect to the static field of the MR scanner on the needle artefact was investigated.

Results: The risk analyses met patient safety requirements. No RF induced local heating around the needle tip was observed. The average in-plane error in 19 measurements was 3.0 mm (range 0-5.6 mm). The average time needed for manipulation to place the needle guide in the desired position was 5 min (range 3-8 min). Total procedure time was 30 min. The needle artefact size increases with the insertion angle with respect to the static field of the MR scanner.

Conclusions: The new MR compatible manipulator can be used safely for patient care. It showed a high accuracy and short total procedure time, demonstrating great potential to improve the transrectal prostate biopsy procedure.

6.0

Introduction

The recent symbiosis between robotics and medical science has made a rapid development, particularly in imaging and interventions. Different imaging modalities provide feedback to interventional devices which are crucial in precise positioning tasks such as needle insertion, biopsy interventions, and catheter placement (1). In the detection of prostate cancer, the most frequently diagnosed form of noncutaneous cancer in men (2), this fusion may help to improve detection rate. The detection rate for transrectal ultrasound (TRUS)-guided biopsies is low (3) Despite the low detection rate and high false negative biopsy rate, TRUS-guided biopsy is still the standard procedure (4) Magnetic resonance (MR) imaging can be used as a diagnostic tool to detect, localize, and stage prostate cancer (5) The detection rate is improved in patients with elevated prostate specific antigen and repetitive negative TRUS-guided biopsies using MR-guided prostate biopsies (6-9)

MR imaging has the reputation of being expensive. This seems to be conceivable when comparing a MR-guided biopsy session with a conventional TRUS-guided biopsy session in the detection of prostate cancer. Nevertheless, it should be noted that the detection rate of prostate cancer in patients after the first negative TRUS-guided biopsy session is 22% and 14% for the third biopsy session. Generally, multiple TRUS-guided biopsy sessions are needed. The detection rate of MR-guided biopsies after two or greater negative TRUS-guided biopsy session is 59% (10). These numbers showed the potential of MR-guided biopsies.

In literature, both manually and mechanically actuated experimental MR compatible biopsy devices are described (11-17). Most of these devices have a needle entrance pathway (transgluteal and transperineal) where local anaesthesia is needed, which is more invasive in comparison with the clinically most commonly used transrectal pathway, where no anaesthesia is needed. Furthermore, the transperineal pathway has a longer trajectory to the prostate with more critical structures compared to the transrectal pathway. So far, the only commercially available transrectal MR-guided prostate biopsy device is a manually adjustable standard for needle guide positioning (6, 18, 19) This device cannot be controlled from distance, as opposed to the experimental devices that are mechanically actuated from outside the magnet room. A needle guide filled with gadolinium-doped water is inserted in the rectum of the patient. Based on the acquired MR images, the needle guide is manually positioned in the direction of the region of interest. This procedure is unpleasant for the patient, operator dependent, and time consuming. For these reasons an in-house MR-compatible robotic manipulator is developed with which the needle guide direction can be controlled outside the magnet room with real-time MR guidance. Consequently the patient does not need to be moved in and out of the magnet bore during needle guide repositioning. It is therefore conceivable that this robotic manipulator may improve procedure time, enhance patient comfort, and improve needle guide positioning.

To our knowledge, this is the first pneumatically actuated and magnetic field compatible manipulator for needle guide positioning under real-time MR-guidance, to perform transrectal prostate biopsies. The purpose of our phantom study was therefore to assess the accuracy and safety of the new transrectal MR compatible manipulator for guidance of prostate biopsies.

Materials and methods

System

The system consists of the robotic manipulator and its controller unit. The controller unit includes a computer, motion control elements, and electropneumatic and electronic interfaces which are located outside the MR cage of Faraday. Plastic tubes connect the manipulator to the control unit (Fig. 1). The entire manipulator

6.0

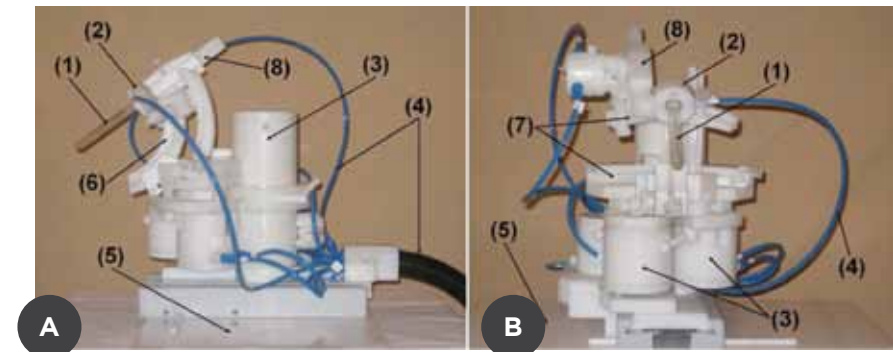


Figure 1: The robot shown from the side (A) and front (B). Most important parts are marked, with (1) needle guide, (2) safety mechanism with the suction cup, (3) pneumatic motors, (4) tubings to the motors, (5) ground plate for installation on MR table, (6) angulation rail to move the needle guide in the sagittal plane, (7) angulation rail to move the needle guide in the coronal plane, and the (8) tapping mechanism to introduce the needle guide.

consists of plastic to achieve magnetic field compatibility, for assuring patient safety and prevention of any signal artefacts. The manipulator is designed to interact with the patient within any standard clinical closed-bore MR system. In this study a closed-bore 3T (gradient strength of 40 mT/m) system was used (Magnetom Trio, Siemens Medical Solutions, Erlangen, Germany) with the body coil of the system as the radiofrequency transmit coil and a spine and body-array coil for MR signal reception. Phase maps of a localizer image sequence (sagittal, coronal, and axial gradient echo images with an echo time of 10 ms) of a volunteer were made with and without the manipulator in correct position to ascertain that the MR compatible manipulator did not disturb the homogeneity of the magnetic field. None of the images in this study were corrected for distortions. Compressed air used in the pneumatic motors is generated in the controller unit and is transmitted through the plastic tubings (Fig. 1). Valves located in the

controller unit generate pressure waves to set the motors in motion. The graphical user interface (GUI) for motion control is connected to the controller unit. By selecting the desired motion control button in the GUI, the corresponding valve is opened and thereby generating a pressure wave to the corresponding motor, resulting in movement of the needle guide in the desired position/direction. No electricity is required inside the MR magnet room.

The needle guide can be manipulated with five degrees of freedom (DOFs), which allows positioning of the end effector in the desired position. The angle of the needle guide with the main magnetic field could range from 30° to 55° in the sagittal plane and plus or minus 26° in the coronal plane.

To assure patient safety and meet standard safety requirements for the use in a medical environment, the needle guide has a mechanical safety mechanism consisting of a suction cup (Fig. 1). When the force from the end effector applied to the patients rectal wall reaches a primary set value, this suction cup will automatically release, preventing the end effector from harming the patient. The suction cup consists of a seal, underpressure generated in the suction cup results in fixation of the needle guide to the manipulator.

Patient safety

In a multidisciplinary group consisting of radiologists and (medical) physicists, a failure mode and effect analysis (FMEA) was performed. A FMEA is a systematic method to identify and prevent product and process problems before they can occur (20, 21). In this study a FMEA is performed to identify possible risks and hazards due the procedure or the manipulator itself, therefore ensuring that safety requirements are met.

To assure patient safety, the mechanical safety mechanism is tested using a force dynamometer (Correx, Haag-Streit, 0-2000 g, Bern, Switzerland). In a previous study of the mechanical properties of the human gastrointestinal tract, it was found that a force of 60 N/cm² can cause irregularities of the serosa and internal muscular layer of the human small bowel, whereas the mucosa, submucosa, and external muscular layer remained intact (22). The force needed to release the suction cup was determined at three different positions and directions on the needle guide (Figs. 2a-2c) Measurements of this force were repeated ten times. The results are presented as mean ± standard deviation.

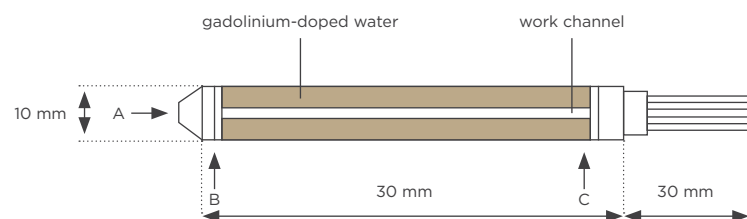


Figure 2: Needle guide with the gadolinium-doped water reservoir (Invivo, Schwerin, Germany) to make the needle guide visible on MR images and the work channel (for needle insertion) are shown. The arrows A, B, and C represent the direction of the forces applied on the needle guide during the safety experiments.

Depending on size and material, heating of metal wire or needle can occur due to deposited radio frequency (RF) power of the MR pulse sequence (23). To assure patient safety in future experiments, possible heating of the needle tip in the agar gel was studied with temperature mapping of the agar gel immediately after excessive RF power deposition. Temperature maps of the agar gel were made based on the difference in chemical shift of water with temperature, reflected in a phase shift of the water signal of a MR image between two experiments. After an initial gradient echo image (repetition time (ms); TR/echo time (ms); TE/flip angle (degrees); FA = 100/20/25; bandwidth 260 Hz/pixel; resolution 1.56 x 1.56 x 5.0 mm; acquisition time 13 s) as a reference phase map, a multiple spin echo sequence with a continuous power of 148 W for 104 s was applied to a 1 kg agar phantom to heat the sample (TR/TE = 8000/107; bandwidth of 465 Hz/pixel). After heating with RF, the temperature map was constructed with the phase map difference of a second gradient echo image and the reference phase map.

Accuracy measurements

To evaluate the ability of sampling with the manipulator, a phantom made of agar was used. Small plastic beads located in the agar represented targets. All beads were imbedded in the agar at the same depth (3 cm) and distance (2-3 cm) between them. The beads were 2 mm in diameter.

A schematic representation of the steps taken to perform a biopsy is illustrated in the flow chart in Figure 3. After the manipulator was connected to the controller unit, the phantom and manipulator were placed and secured on the table of the MR system (step 1). A body-array surface coil was used for MR signal reception (Fig. 4 - page 88).

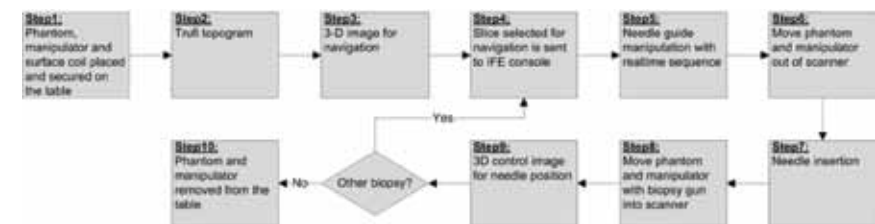


Figure 3: Flow chart of the biopsy procedure showing the different steps during the biopsy procedure.

Once the manipulator and phantom were fixed within the MR system, a T1-weighted 3D volumetric gradient echo sequence was used to acquire an image set (step 2) (TR/TE/FA = 6.5/2.5/10; resolution of 0.72 x 0.72 x 0.72 mm; readout gradient direction H>>F; readout gradient strength = 6.5 mT/m; acquisition time of 2 min and 20 s). The acquired 3D volume was used to select the target (step 3) and as a reference to navigate on during positioning of the needle guide with real-time MR imaging. After this initial target selection, a software package (interactive

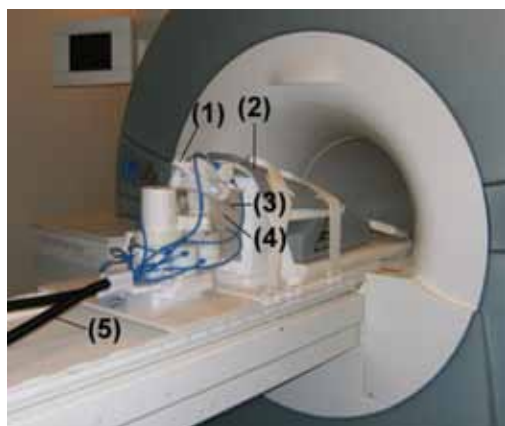


Figure 4: Measurement set up with the biopsy gun; (1) the needle is inserted in the phantom (4) through the needle guide (3). A body-array surface coil was used for MR signal reception (2). Plastic tubings connect the manipulator to the control room (5).

front end (IFE); work in-progress package; Siemens, Erlangen, Germany) was used to orient and direct the needle guide in the desired direction (step 4). The IFE software provides both 2D and 3D displays of real-time images. Manipulation of images and relevant controls can be performed in a single screen to simplify user interaction (24, 25). This software package uses a truFi sequence (Siemens, Erlangen, Germany) which supports interactive changes of imaging parameters during real-time imaging, such as image position/orientation. The sequence is especially designed to assist MR-guided interventional procedures which require interactive slice positioning for path planning and real-time monitoring of the acquired images. The sequence has the following parameters (TR/TE/FA = 732/1.9/70; resolution of 1.65 x 1.65 x 5.0 mm; readout gradient strength = 15.4 mT/m; three slices in different planes (sagittal, coronal, transverse plane); refresh rate = 2.2 s).

After correct positioning of the needle guide (step 5) according to the performing physician, the patient table with the manipulator and phantom is moved out of the magnet bore (step 6), and the biopsy was taken manually (step 7) with a standard biopsy gun (titanium 18-gauge, fully automatic, core-needle, double-shot biopsy gun with needle length of 170 mm and tissue core sampling length of 17 mm (Invivo, Schwerin, Germany)). The setup is returned to its original position in the magnet (step 8). Again a 3D volumetric gradient echo (TR/TE/FA = 4.6/2.0/10; resolution of 0.72 x 0.72 x 0.72 mm; readout gradient direction H>>F; readout gradient strength = 25.5 mT/m; acquisition time of 2 min and 20 s) image was acquired with the needle inserted in the phantom (step 9) to evaluate the accuracy of sampling the target.

The time needed for every step in the biopsy procedure was measured in order to evaluate the time needed for the procedure.

The angle of the titanium needle with the static field (B0) of the MR scanner was of influence on the artefact size of the needle (26). To determine the influence

of the angle on the size of the artefact, different insertion angles relative to the static field were made, and the same 3D image sequence used to determine the accuracy was utilized to measure the artefact size.

Data evaluation

To determine the accuracy for needle positioning, the inplane error was determined because the out of plane error is less critical in the biopsy procedure due to the core sampling length of 17 mm of the biopsy needle (13). The in-plane error is defined as the distance between the centre of the target and the centre of the biopsy needle in the plane perpendicular to the needle. Therefore, the tip of the needle was injected approximately 10 mm beyond the target for hypothetical sampling of the target in the centre of the 17 mm biopsy sampling core. In other words, we inserted the needle deep enough to be sure the tip of the needle was beyond the target. The in-plane error, which was the distance between the centre of the target and centre of the needle, was calculated using the following formula:

$$\sqrt{(x_{\text{needle}} - x_{\text{target}})^2 + (y_{\text{needle}} - y_{\text{target}})^2 + (z_{\text{needle}} - z_{\text{target}})^2}$$

The x, y, and z coordinates in the patient coordinate system were acquired from an image slice perpendicular to the needle guide, where both target and biopsy needle are visible (Fig. 5). The image slices perpendicular to the needle guide were reconstructed from the original 3D images. For this reason the coordinate system of the original image was still valid and, therefore, the distance needed to be calculated from all three dimensions. With the commercially available viewing program DYNACAD (Invivo, Schwerin, Germany), the three-dimensional coordinate positions of the centre of the needle and target were provided from the reconstructed 3D MR images.

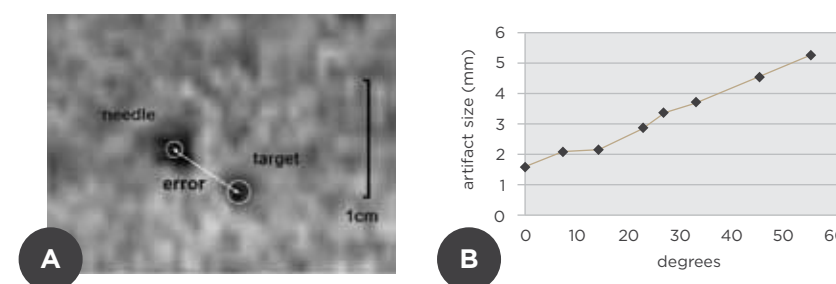


Figure 5: In the left panel (A) an image of the phantom is shown where both needle and target are visible. The image slice is perpendicular to the needle. The white double arrow represents the in-plane error. From this image it can be seen that the needle artefact is bigger than the real needle diameter (white circle). The influence of the angle with the static field of the MR scanner on the needle artefact is shown in the right panel (B).

A 3D image set with isotropic voxels was chosen to be sure that the measured distance in every direction will have the same error due to the voxel size and to minimize this error in the reconstructed images, where voxels are not square anymore due to the angulation.

Results

System

In total, 19 biopsies in phantoms were performed. No technical problems occurred during the procedure and all predefined targets could be reached. No artefacts from the manipulator were seen on the MR images. Phase maps in all orientations with and without the manipulator in place did not show any differences (data not shown), illustrating that the manipulator did not interfere with the magnetic field homogeneity in any way. The simple interface for manipulation, five DOFs, and fast manipulation speed of the end effector made it effortless to reach a target. Therefore, most of the manipulation time was spent on fine tuning of the final needle guide position, even when two predefined targets were far apart.

Patient safety

The FMEA risk analysis showed minor items for improvement. Most important failure modes observed were incorrect installation of the manipulator on the MR table and incorrect slice selection through the needle guide. Therefore, small technical adaptations were performed such as improved connection of the tubings on the MR table to prevent damage. Also the instructions for correct image slice selection were improved. Most important recommendation in this risk analysis was to test the mechanical safety mechanism. The mean (\pm standard deviation) forces required before the safety mechanism was activated during positioning of the needle guide were 5.5 ± 0.3 , 8.1 ± 0.3 , and 15.1 ± 0.9 N for position and directions A (needle guide tip), B, and C, respectively (Fig. 2). If we assume 20 N as the maximum force that can be applied on the needle guide (the mechanical safety tests show that this is in the direction of arrow C) before the safety mechanism will be activated, which includes a safety margin of 4.9 N, we can estimate the minimal contact surface needed to refrain from damaging the rectal wall. Taking 60 N/cm^2 as the maximum allowed force per surface on the patient in order to prevent bowel wall damage (22), the minimal contact surface between the needle guide and rectal wall of 0.3 cm^2 is allowed. Regarding these results, the flexibility of the rectal wall, and the estimated surface of the tip of the needle guide (1.8 cm^2), we can conclude that the forces applied on the rectal wall by the manipulator cannot cause harm to the patient.

The 1 kg agar phantom did heat up a few degrees due to the applied continuous power of 148 W for 104 s with the high-power multiple spin echo pulse sequence. Temperature mapping showed an inhomogeneous increase in temperature of the agar phantom, with more heat deposited at the bottom of the phantom than near the top. However, from the temperature map after RF heating (Fig. 6), it can be seen that there is no local heating around the needle tip in this phantom setup.

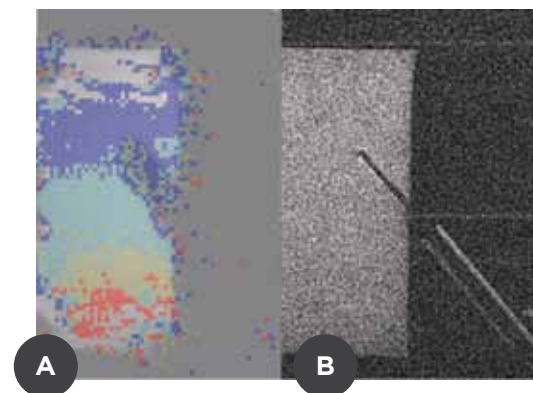


Figure 6: Temperature map of a 1 kg agar phantom (A) after applying a continuous power of 148 W for 104 s to a 1 kg phantom. The temperature map showed an inhomogeneous increase in temperature of the agar phantom. However, no local heating of the needle tip was seen. The colours indicate the relative temperature increase. Blue indicates an increase of 0.0° - 1.0° , cyan of 1.0° - 2.0° , yellow 2.0° - 2.5° , and red 2.5° - 3.0° with respect to the reference image made before applying a continuous power of 148 W for 104 s. An anatomical image of the set up is shown in the right panel (B).

Accuracy measurements

The installation of the manipulator on the MR table and the connection to the controller unit was accomplished within 10 min (step1; Fig. 3). The average time needed for manipulation to place the needle guide in the desired position (step 4) was 5 min (range 3-8 min). Total procedure time to perform a biopsy was less than 30 min for each sample (steps 1-10). To perform an additional biopsy (steps 4-9), 11 min extra to total procedure time was needed on average.

For needle placement the average in-plane error was 3.0 mm (range 0-5.6 mm; Fig. 7). In 3 out of 19 measurements, there was an exact hit of the needle and target.

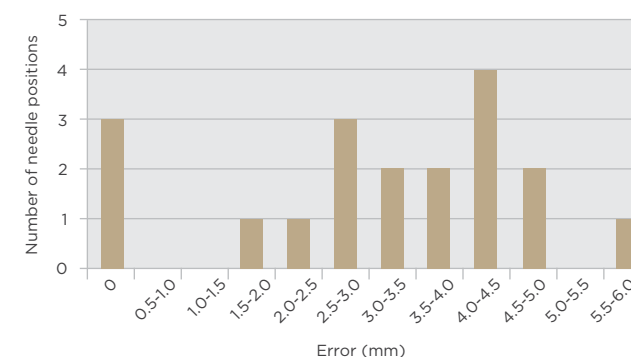


Figure 7: Histogram of needle placement error (n=19), which is defined as the in-plane distance between the centre of the target and the centre of the needle. In three cases a direct hit of the target (error = 0 mm) resulted in movement of the plastic bead along with the needle tip in the agar phantom. In one case the bead probably bounced off the needle resulting in an error of 1.6 mm (half the diameter of the needle plus half the diameter of the target).

As a result the plastic bead moved with the needle in the agar phantom and was seen on the needle tip. In the other 16 biopsies the needle missed the target or bounced off on the plastic beads.

An additional difficulty in assessing the accuracy of the procedure was the dependency of the apparent size of the needle in relation to the insertion angle of the needle with respect to the static magnetic field of the MR scanner. The size of the void in the images at the position of the needle increases with the angle between the needle and the static magnetic field (Fig. 5).

Discussion

Our MR-compatible transrectal prostate biopsy manipulator demonstrated promising results with respect to the precision of needle positioning and short manipulation time. Furthermore, the manipulator prevented the need of moving the phantom in and out of the scanner bore for manipulation and imaging of the needle guide. This will be an enormous advantage when performing the biopsy procedure with the manipulator in patients.

Safety

Regarding the mechanical safety mechanism tests, we can conclude that the manipulator cannot harm the patient. However, it should be noted that the utilized 20 N/cm² as a measure for rectal wall damage are ex vivo laboratory results for damage in the small intestine. Therefore, extra safety margins were taken into account for the calculations.

Local heating of the needle tip was not seen, in this experimental setup, after applying a continuous power of 148 W for 104 s to a 1 kg phantom. In patients in the 3T MR system, the amount of RF power that is allowed to be deposited in the body is the SAR limit of 4 W/kg averaged over a period of 6 min (this is only 9% of the RF power deposited in the phantom). According to these results it is safe to perform in vivo accuracy studies in the future without causing heating damage with the currently used needles to the patient. Nevertheless, care should be taken into account when performing in vivo studies since these results are obtained from one experiment with a particular setup. In our experiment we neither investigated the influence of the surrounding medium of the needle nor differences in length, angle, and position of the needle with respect to the static magnetic field.

Accuracy measurements

We found an average in-plane error of 3.0 mm (range 0-5.6 mm) which is comparable to other devices used for prostate biopsies. Preliminary results of Fischer et al. (27) showed that their transperineal robot successfully punctured five out of five 10 mm targets. The transperineal robot described by Muntener et al. is able to perform biopsies with a median error of 2.02 mm (range 0.86-3.18 mm) (7). These results suggest that these devices, including our manipulator, are

able to puncture most clinically relevant tumours as 80% of the tumours with a volume of less than 0.5 mL (diameter = 1.0 cm) are unlikely to be important during the life of a patient (28).

The average total procedure time was less than 30 min which is comparable with the time Muntener et al. (7) described in their study (30-35 min). When comparing with the MR-compatible biopsy device (Invivo, Schwerin, Germany) used in clinical practice, the procedure time found in this phantom study is shorter (18). However, it should be noted that it is difficult to compare phantom studies with patient studies since more precautions are taken when performing a biopsy on a patient. Our results with respect to the procedure time are promising, taking into account that the learning curve for using the manipulator is expected to optimize the procedure times even further. Most procedure time is spent in installation and removal of the manipulator and phantom from the MR table.

The interface for manipulation of the needle guide is user friendly and does not need a lot of experience from the practitioner. This interface in combination with the IFE software, for interactive changes of imaging parameters during real-time MR imaging, brings manipulation and orientation of the needle guide more together. Manipulation under real-time imaging enables monitoring of progress for the performing physician during intervention.

The pneumatic robot that Fischer et al. (27) described also makes use of real-time imaging during needle guide positioning. However, the perineum is used as the entrance pathway which needs local anaesthesia to ease patient discomfort and has a longer distance to the prostate (which may result in a larger biopsy error) when compared to our manipulator using the transrectal entrance pathway.

Limitations and further improvements

By calculating the accuracy as the distance between the coordinates of the centre of the needle and the centre of the target rather than the edge of the needle and target, an error is introduced when the needle touches the target. The target is a plastic bead which can be displaced in the gel by a direct hit of the needle resulting in an error of 1.6 mm (half the diameter of the needle (0.6 mm) plus half the diameter of the target (1 mm)). This may have occurred in one needle (error of 1.5-2 mm) (Fig. 7).

The cannula of the needle guide is a fragment wider than the biopsy needle. This may result in an error in needle positioning due to the angle of insertion. This error increases with insertion depth.

The asymmetrical shape of the needle tip and tissue inhomogeneities may result in deflection of the needle (29, 30). Bosch et al. (17) used a tapping technique to minimize tissue deformation. Although deflection of the needle contributes to the measured error, we did not investigate this aspect of needle placement error since this is beyond the scope of this study.

During manipulation under real-time imaging, the practitioner has to manually adjust the image slice direction within the IFE software to see whether the needle guide points in the correct direction. However, it should be noted that manipulation time is only 5 min and probably will become shorter taking into

account that the learning curve for using the manipulator is expected to optimize the procedure time even further.

During manipulation of the pneumatically driven needle guide, some delay was seen resulting in overshoots of the needle guide toward the target. This delay is caused by the near-real-time imaging sequence (refresh rate of 2.2 s) and by the fact that the pneumatic motors not directly stop moving after release of the motion button in the GUI.

The apparent size of the needle changes with the insertion angle and can be up to four times the actual needle size (5.3 mm). Although this is not of influence on positioning the needle guide with the manipulator (needle is not present yet), it could introduce a systematic bias in the calculated sampling error. The error is calculated from the centre of the needle position to the centre of the plastic bead. This may result in an error when the exact location of the needle within the signal void in the image is not known.

In this study we did not investigate the required insertion depth of the needle. It is expected that the insertion depth will not be a problem since the sampling length of the biopsy needle is 17 mm. However, the insertion depth should be taken into account in future patient studies.

The range of the manipulator is comparable with the manual device, used in clinical practice, which can range from 30° to 65° in the sagittal plane and plus or minus 20° in the coronal plane. It is therefore conceivable that the manipulator can cover the whole prostate. However, apical lesion may become a problem since the range of the manipulator in the sagittal plane is 30-50 which is 15° less compared to the range of the manual device (30°-65°). In a planning study for brachytherapy performed by van Gellekom et al. (31), they showed that it is feasible to cover the entire prostate with the divergent single needle method. They found that the limited space in the scanner bore and internal patient anatomy were the major limitations for possible needle trajectories. Using the transrectal pathway may overcome these limitations when compared with the transperineal pathway.

The applied sequences have not been tested on patients since we optimized the sequences to obtain the best image contrast in the agar phantom. Before starting patient studies, these sequences have to be optimized to obtain the best image contrast in patients and minimize needle artefacts.

In conclusion we can state that the new MR compatible manipulator is safe enough to do the first feasibility tests. It showed a high accuracy and short total procedure time, demonstrating great potential to improve the transrectal prostate biopsy procedure. The next step therefore is to establish the clinical feasibility of the system.

References

1. Elhawary H, Tse ZT, Hamed A, et al. The case for MR-compatible robotics: a review of the state of the art. *Int J Med Robot.* 2008;4(2):105-13.
2. Jemal A, Siegel R, Ward E, et al. Cancer statistics, 2008. *CA Cancer J Clin.* 2008;58(2):71-96.
3. Lujan M, Paez A, Santonja C, et al. Prostate cancer detection and tumor characteristics in men with multiple biopsy sessions. *Prostate Cancer Prostatic Dis.* 2004;7(3):238-42.
4. Rabbani F, Stroumbakis N, Kava BR, et al. Incidence and clinical significance of false-negative sextant prostate biopsies. *J Urol.* 1998;159(4):1247-50.
5. Futterer JJ, Barentsz J, Heijmink ST. Imaging modalities for prostate cancer. *Expert Rev Anticancer Ther.* 2009;9(7):923-37.
6. Anastasiadis AG, Lichy MP, Nagele U, et al. MRI-guided biopsy of the prostate increases diagnostic performance in men with elevated or increasing PSA levels after previous negative TRUS biopsies. *Eur Urol.* 2006;50(4):738-48; discussion 48-9.
7. Muntener M, Patriciu A, Petrisor D, et al. Transperineal prostate intervention: robot for fully automated MR imaging--system description and proof of principle in a canine model. *Radiology.* 2008;247(2):543-9.
8. Hambrock T, Futterer JJ, Huisman HJ, et al. Thirty-two-channel coil 3T magnetic resonance-guided biopsies of prostate tumor suspicious regions identified on multimodality 3T magnetic resonance imaging: technique and feasibility. *Invest Radiol.* 2008;43(10):686-94.
9. Beyersdorff D, Taupitz M, Winkelmann B, et al. Patients with a history of elevated prostate-specific antigen levels and negative transrectal US-guided quadrant or sextant biopsy results: value of MR imaging. *Radiology.* 2002;224(3):701-6.
10. Hambrock T, Somford DM, Hoeks C, et al. Magnetic resonance imaging guided prostate biopsy in men with repeat negative biopsies and increased prostate specific antigen. *J Urol.* 2010;183(2):520-7.
11. Fichtinger G, Krieger A, Susil RC, et al. Transrectal prostate biopsy inside closed MRI scanner with remote actuation, under real-time image guidance. *Medical Image Computing and Computer-Assisted Intervention-Miccai 2002, Pt 1.* 2002;2488:91-8.
12. Krieger A, Csoma C, Lordachital, II, et al. Design and preliminary accuracy studies of an MRI-guided transrectal prostate intervention system. *Med Image Comput Comput Assist Interv.* 2007;10(Pt 2):59-67.
13. Susil RC, Menard C, Krieger A, et al. Transrectal prostate biopsy and fiducial marker placement in a standard 1.5T magnetic resonance imaging scanner. *J Urol.* 2006;175(1):113-20.
14. Stoianovici D, Song D, Petrisor D, et al. "MRI Stealth" robot for prostate interventions. *Minim Invasive Ther Allied Technol.* 2007;16(4):241-8.
15. Zangos S, Herzog C, Eichler K, et al. MR-compatible assistance system for puncture in a high-field system: device and feasibility of transgluteal biopsies of the prostate gland. *Eur Radiol.* 2007;17(4):1118-24.
16. Cleary K, Melzer A, Watson V, et al. Interventional robotic systems: applications and technology state-of-the-art. *Minim Invasive Ther Allied Technol.* 2006;15(2):101-13.
17. van den Bosch MR, Moman MR, van Vulpen M, et al. MRI-guided robotic system for transperineal prostate interventions: proof of principle. *Phys Med Biol.* 2010;55(5):N133-40.
18. Beyersdorff D, Winkel A, Hamm B, et al. MR imaging-guided prostate biopsy with a closed MR unit at 1.5 T: initial results. *Radiology.* 2005;234(2):576-81.
19. Yakar D, Hambrock T, Huisman H, et al. Feasibility of 3T dynamic contrast-enhanced magnetic resonance-guided biopsy in localizing local recurrence of prostate cancer after external beam radiation therapy. *Invest Radiol.* 2010;45(3):121-5.

20. Abujudeh HH, Kaewlai R. Radiology failure mode and effect analysis: what is it? *Radiology*. 2009;252(2):544-50.
21. McDermott REM, R.J., Beauregard, M.R. The basics of FMEA. London: CRC Press, 2008: 3-8.
22. Egorov VI, Schastlivtsev IV, Prut EV, et al. Mechanical properties of the human gastrointestinal tract. *J Biomech*. 2002;35(10):1417-25.
23. Yeung CJ, Atalar E. RF transmit power limit for the barewire loopless catheter antenna. *J Magn Reson Imaging*. 2000;12(1):86-91.
24. Yutzy SR, Duerk JL. Pulse sequences and system interfaces for interventional and real-time MRI. *J Magn Reson Imaging*. 2008;27(2):267-75.
25. Lorenz SRK, K.J.; Zuehlsdorff, S.; Speier, P.; Caylus, M.; Borys, W.; Moeller, T.; Guttman, M.A. Interactive frontend (IFE): A platform for graphical MR scanner control and scan automation. *Intl Soc Mag Reson Med*2005; 2170.
26. Frahm C, Gehl HB, Melchert UH, et al. Visualization of magnetic resonance-compatible needles at 1.5 and 0.2 Tesla. *Cardiovasc Intervent Radiol*. 1996;19(5):335-40.
27. Fischer GS, Iordachita I, Csoma C, et al. MRI-Compatible Pneumatic Robot for Transperineal Prostate Needle Placement. *IEEE ASME Trans Mechatron*. 2008;13(3):295-305.
28. Stamey TA, Freiha FS, McNeal JE, et al. Localized prostate cancer. Relationship of tumor volume to clinical significance for treatment of prostate cancer. *Cancer*. 1993;71(3 Suppl):933-8.
29. Abolhassani N, Patel R, Moallem M. Needle insertion into soft tissue: a survey. *Med Eng Phys*. 2007;29(4):413-31.
30. Blumenfeld P, Hata N, DiMaio S, et al. Transperineal prostate biopsy under magnetic resonance image guidance: a needle placement accuracy study. *J Magn Reson Imaging*. 2007;26(3):688-94.
31. Van Gellekom MP, Moerland MA, Battermann JJ, et al. MRI-guided prostate brachytherapy with single needle method--a planning study. *Radiother Oncol*. 2004;71(3):327-32.

CHAPTER 7.0 EVALUATION OF A ROBOTIC TECHNIQUE FOR TRANSRECTAL MR-GUIDED PROSTATE BIOPSIES

*Martijn G. Schouten, Joyce G.R. Bomers, Derya Yakar,
Henkjan Huisman, Eva Rothgang, Dennis G.H. Bosboom,
Tom W.J. Scheenen, Sarthak Misra, Jurgen J. Fütterer*

European Radiology 2012 Feb;22(2):476-83

Abstract

Objectives: To evaluate the accuracy and speed of a novel robotic technique as an aid to perform magnetic resonance (MR)-guided prostate biopsies on patients with cancer suspicious regions.

Methods: A pneumatic controlled MR-compatible manipulator with 5 degrees of freedom was developed in-house to guide biopsies under real-time imaging. From 13 consecutive biopsy procedures, the targeting error, biopsy error and target displacement were calculated to evaluate the accuracy. The time was recorded to evaluate manipulation and procedure time.

Results: The robotic and manual techniques demonstrated comparable results regarding mean targeting error (5.7 vs 5.8 mm, respectively) and mean target displacement (6.6 vs 6.0 mm, respectively). The mean biopsy error was larger (6.5 vs 4.4 mm) when using the robotic technique, although not significant. Mean procedure and manipulation time were 76 min and 6 min, respectively using the robotic technique and 61 and 8 min with the manual technique.

Conclusions: Although comparable results regarding accuracy and speed were found, the extended technical effort of the robotic technique make the manual technique - currently - more suitable to perform MR-guided biopsies. Furthermore, this study provided a better insight in displacement of the target during in vivo biopsy procedures.

7.0

Introduction

The detection rate of prostate cancer in men with elevated and/or rising prostate specific antigen (PSA) after negative transrectal ultrasound (TRUS)-guided biopsy sessions is poor. Hambrook et al. found a cancer detection rate of 59%, in men with an elevated PSA and multiple negative TRUS-guided biopsy (≥ 2) sessions, for magnetic resonance (MR)-guided biopsies. This is an improvement when compared to 8 to 12-core TRUS-guided biopsy schemes with a detection rate around 17% (TRUS-guided biopsy ≥ 1) (1-3). Nevertheless, MR-guided biopsy is unpleasant for the patient and time-consuming for the radiologist. For these reasons an in-house pneumatically actuated MR compatible robot was developed where needle-guide direction can be controlled in real-time inside the controller room (4). Consequently, the patient remains inside the scanner bore. This may decrease procedure time, enhance patient comfort and improve needle-guide positioning.

Eighty-percent of the tumours with a volume larger than 0.5 cm^3 (diameter=1.0 cm) are likely to be clinically significant (5). Therefore, it is desirable to have a technique with a biopsy error smaller than 5 mm. Different factors, such as needle-guide positioning, patient and prostate motion, and tissue deformation influence the accuracy of needle positioning (6-8). Consequently, the needle does not always reach the cancer suspicious lesion (CSL).

In a phantom study the new robotic technique demonstrated a short manipulation time of 5 min (range 3-8 min) and a high accuracy of 3.0 mm (range 0-5.6 mm) for needle positioning (4). Yakar et al. demonstrated that it is technical feasible to perform transrectal prostate biopsies using the novel robotic technique (n=10) (Fig. 1) (9). To evaluate and optimize the biopsy procedure in the future, it is necessary to identify and quantify the cause of the biopsy error. Therefore, the purpose of this study was to evaluate the accuracy and speed of the novel robotic technique as an aid to perform MR-guided biopsy on patients with CSLs.

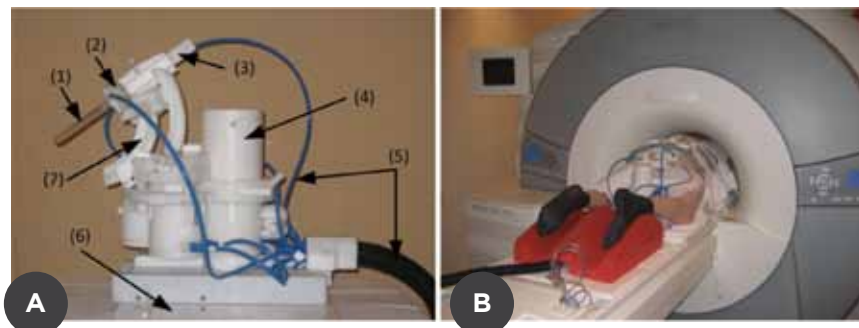


Figure 1: (a) the robot with (1) the needle guide, (2) safety mechanism with the suction cup, (3) tapping mechanism to introduce the needle guide, (4) pneumatic motor, (5) tubings to the motors, (6) ground plate for installation on the MR table, (7) angulation rail to move the needle guide in the coronal plane. (b) set-up of a patient with the robotic technique on the table of the MR system. The patient was positioned in prone position in the MR system. After the needle guide was inserted rectally it was attached to the robot

Materials and methods

Patients

This study was approved by the ethics review board and written informed consent was obtained from all patients who were biopsied with the robotic technique. From February to September 2010, 13 consecutive patients with an elevated PSA ($>4 \text{ ng/mL}$) and at least one negative TRUS-guided biopsy session were included. Patient were included in the robotic patient population based on their willingness. The manual patient population was matched to the robotic population. Prior to the MR-guided, patients received a 3T (Magnetom TRIO, Siemens, Germany) multi-parametric MRI examination of the prostate for identification of possible CSLs. T2-weighted images in three orthogonal planes, transversal diffusion weighted images (DWI) and dynamic contrast-enhanced (DCE)-MR images (Table 1 - page 102) were obtained during and after injection of 15 mL gadopentetate dimeglumine with a power injector (Guerbet, Gorinchem, Netherlands). To evaluate the CSL for clinical significance, the criteria for MR-guided biopsy reported by Hambrook et al. were applied (3).

CSLs were determined in consensus by 2 readers with at least 6 years of experience in prostate MR reading. From each CSL the volume (in mL) was determined on the MR images, assuming that the lesions were ellipsoids.

MR-guided biopsy

MR-guided biopsy were performed within 12 weeks after the diagnostic multi-parametric MR examination. Antibiotic prophylaxis was given with 500 mg ciprofloxacin in the morning and evening for three consecutive days, starting the day before biopsy. A schematic representation of the steps taken to perform a biopsy is illustrated in the flow chart (Fig. 2).

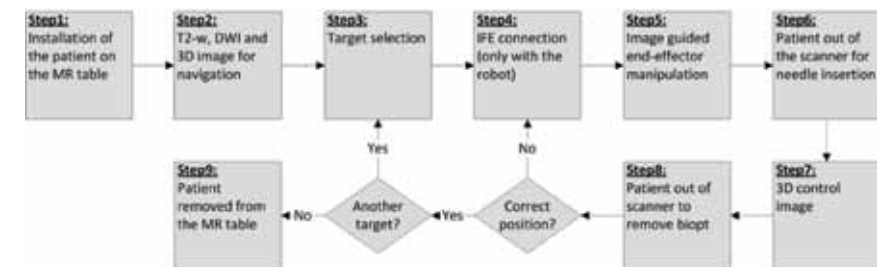


Figure 2: Flow chart of the biopsy procedure for both the robotic and manual techniques. Scan plane adjustments were only performed with the IFE software (step 4) when using the robotic technique

Sequence	TR/TE/FA ms/ms/degrees	Resolution (mm)	Acquisition time (minutes)
Diagnostic multi-parametric image sequences			
DWI, b-values: 50, 500, and 800 s/mm ²	2300-2500/61-64	2.0 x 2.0 x 4.0	3:08
Transversal, sagittal and coronal T2-weighted turbo spin echo	4480-4950/103-110/120	0.6 x 0.6 x 3.0	3:22-4:43
DCE-MRI 3D T1-w spoiled gradient-echo	32/1.47/10	1.8 x 1.8 x 4.0	2:43
Image sequences during biopsy procedure			
DWI, b-values: 0, 100, 500 and 800 s/mm ²	2000/67	1.8 x 1.8 x 4.0	2:06
T2-weighted turbo spin echo	3620/103/120	0.8 x 0.8 x 4.0	3:26
Transversal and sagittal TRUFI image (manual technique)	4.48/2.24/70	1.1 x 1.1 x 3.0	7.5 and 8.9 s
Transversal, sagittal and coronal TRUFI image (robotic technique)	894/2.3/60	1.6 x 1.6 x 5.0	0.9 s/slice
T1-w 3D volumetric gradient echo ¹	4.5/2.2/43	1.0 x 1.0 x 1.0	2:20
T2-weighted 3D volumetric spin echo	1000/102/100	1.0 x 1.0 x 1.0	2:36

Table 1: Imaging protocol with sequence specifications. Volumetric images were utilized to identify anatomical landmarks used to quantify target displacement. DWI = diffusion weighted imaging, TR = repetition time, TE = echo time, FA = flip angle, DCE = dynamic contrast enhanced, TRUFI = true-FISP

¹ The initial two volumetric images (2/13) were gradient echo sequences (first 2 procedures using the robotic technique).

A needle-guide filled with gadolinium-doped water was inserted in the rectum of the patient. Subsequently, the needle-guide was mounted to the robotic or manual device (Step 1). The MR imaging protocol (Step 2) for target selection and to navigate on during the biopsy procedure is shown in Table 1.

Targets were selected (Step 3) on these images based on the CSLs found in the diagnostic MRI examination. Manipulation of the needle-guide was done using either the robotic or manual technique (Step 5). After correct alignment of the needle-guide the insertion depth of the needle was measured on a transversal true-FISP (TRUFI) image (Table 1). The patient was slid out the gantry to insert the biopsy needle manually (titanium 18-gauge, fully automatic, core-needle, double-shot biopsy gun with needle length of 175, sampling length of 17 mm (Invivo, Schwerin, Germany).

A T2-weighted 3D volumetric gradient-echo (first two procedures with the robotic technique) or a T2-weighted 3D volumetric spin-echo image (all other patients) was acquired with the needle inserted (Step 7). This was the same 3D volumetric image (Table 1) as acquired in step 2. When the needle was in correct position, confirmed on the control images, another target could be targeted (Steps 3-8) or the patient was removed from the MR table (Step 9).

Needle-guide positioning: robotic technique

The robotic system has five degrees of freedom: translations in three directions (anterior-posterior, inferior-superior, lateral) and rotations in two directions (inferior-superior, lateral). The angle of the needle-guide with the main magnetic field could range from 30° to 55° in the inferior-superior direction and plus or minus 26° in the lateral direction (4).

With a simple graphical user interface the direction of the needle-guide can be adjusted (9). A software package (Interactive Front End (IFE); Siemens Corporate Research, Baltimore (MD), USA) was used to orient and direct the needle-guide in the desired direction (Step 5) under real-time image guidance (Table 1). Manipulation of images and relevant controls can be performed during imaging which allows interactive slice positioning for path planning and real-time monitoring (10, 11).

Needle-guide positioning: manual technique

Transversal and sagittal TRUFI images (Table 1) through the needle-guide were acquired to determine needle-guide direction. The patient was withdrawn from the scanner bore and the radiologist manually adjusted the biopsy device to point the needle-guide towards the target. To confirm correct positioning of the needle guide sagittal and transversal TRUFI images were acquired through the needle-guide again. These actions were repeated until the needle-guide was in correct position (12).

Total procedure time and manipulation time were recorded for both the robotic and manual techniques.

Measurements

Motion and deformation of the prostate may occur during the biopsy procedure. This will have effect on the position of the target. Since targeting of the CSL in both methods was done on the images acquired in Step 2, which do not take deformation and motion into account, it is important to distinguish between targeting and biopsy error (Fig. 3 - page 104).

Targeting error (ϵ) The targeting error is defined as the normal (shortest) distance from the needle trajectory to the original target location (Fig. 3). This error does not take tissue deformation and patient motion into consideration. This error is a measure for needle-guide positioning towards the intended target.

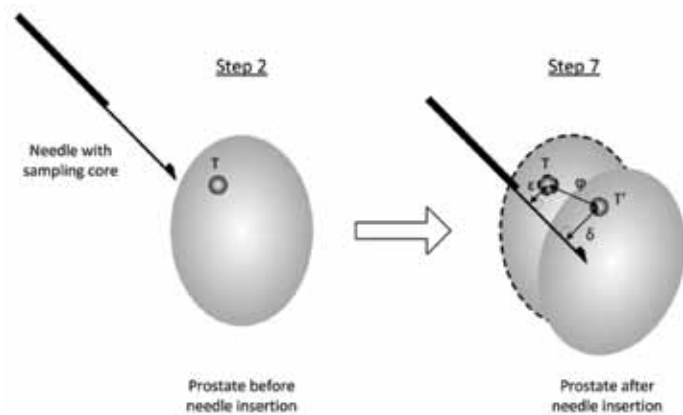


Figure 3: Representation of the needle inside the prostate, illustrating targeting error (ϵ), target displacement (ϕ) and biopsy error (δ). The targeting error, defined as the normal distance from needle to the original target coordinate (T), is shown. Target displacement, defined as the distance between original target (T) and transformed target (T'), is represented by ϕ . Furthermore, the biopsy error (δ) is shown, which is defined as the normal distance between transformed target (T') and needle

Biopsy error (δ) The biopsy error is defined as the normal distance from the needle to the transformed target location (the actual target location after needle insertion). The coordinates of the transformed target are corrected for tissue deformation, as well as patient and prostate motion. The transformed target coordinates were calculated by adding the target displacement vector to the original target coordinates.

Target displacement (ϕ) The target displacement vector is defined by the distance and angle between the original and transformed target location. The target displacement (ϕ) is the length of this vector. The 3D volumetric images made before (Step 2) and after needle insertion (Step 7) were used to determine the target displacement vector. In these images identical anatomical landmarks around the target (mean 13.7 mm; range 2.3-48.4 mm) were manually selected with the aid of an open source fusion package (13). Calcifications, benign prostate hyperplasia (BPH) nodules, the verumontanum and the urethra were used as anatomical landmarks. Coordinates of these anatomical landmarks (≥ 5) were used to create a 3D vector field. The arrows represent the direction and distance of displacement of anatomical landmarks (Fig. 4). The mean vector of this vector field is a quantitative measure for localized target displacement, since anatomical landmarks around the target were selected.

To calculate the targeting and biopsy error the needle trajectory was determined by fitting a line through multiple points (≥ 8) within the needle artefact using linear regression in 3D-space. These points were obtained from the 3D volumetric MR images obtained in Step 7.

Target coordinates (CSLs) were obtained from the T2-weighted and DW images acquired in Step 2.

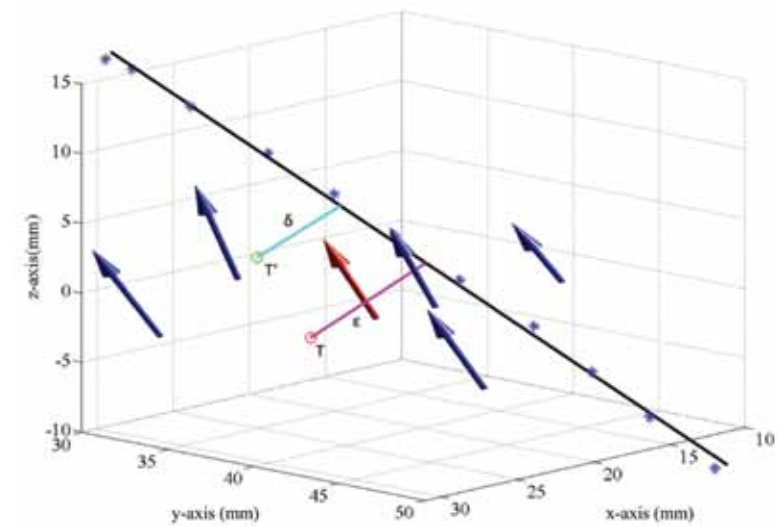


Figure 4: 3D vector field: The blue arrows represent the direction and displacement of the anatomical landmarks. The red arrow is the mean vector representing target displacement. Furthermore, the needle trajectory (black line), targeting error (ϵ), original target (T), biopsy error (δ) and transformed target (T') are shown.

The angle between needle trajectory and target displacement direction was calculated in order to see whether the target moved along the needle trajectory or in a random direction (Fig. 5).

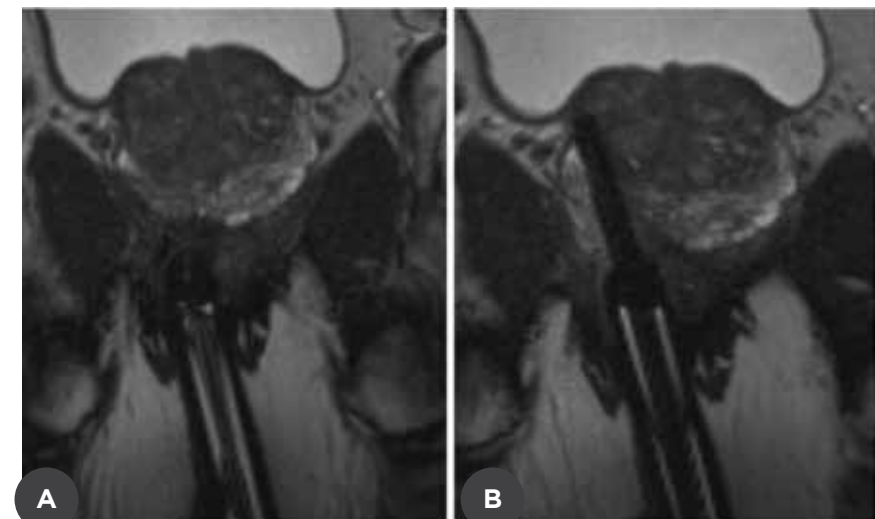


Figure 5: Transversal TRUFI image through the needle guide before (a) and after (b) needle insertion in the prostate

Statistical analysis

Two-tailed independent t-tests were performed to determine whether there were significant differences between the robotic and manual techniques for targeting error, biopsy error, target displacement, procedure and manipulation time. Differences were considered to be significant at $p < 0.05$. Statistical analysis were performed with SPSS, version 16.0.01 (Chicago, Illinois).

Results

In total, 13 patients with 32 needle positions were analyzed. Table 2 describes the patient characteristics and biopsy results for both techniques.

Patient characteristics	Robotic	Manual
Number of patients	8	5
Number of needle placements	19	13
Median needle positions per patient	1.5 (range 1-3)	2 (range 1-4)
Mean PSA (ng/mL)	15 (range 8-28)	14 (range 7-19)
Mean prostate volume (mL)	67 (range 44-98)	72 (range 49-100)
Median number of repeated negative TRUS-guided biopsy sessions	2 (range 1-4)	2 (range 1-4)
Median lesion volume on MR images (cc)	0.85 (0.38-1.61)	0.91 (0.6-3.19)
Histopathological findings (nr. of patients)	non-malignant (3), prostatitis (3), cancer (2)	non-malignant (2), prostatitis (2), cancer (1)

Table 2: Patient characteristics and biopsy results for both the robotic and manual techniques.

Since the majority of previous negative TRUS-guided biopsy had been performed outside our institution, information on the number of cores was not available for most patients.

Accuracy

The mean targeting error for both the robotic and manual techniques was almost similar (5.7 vs 5.8 mm respectively, $p=0.928$) (Fig. 6). The mean biopsy error was less (4.4 vs 6.5 mm) with the manual technique compared to the robotic technique ($p=0.054$). Target displacement was larger with the robotic technique (6.6 vs 6.0 mm, $p=0.439$).

Direction of target displacement

The mean angle between needle trajectory and target displacement direction for the robotic and manual techniques was 36.7° (range $4.0-82.2^\circ$) and 37.6° (range $7.7-73.3^\circ$), respectively.

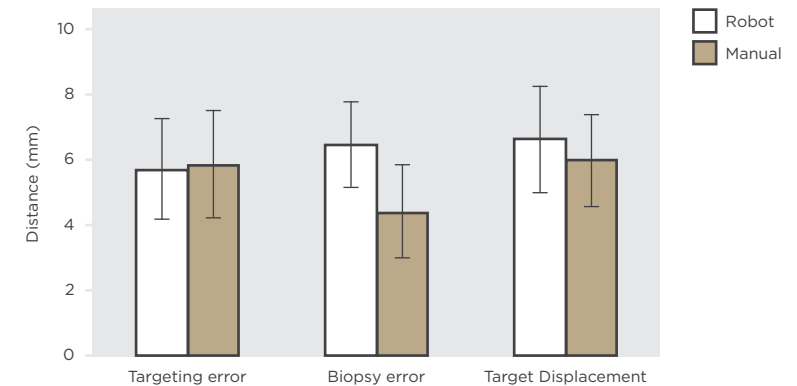


Figure 6: Histogram showing the mean targeting error, biopsy error and target displacement for both the robotic and manual techniques. The error bars represent the standard deviation.

Time

The mean time to perform a biopsy procedure using the robotic technique was 76 min (range 60-100 min) and 61 min (range 52-64 min) with the manual technique. The total procedure time includes the extra time to acquire the 3D volumetric images (2:36 min each). The mean manipulation time to move from target to target was 6 min (range 3-11 min) with the robotic technique and 8 min (range 5-11 min) with the manual technique. The differences in manipulation time and procedure time between both techniques were not significant.

Discussion

The robotic and manual techniques demonstrated comparable results regarding targeting error and target displacement. The biopsy error was larger when using the robotic technique, however not statistically significant. The robotic technique prevented the need of moving the patient in and out of the scanner bore for manipulation and imaging of the needle-guide. Most of the target displacement found in our study was in the direction of the needle trajectory.

Several robots for transperineal seed delivery in brachytherapy have been described in literature (14-17). The robotic and manual techniques for transrectal biopsies demonstrated a larger targeting error (5.7 and 5 mm respectively) compared to other robotic techniques. Muntener et al. found a targeting error of 2.02 mm (range 0.86-3.18 mm) with their robot in a canine model (16). Zangos et al. describe a transgluteal approach for prostate biopsy with a targeting error of 0.9 mm (range, 0.3-1.6 mm) (18). The targeting error, biopsy error and target displacement for a transrectal biopsy device were 2.2 mm (range 0.5-5.7 mm), 5.1 mm (range 1.6-11.0 mm) and 5.4 mm (range 1.6-11.1 mm) respectively. Although the targeting error was less compared to our results, the biopsy error and target displacement were in concordance with our results (19).

MR-guided TRUS biopsy may be an alternative to MR-guided biopsy in the future because its availability and is probably less expensive. However, initial results show registration errors around three millimeter in phantoms and patients (20-23). In addition to this error is the targeting error and tissue deformation which together determine the ability to sample a CSL.

The anatomical landmarks chosen in the MR images to determine target displacement were selected manually. This may have introduced an error, since it is difficult to select exactly the same position. Automatic registration would be an alternative to diminish this error. However, automatic registration is difficult and introduces errors as well (15). Furthermore, the images that need to be registered are different in the area of the target, because of the presence of the needle, causing a line shape void in the area where best registration is needed.

The biopsy procedures with the robotic and manual techniques were not performed by the same radiologist. To overcome the limitation of inter-variability, the performing physician of each procedure performed the biopsy session in consensus with the first author who attended all sessions. Despite the fact that patient selection for each technique was not randomly chosen, both groups had similar patient characteristics (Table 2). The number of cores taken during TRUS-guided biopsy was not available for most patients in both groups.

In the first patient a gradient-echo sequence was used to determine needle trajectory and target displacement. The needle artefact size was acceptable, varying from 3.5 mm to 4.5 mm. In the second patient, the angle of the needle with the static magnetic field was larger. As a result, the artefact size of the needle increased to 8.5 mm. Therefore, we decided to use a 3D spin-echo sequence in which the signal void around the needle was less influenced by distortions of the magnetic field. Needle artefact size now varied from 3.8 to 4.7 mm.

The quantitative method described to determine target displacement cannot discriminate between patient motion, prostate motion and tissue deformation. However, our results demonstrated that most target displacement was in the direction of the needle trajectory suggesting that most of the target displacement was caused by needle insertion.

Hambrock et al. found a median imaging time of 35 min for MR-guided biopsy (24). In our study, we reported the total procedure times (including patient preparation) for the robotic and manual techniques. Although manipulation time was shorter when using the robotic technique, the total procedure time was longer compared to the manual technique. Positioning of the patient was a precise and time-consuming process. In case of incorrect positioning the whole set-up did not fit inside the scanner bore, or the range of motion of the robotic technique was impaired. Furthermore, a connection with the IFE software was necessary for real-time image guidance. Even for small adjustments in needle-guide direction, a interaction with the IFE was necessary including manual selection of the correct slice direction through the needle guide. Furthermore, some actions were only possible from behind the MR-console (e.g. measurement tool); the operator had to switch constantly between MR console and IFE monitor during the procedure. Altogether this led to an extension of the procedure time.

Image registration during the biopsy procedure can correct for target displacement and may attribute to reduce the biopsy error (25). Nevertheless, image registration is often a time consuming process. Furthermore, our results suggested that movement of the target was mainly caused by needle insertion. Image registration would not correct for prostate motion due to needle insertion. Deformation models of the prostate to predict tissue deformation due to needle insertion may help to overcome this problem (26). Other alternatives are different techniques for needle insertion, such as rotating needles and tapping devices (27-30).

Promising treatment types in the MR-scanner such as focal cryosurgery (31) and laser ablation (32) are now under investigation. Major advantages of treatment in the MR scanner are the ability of soft tissue imaging and monitoring (for example temperature mapping) (33). Robotics will play an important role in the future during treatment in the MR since accurate needle placement is required.

In spite of the fact that the results are comparable regarding accuracy and speed, the larger biopsy error and the extended technical effort of the robotic technique make the manual technique - currently - more suitable to perform MR-guided biopsy. Furthermore, this study provided a better insight in displacement of the target during in-vivo biopsy procedures.

References

1. Mian BM, Naya Y, Okihara K et al. Predictors of cancer in repeat extended multisite prostate biopsy in men with previous negative extended multisite biopsy. *Urology* 2002;60:836-840
2. Roehl KA, Antonor JA, Catalona WJ. Serial biopsy results in prostate cancer screening study. *J Urol* 2002;167:2435-2439
3. Hambrock T, Somford DM, Hoeks C et al. Magnetic resonance imaging guided prostate biopsy in men with repeat negative biopsies and increased prostate specific antigen. *J Urol* 2010;183:520-527
4. Schouten MG, Ansems J, Renema WKJ et al. The accuracy and safety aspects of a novel robotic needle guide manipulator to perform transrectal prostate biopsies. *Med Phys* 2010;37:4744-4750
5. Stamey TA, Freiha FS, McNeal JE et al. Localized prostate cancer. Relationship of tumor volume to clinical significance for treatment of prostate cancer. *Cancer* 1993;71:933-938
6. Stone NN, Roy J, Hong S et al. Prostate gland motion and deformation caused by needle placement during brachytherapy. *Brachytherapy* 2002;1:154-160
7. Lagerburg V, Moerland MA, Lagendijk JJ et al. Measurement of prostate rotation during insertion of needles for brachytherapy. *Radiother Oncol* 2005;77:318-323
8. Damore SJ, Syed AM, Puthawala AA et al. Needle displacement during HDR brachytherapy in the treatment of prostate cancer. *Int J Radiat Oncol Biol Phys* 2000;46:1205-1211
9. Yakar D, Schouten MG, Bosboom DG et al. Feasibility of a pneumatically actuated mr-compatible robot for transrectal prostate biopsy guidance. *Radiology*. 2011
10. Lorenz SR, Kirchberg KJ, Zuehlsdorff S et al. Interactive frontend (IFE): a platform for graphical MR scanner control and scan automation. *Proc Intl Soc Mag Reson Med* 2005;13:2170
11. Yutzey SR, Duerk JL. Pulse sequences and system interfaces for interventional and real-time MRI. *J Magn Reson Imaging* 2008;27:267-275
12. Beyersdorff D, Winkel A, Hamm B et al. MR imaging-guided prostate biopsy with a closed MR unit at 1.5 T: initial results. *Radiology* 2005;234:576-581
13. Huisman HJ, Fütterer JJ, van Lin EN et al. Prostate cancer: precision of integrating functional MR imaging with radiation therapy treatment by using fiducial gold markers. *Radiology* 2005;236:311-317
14. Fischer GS, Iordachita I, Csoma C et al. MRI-compatible pneumatic robot for transperineal prostate needle placement. *IEEE/ASME Trans Mechatron* 2008;13:295-305
15. Tokuda J, Fischer GS, DiMaio SP et al. Integrated navigation and control software system for MRI-guided robotic prostate interventions. *Comput Med Imaging Graph* 2010;34:3-8
16. Muntener M, Patriciu A, Petrisor D et al. Transperineal prostate intervention: robot for fully automated MR imaging system description and proof of principle in a canine model. *Radiology* 2008;247:543-549
17. van den Bosch MR, Moman MR, van Vulpen VM et al. MRI-guided robotic system for transperineal prostate interventions: proof of principle. *Phys Med Biol* 2010;55:133-140
18. Zangos S, Melzer A, Eichler K. MR-compatible assistance system for biopsy in a high-field-strength system: initial results in patients with suspicious prostate lesions. *Radiology* 2011;59:903-10
19. Xu H, Lasso A, Vikal S et al. Accuracy validation for MRI-guided robotic prostate biopsy. *Medical Imaging* 2010;762517-762518
20. Hu Y, Ahmed HU, Taylor Z et al. MR to ultrasound registration for image-guided prostate interventions. *Med Image Anal*. 2010
21. Karnik VV, Fenster A, Bax J et al. Assessment of image registration accuracy in three dimensional transrectal ultrasound guided biopsy. *Med Phys* 2010;37:802-813
22. Martin S, Baumann M, Daanen V et al. MR prior based automatic segmentation of the prostate in TRUS images for MR/ TRUS data fusion. *Biomedical Imaging: From Nano to Macro, IEEE International Symposium* 2010;640-643
23. Singh AK, Kruecker J, Xu S et al. Initial clinical experience with real-time transrectal ultrasonography-magnetic resonance imaging fusion-guided prostate biopsy. *BJU Int* 2008;101:842-845
24. Hambrock T, Fütterer JJ, Huisman HJ et al. Thirty-twochannel coil 3T magnetic resonance-guided biopsies of prostate tumor suspicious regions identified on multimodality 3T magnetic resonance imaging: technique and feasibility. *Invest Radiol* 2008;43:686-694
25. Tadayyon H, Lasso A, Gill S et al. Target motion compensation in MRI-Guided prostate biopsy with static images. *EMBS Engineering in Medicine and Biology Society (EMBC), Annual International Conference* 2010;5416-5419
26. Misra S, Macura KJ, Ramesh KT et al. The importance of organ geometry and boundary constraints for planning of medical interventions. *Med Eng Phys* 2009;31:195-206
27. Abolhassani N, Patel R, Moallem M. Control of soft tissue deformation during robotic needle insertion. *Minim Invasive Ther Allied Technol* 2006;15:165-176
28. Lagerburg V, Moerland MA, van Vulpen VM et al. A new robotic needle insertion method to minimise attendant prostate motion. *Radiother Oncol* 2006;80:73-77
29. Lagerburg V, Moerland MA, Konings MK et al. Development of a tapping device: a new needle insertion method for prostate brachytherapy. *Phys Med Biol* 2006;51:891-902
30. Meltner MA, Ferrier NJ, Thomadsen BR. Observations on rotating needle insertions using a brachytherapy robot. *Phys Med Biol* 2007;52:6027-6037
31. Lambert EH, Bolte K, Masson P et al. Focal cryosurgery: encouraging health outcomes for unifocal prostate cancer. *Urology* 2007;69:1117-1120
32. Lindner U, Lawrentschuk N, Weersink RA et al. Focal laser ablation for prostate cancer followed by radical prostatectomy: validation of focal therapy and imaging accuracy. *Eur Urol* 2010;57:1111-1114
33. de Senneville BD, Mougnot C, Quesson B et al. MR thermometry for monitoring tumor ablation. *Eur Radiol* 2007;17:2401-2410

CHAPTER 8.0 AUTOMATED REAL-TIME NEEDLE-GUIDE TRACKING FOR FAST 3T MR-GUIDED TRANSRECTAL PROSTATE BIOPSY: A FEASIBILITY STUDY

*Patrik Zamecnik, Martijn G. Schouten, Axel J. Krafft,
Florian Maier, Heinz-Peter Schlemmer, Jelle O. Barentsz,
Michael Bock, Jurgen J. Fütterer*

Radiology 2014 Dec;273(3):879-86

Abstract

Purpose: To assess the feasibility of automatic needle-guide tracking by using a real-time phase-only cross correlation (POCC) algorithm-based sequence for transrectal 3T in bore magnetic resonance (MR)-guided prostate biopsies.

Materials and methods: This study was approved by the ethics review board, and written informed consent was obtained from all patients. Eleven patients with a prostate-specific antigen level of at least 4 ng/mL and at least one transrectal ultrasonography-guided biopsy session with negative findings were enrolled. Cancer suspicious lesions were identified on 3T multi-parametric MR images. During a subsequent MR-guided biopsy, the cancer suspicious lesions were reidentified and targeted by using the POCC-based tracking sequence. Besides testing a general technical feasibility of the biopsy procedure by using the POCC-based tracking sequence, the procedure times were measured, and a pathologic analysis of the biopsy cores was performed.

Results: Thirty-eight core samples were obtained from 25 cancer suspicious lesions. It was technically feasible to perform the POCC-based biopsies in all cancer suspicious lesions in each patient, with adequate biopsy samples obtained with each biopsy attempt. The median size of the cancer suspicious lesions was 8 mm (range, 4-13 mm). In each cancer suspicious lesion (median number per patient, two; range, 1-4), a median of one core sample per lesion was obtained (range, 1-3). The median time for guidance per target was 1.5 minutes (range, 0.7-5 minutes). Nineteen of 38 core biopsy samples contained cancer.

Conclusion: This study shows that it is feasible to perform transrectal 3T MR-guided biopsies by using a POCC algorithm based real-time tracking sequence.

Introduction

Currently, a systematic transrectal ultrasonography (TRUS)-guided biopsy session with up to 10-12 biopsy cores is the reference standard for prostate cancer detection. However, the sensitivity for prostate cancer detection with TRUS is poor: In men clinically suspected of having this disease, detection rates of 30%-40% have been reported (1,2). TRUS-guided prostate biopsies may have false-negative rates of up to 23% (3). For a second TRUS-guided biopsy, the cancer detection rate was only in the range of 10%-17% (4-6).

Multi-parametric magnetic resonance (MR) imaging is currently the preferred imaging modality for the prostate (7). On the basis of these results, MR-compatible biopsy systems were developed to allow the use of MR imaging to guide prostate biopsies. Initial results with MR-guided prostate biopsies were very promising, showing high tumor detection rates (up to 59% in patients with repeat negative TRUS-guided biopsy findings) and reduced number of biopsy cores per patient (8-10). Unfortunately, the mean procedure time for an in-bore MR-guided biopsy is substantially longer than that with the TRUS-guided biopsy session (range, 39-76 minutes vs 15-20 minutes) (11,12), which considerably limits the clinical applicability of the procedure. Long procedure times in the MR imaging environment are primarily caused by the time required for manual alignment of the imaging planes with the biopsy needle trajectory.

A fast real-time tracking sequence by using a phase-only cross correlation (POCC) algorithm was developed (13,14), which showed promising experimental results in animals (15). For this kind of real-time instrument or needle-guide tracking, a combination of the POCC algorithm and a common fast imaging sequence (for example, fast low-angle shot or balanced steady-state free precession) is used. The POCC algorithm-based tracking sequence is able to automatically recognize the position of the needle guide and align the imaging plane with the needle axis in nearly real time. Thus, imaging is linked to the device, and instrument handling becomes very similar to that in a TRUS-guided biopsy. In particular, the time-consuming procedure steps during guidance (requiring the physician to walk in and out of the imaging room to adjust the needle guide during the procedure) are eliminated, which may result in a substantial reduction in procedure time.

The POCC-based tracking sequence was previously evaluated for geometric accuracy and operational stability, with a mean target accuracy \pm standard deviation of 1.5 mm \pm 0.9, and it has been used successfully in MR interventions in animal experiments (15).

The purpose of this study was to assess the feasibility of automatic needle-guide tracking by using a real-time POCC algorithm-based sequence for transrectal 3T in-bore MR-guided prostate biopsies.

Materials and methods

Patients

This study was approved by the ethics review board, and written informed consent was obtained from all patients. Eleven men with a prostate specific antigen (PSA) level of 4 ng/mL and higher and a history of at least one previous negative TRUS-guided biopsy finding were enrolled in our study (the patients' characteristics are summarized in Table 1). This study was performed during May and June 2011. All patients had cancer suspicious lesions (CSLs) identified in a diagnostic 3T multi-parametric MR examination that consisted of T2-weighted, diffusion-weighted, and dynamic contrast material-enhanced imaging. In a subsequent MR-guided biopsy session, the CSLs were reidentified and targeted by using a real-time POCC-based automatic tracking sequence. Exclusion criteria for this study were general contraindications to MR imaging.

Parameter	Value
Number of patients	11
Median patient age (years)	64 (range: 59-71)
Median PSA level (ng/mL)	13.9 (range: 5-36.6)
Median no. of negative TRUS-guided biopsy procedures per patient	2 (range: 1-4)
Mean prostate volume (mL)	72 (range 49-100)
Median number of repeated negative TRUS-guided biopsy sessions	2 (range 1-4)

Table 1: Patient characteristics. PSA = prostate-specific antigen

Multi-parametric MR imaging

Diagnostic MR imaging of the prostate was performed with a 3T MR system (Skyra; Siemens Healthcare, Erlangen, Germany) and a pelvic phased-array coil. Peristalsis was suppressed with an intramuscular administration of 20 mg butylscopolamine bromide (Buscopan; Boehringer-Ingelheim, Ingelheim, Germany) and 1 mg glucagon (Glucagen; Nordisk, Gentofte, Denmark) approximately 5 minutes before imaging.

The multi-parametric MR imaging protocol included T2-weighted imaging in sagittal, coronal, and axial planes and axial diffusion-weighted imaging (DWI) from which maps of the apparent diffusion coefficient (ADC) were calculated automatically. By using intravenous administration of contrast agent (0.1 mmol/kg body weight of gadoterate meglumine [Dotarem] administered with a 3 mL/sec flow; Guerbet, Paris, France), dynamic contrast-enhanced (DCE) MR imaging was performed by using a three dimensional T1-weighted sequence with the same section orientation and image center as those with the transverse T2-weighted sequence. The contrast agent was injected after 9 seconds (ie, after two

repetitions of T1-weighted image acquisitions) after the sequence was started. Detailed pulse sequence parameters are provided in Table 2. Before contrast agent injection, the same transverse three-dimensional T1-weighted gradient-echo sequence was used (with the exception of repetition time msec/ echo time msec of 800/1.6 and a flip angle of 8°) to obtain proton-density images at identical section locations to allow calculation of the relative gadolinium chelate concentration curves (16).

Sequence	Repetition time/ Echo time (msec)	Slice thickness (mm)	Field of view (mm ²)	Matrix	Additional parameters
T2-weighted turbo spin echo	4010/107	3	180x180	320x320	Flip angle: 120°
Diffusion weighted image	2300/61	3	256x256	128x128	b-values: 50, 500, and 800 s/mm ²
Dynamic contrast enhanced (3D-gradient echo)	32/1.47	3	230x230	128x128	35 measurements within 180 s Flip angle: 10°
Balanced steady-state free precession (confirmation scan)	4.4/2.2	3	228x228	256x256	Flip angle: 70° Scan duration: 9s
Balanced steady-state free precession (phase-only cross correlation)	4/1.9	4	280x280	256x256	Temporal resolution: 1/s Flip angle: 70°

Table 2: sequence parameters used for multi-parametric MR imaging and POCC guidance.

Multi-parametric MR image interpretation

Images in all patients were interpreted together by two radiologists with 7 and 5 years of experience in prostate MR imaging, and the final diagnosis was achieved in consensus. The interpretation of diagnostic MR images was performed by using the volume transfer constant pharmacokinetic parameter maps calculated from DCE MR imaging acquisitions based on the standard two-compartment model (17) with corrected curve fit algorithm (16) and DWI and ADC maps. Both the pharmacokinetic parameter and the ADC maps were overlaid as colour maps on the T2-weighted MR images. The CSLs were defined by using the Prostate

Imaging Reporting and Data System, or PIRADS, classification, according to European Society of Urogenital Radiology prostate MR guidelines in 2012 (18). The CSLs were defined as lesions with final PIRADS scores of 4 and 5, where clinically significant cancer is likely or highly likely to be present.

MR-guided biopsy procedure

The biopsy was performed by one of the two evaluating radiologists. A manually adjustable MR-compatible biopsy instrument holder (DynaTrim; Invivo, Schwerin, Germany) was used as described previously to hold the MR compatible biopsy device (10,11,19). The holder contains a plastic cylinder (Invivo) filled with contrast agent solution (ratio of gadopentetate dimeglumine to water, 1:100), which serves as passive endorectal marker and needle guide. The spine and body array coils of the MR imaging system (Trio; Siemens Healthcare) were used for MR signal reception. After positioning of the patient in prone position, the passive marker (needle guide) was inserted into the patient's rectum. To facilitate the insertion of the needle guide and for local anaesthesia, a topical anaesthetic gel was used. The needle guide was connected to the instrument holder, and the holder was fixed on the MR table. The biopsy MR protocol consisted of a short diagnostic part (reidentification of the CSLs) and the biopsy protocols. The diagnostic part included axial T2-weighted turbo spin-echo and DWI sequences to assess the position of the needle guide and to reidentify the CSLs within the prostate by means of comparison with the prior diagnostic multi-parametric MR images. A workstation that showed the prior diagnostic MR images was installed next to the MR console to facilitate the identification of the CSLs.

After lesion identification, the needle guide was slowly moved inside the rectum and aligned with the CSLs by using the real-time POCC-based tracking sequence, providing T2-weighted images (balanced steady-state free precession or true fast imaging with steady-state precession sequence; 4.0/1.9; flip angle, 70°; resolution, 1.2 x 1.2 x 4.0 mm; and temporal resolution, one image acquired per second). Then, the performing physician in the MR room reached into the imaging bore to manipulate the needle guide orientation. The sequence automatically aligned the imaging plane with the symmetry axis of the needle guide (Fig. 1 - page 118). The POCC algorithm-based tracking sequence worked as follows: As a start, two parallel so-called tracking sections (in our study, T1-weighted fast low-angle shot sequence; distance between these sections > 40 mm) are manually positioned perpendicular to the needle guide symmetry axis. The needle guide appears on these tracking sections as a ringlike structure. By using the POCC algorithm, the three dimensional positions of these ringlike structures are calculated (13,15). In this manner, the axis of the needle guide is defined, and the targeting image plane - which is then finally displayed to the performing physician - is automatically aligned with it. For the targeting image, a balanced steady state free precession sequence was used to provide contrast enhancement on T2-weighted images. The image plane could be changed manually (sagittal, axial, or coronal view) by the imaging operator to position the needle guide in three dimensions. For online guidance, the real-time images were projected directly into the MR room through

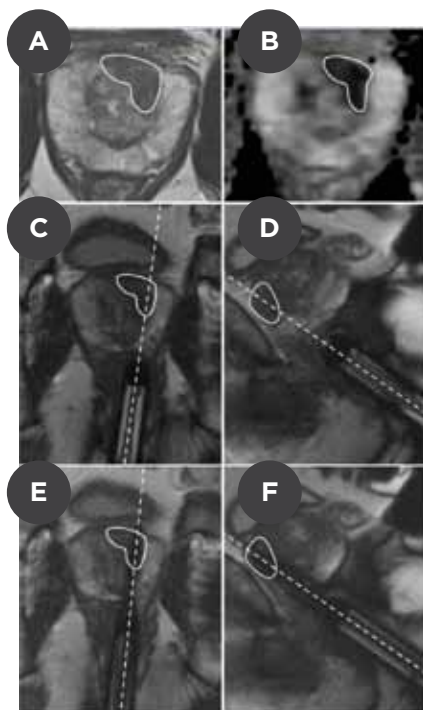


Figure 1: Images in a 64-year-old man with prostate cancer (Gleason score: 4+4=8) in the left anterior apical part of the transition zone (delineated with solid line) (A-F). Diagnostic axial T2-weighted turbo spin-echo image (A). Diagnostic axial ADC map (B). Axial (C) and sagittal (D) images used for needle guide positioning. The dotted line illustrates the axis of the endorectal marker (ie, the trajectory of the biopsy needle). Needle position confirmation acquisition shows the position of the biopsy needle in the cancer suspicious lesion (E,F).

the MR-room window by using a video projector located outside the MR room (Fig. 2). When the calculated needle-guide axis (ie, the planned needle trajectory that was overlaid onto the real-time image as a green line) was aligned with the CSLs, the instrument holder was fixed, and the POCC sequence was stopped. Two additional confirmation acquisitions (in axial and sagittal planes) performed by using a standard balanced steady-state free precession sequence (duration, 9 seconds each; for detailed parameters, see Table 2) were used to control the position of the needle guide before executing the biopsy. After the confirmation acquisitions, the MR table was moved out of the imager, and a biopsy sample was obtained by using an MR-compatible, 18-gauge fully automatic core-needle double-shot biopsy gun (Invivo) with a needle length of 175 mm and a tissue core sampling length of 17 mm. After the biopsy sample was obtained, the patient was placed back into the imager, while the needle was left in situ to verify the needle position in the target by using the balanced steady-state free precession sequence (the same as done for the confirmation acquisition; see Table 2) in two orientations, axial and sagittal. In the case of additional CSLs, the guidance process was continued. From small lesions (<7 mm in diameter), more additional biopsy samples were obtained to acquire enough biopsy material for pathologic evaluation. During the whole biopsy procedure, the patient remained in a prone position. The clinical status of the patient was monitored by the performing physician while performing the biopsy (in terms of pain or bleeding), as well as after the biopsy (in terms of infection).



Figure 2: Photographs demonstrate the interaction between the physician performing the real-time biopsy (left) and the imaging operator (right). The physician performing the biopsy is looking backward to the screen with the real-time images (the monitor is hanging on the cabin window) while moving the needle guide with his hand inside of the imager. The operator is controlling the POCC sequence, including the change of real-time imaging section orientation (on demand, for example from axial to sagittal orientation).

Procedure time assessment

The procedure times were assessed by the retrospective evaluation of the Digital Imaging and Communications in Medicine (DICOM) header information of the acquired images. The following time parameters were assessed: guidance time (time needed for movement of the needle guide until the alignment of its axis with the CSLs or between two lesions) and sampling time (time needed for performing of the sampling and the confirmation acquisitions). The entire biopsy procedure time was defined as a sum of the guidance and sampling times.

Evaluation of the biopsy targeting accuracy

For each of the CSLs, the geometric distance (d) between the biopsy needle axis and corresponding center point of the lesion was calculated to assess the targeting accuracy. The center points of the lesions were defined by conducting image analysis of the ADC images as the point with the lowest ADC value. Distance (d) was defined as the geometric distance between the needle axis and the center point of the lesions (Fig. 3).

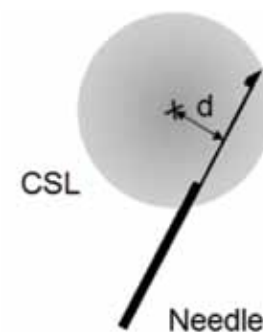


Figure 3: Schematic illustrates the calculation of the distance d for quantification of the accuracy of the biopsy by using the POCC tracking sequence. x is the center point of a cancer suspicious lesion (CSL), defined as the lowest ADC value within the lesion.

Histopathologic analysis

All biopsy samples were analyzed by means of standard histopathologic examination to confirm the presence of prostate cancer or benign findings. Therefore, samples were routinely fixed in formalin, embedded in paraffin, and stained with hematoxylin-eosin with subsequent evaluation. For every sample that was positive for prostate cancer, a Gleason score and tumour volume percentage in the sample was determined.

Results

POCC guidance, CSLs, and samples

A total of 25 CSLs were identified in 11 patients, and 38 core biopsy samples were obtained. The median of the maximum diameter of CSLs on T2-weighted images was 8 mm (range, 4-13 mm). All detailed specifications of the CSLs are summarized in Table 3. All biopsy samples were obtained with the first attempt in each patient, and biopsy samples were obtained from all CSLs.

In some cases it was uncomfortable for the performing physician to manipulate the needle guide, because it was located near the isocenter of the closed-bore magnet (potentially a long distance from the gantry); however, the whole procedure was technically feasible. If the needle guide was manipulated during guidance by more than 50° in less than 1 second, the orientation - and, consequently, the guidance - was lost. In such cases, a manual restart of the sequence was needed, which took about 20-30 seconds. This occurred two times during our study, when the marker was rapidly repositioned to the contralateral side of the prostate.

There were no complications during or after the biopsy in terms of severe pain (no pain relievers were needed), bleeding, or infection. A median of two CSLs (range, 1-4 lesions) per patient were targeted. A median of one core sample per lesion was obtained (range, 1-3 samples), and a median of three biopsy samples (range, 1-6 samples) per patient was obtained.

Procedure time and targeting accuracy

The median time needed for the entire biopsy procedure (ie, time needed for guidance and biopsy sampling of all CSLs per patient) was 32 minutes (range, 14-48 minutes). The median time for guidance per target (movement of the needle guide between two lesions) was 1.5 minutes (range, 0.7-5 minutes). The mean measured displacement from the target center (d) in all lesions was 1.7 mm ± 0.8.

Histopathologic findings

In seven of 11 patients, a diagnosis of prostate cancer was assigned on the basis of the biopsy samples obtained (detection rate of 64%). Nineteen of 38 core biopsy samples (50%) contained prostate cancer (Gleason scores: 3+3, 3+5, 3+4, and 4+3). Eleven core biopsy samples contained prostatitis. In eight core samples, fibrotic or unspecific changes were found.

Parameter	Value
Number of CSLs	25
Median maximum diameter of CSLs on T2-weighted images (mm)	8 (range: 4-13)
Median maximum diameter of CSLs on DWI images (mm)	7 (range: 3-11)
Number of CSLs localized in the right apex	
Peripheral zone	3
Transition zone	1
Number of CSLs localized in the right mid prostate	
Peripheral zone	6
Transition zone	2
Number of CSLs localized in the right basis	
Peripheral zone	1
Transition zone	1
Number of CSLs localized in the left apex	
Peripheral zone	3
Transition zone	0
Number of CSLs localized in the left mid prostate	
Peripheral zone	3
Transition zone	1
Number of CSLs localized in the left basis	
Peripheral zone	4
Transition zone	0
Median distance of the CSLs from the anterior rectum wall (mm)	19 (range: 8-38)
Median distance of the CSLs from the midline left (mm)	14 (range: 5-26)
Median distance of the CSLs from the midline right (mm)	17 (range: 9-27)

Table 3: characteristics of the cancer suspicious lesions (CSLs). PZ = peripheral zone, TZ = transition zone

Discussion

In this study, all CSLs could be identified during the targeting process by using the POCC approach, and biopsies were performed. While this study was not designed to prove the detection rate in patients with clinical suspicion of prostate cancer, our detection rate (64%, seven of 11 patients) was consistent and even higher than that reported in other studies of MR-guided prostate biopsies (8-11). The mean measured distance from the center of the target CSLs was 1.7 mm ±

0.8. This is consistent with the result reported in our prior animal experiment with the POCC-based tracking sequence ($1.5 \text{ mm} \pm 0.9$) (15). Our current results show sufficient clinical accuracy comparable to that reported with other MR-guided prostate biopsy techniques (8,11,20).

The automated POCC algorithm - based tracking sequence substantially accelerates and shortens the biopsy procedure time, since walking into the imaging room repeatedly to adjust the needle guide direction and the manual adjustments of the confirmation acquisitions is no longer necessary. In our study, however, we performed additional confirmation acquisitions directly before biopsy to confirm the orientation of the needle guide in relation to the CSL before needle insertion. In our study, there was no patient that needed additional readjustment of the needle after the additional confirmation acquisition.

During our study, safe and precise guidance was demonstrated. The automatic section alignment of the POCC algorithm-based tracking sequence facilitated the targeting process and made handling very similar to that in ultrasound-guided procedures. The temporal resolution of the sequence during tracking of 1 second per section was fast enough to target the CSL in nearly real time. Compared with the published mean procedure times for MR-guided biopsies (range, 39-76 minutes) (11,12), a considerable time improvement was achieved in this study. The entire biopsy procedure time needed was about 30 minutes (median, 32 minutes). The median time for guidance per target (ie, movement of the needle guide between two CSLs) was only 1.5 minutes. However, these results need to be validated in future studies with larger numbers of patients. Even though our procedure time is still longer than that for TRUS-guided biopsies, reduction in procedure time may be achieved after more training of the personnel.

One of the major factors hampering the availability of any new MR-based diagnostic or therapeutic technique is the need for additional, often specially designed and therefore costly MR-compatible hardware. In contrast, our study was performed by using standard, commercially available hardware only (instrument holder, needle guide, and biopsy needle), without any need for new hardware or hardware modifications of the closed-bore MR system. This fact could be very important for the potential availability of this technique in the future. Because of the versatility of the POCC algorithm-based tracking sequence, it can also be used to guide focal therapies (for example, cryoablation or laser-induced thermoablation) (21,22).

First studies were conducted to evaluate the new prostate biopsy technique with MR imaging/TRUS fusion. This technique was developed to make the TRUS-guided biopsies more accurate by using fused MR imaging and real-time TRUS images during the biopsy. The first published results are promising in terms of tumour detection (23,24), but there are no precise data concerning the procedure times. This technique also requires special MR imaging/TRUS-fusion software, which has to be evaluated in a larger number of patients.

During our study, some minor issues arose. It was uncomfortable to reach into the magnet and to hold the needle guide by hand when it was located close to the isocenter of the magnet. Potentially, some performing physicians might not

be able to reach the needle guide, particularly when MR systems with standard bore length and small bore diameters are used or when the patient's legs are in the way, because of the possibly long distance from the gantry to the isocenter of the magnet. Accessibility might be further facilitated in future applications of the sequence, as modern MR systems with wider bore openings and shorter bore lengths become more available.

The most important limitation of our study was that the demonstrated applicability of the POCC algorithm-based sequence for automatic tracking was limited to the transrectal prostate biopsy approach by using a specific commercial needle guide system.

In conclusion, it is feasible to use the POCC-based automatic tracking sequence to perform 3T MR-guided prostate biopsies. This technique has the potential to accelerate MR-guided prostate interventions.

References

1. Halpern EJ, Strup SE. Using gray-scale and color and power Doppler sonography to detect prostatic cancer. *American Journal of Roentgenology*. 2000;174(3):623-627.
2. Terris MK. Sensitivity and specificity of sextant biopsies in the detection of prostate cancer: Preliminary report. *Urology*. 1999;54(3):486-489.
3. Rabbani F, Stroumbakis N, Kava BR, et al. Incidence and clinical significance of false-negative sextant prostate biopsies. *Urologe-Ausgabe A*. 1998;159(4):1247-1250
4. Mian BM, Naya Y, Okihara K, et al. Predictors of cancer in repeat extended multisite prostate biopsy in men with previous negative extended multisite biopsy. *Urology*. 2002;60(5):836-840.
5. Philip J, Hanchanale V, Foster CS, et al. Importance of peripheral biopsies in maximising the detection of early prostate cancer in repeat 12-core biopsy protocols. *BJU Int*. 2006;98(3):559-562.
6. Roehl KA, Antenor JAV, Catalona WJ. Serial biopsy results in prostate cancer screening study. *Journal of Urology*. 2002;167(6):2435-2439.
7. Hoeks CM, Barentsz JO, Hambrock T, et al. Prostate cancer: multiparametric MR imaging for detection, localization, and staging. *Radiology*. 2011;261(1):46-66.
8. Hambrock T, Somford DM, Hoeks C, et al. Magnetic Resonance Imaging Guided Prostate Biopsy in Men With Repeat Negative Biopsies and Increased Prostate Specific Antigen. *Journal of Urology*. 2010;183(2):520-527.
9. Anastasiadis AG, Lichy MP, Nagele U, et al. MRI-guided biopsy of the prostate increases diagnostic performance in men with elevated or increasing PSA levels after previous negative TRUS biopsies. *Eur Urol*. 2006;50(4):738-749.
10. Beyersdorff D, Winkel A, Hamm B, et al. MR imaging-guided prostate biopsy with a closed MR unit at 1.5 T: Initial results. *Radiology*. 2005;234(2):576-581.
11. Pondman KM, Futterer JJ, ten Haken B, et al. MR-guided biopsy of the prostate: An overview of techniques and a systematic review. *Eur Urol*. 2008;54(3):517-527.
12. Zangos S, Herzog C, Eichler K, et al. MR-compatible assistance system for puncture in a high-field system: device and feasibility of transgluteal biopsies of the prostate gland. *Eur Radiol*. 2007;17(4):1118-24.
13. de Oliveira A, Rauschenberg J, Beyersdorff D, et al. Automatic passive tracking of an endorectal prostate biopsy device using phase-only cross-correlation. *Magnetic Resonance in Medicine*. 2008;59(5):1043-50.
14. Maier F, Krafft AJ, Stafford JR, et al. 3D passive marker tracking for MR-guided interventions. *Proc Intl Soc Mag Reson Med*. 2011;3749(19).
15. Krafft AJ, Zamecnik P, Maier F, et al. Passive marker tracking via phase-only cross correlation (POCC) for MR-guided needle interventions: Initial in vivo experience. *Phys Med*. 2012;12.
16. Huisman HJ, Engelbrecht MR, Barentsz JO. Accurate estimation of pharmacokinetic contrast-enhanced dynamic MRI parameters of the prostate. *Journal of Magnetic Resonance Imaging*. 2001;13(4):607-14.
17. Tofts PS, Brix G, Buckley DL, et al. Estimating kinetic parameters from dynamic contrast-enhanced T(1)-weighted MRI of a diffusible tracer: Standardized quantities and symbols. *Journal of Magnetic Resonance Imaging*. 1999;10(3):223-32.
18. Barentsz JO, Richenberg J, Clements R, et al. ESUR prostate MR guidelines 2012. *Eur Radiol*. 2012;22(4):746-57.
19. Nagel KNA, Schouten MG, Hambrock T, et al. Differentiation of Prostatitis and Prostate Cancer by Using Diffusion-weighted MR Imaging and MR-guided Biopsy at 3 T. *Radiology*. 2013;267(1):164-72.
20. Roethke M, Anastasiadis AG, Lichy M, et al. MRI-guided prostate biopsy detects clinically significant cancer: analysis of a cohort of 100 patients after previous negative TRUS biopsy. *World J Urol*. 2012;30(2):213-8.
21. Bomers JGR, Sedelaar JPM, Barentsz JO, et al. MRI-Guided Interventions for the Treatment of Prostate Cancer. *American Journal of Roentgenology*. 2012;199(4):714-20.
22. Gangi A, Tsoumakidou G, Abdelli O, et al. Percutaneous MR-guided cryoablation of prostate cancer: initial experience. *Eur Radiol*. 2012;22(8):1829-35.
23. Hadaschik BA, Kuru TH, Tulea C, et al. A novel stereotactic prostate biopsy system integrating pre-interventional magnetic resonance imaging and live ultrasound fusion. *J Urol*. 2011;186(6): 2214-2220.
24. Roethke MC, Kuru TH, Schultze S, et al. Evaluation of the ESUR PI-RADS scoring system for multiparametric MRI of the prostate with targeted MR/TRUS fusion-guided biopsy at 3.0 Tesla. *Eur Radiol*. 2014;24(2):344-352.

CHAPTER 9.0 SUMMARY AND DISCUSSION

This thesis describes some aspects of the symbiosis between imaging and robotics in magnetic resonance (MR)-guided prostate biopsy. The need for MRI targeted biopsy in the detection of prostate cancer was demonstrated in *chapter 2*. We identified differences between MR image-guided and transrectal ultrasound (TRUS)-guided biopsy regarding cancer locations and aggressiveness in order to get insight in the diagnostic limitations of both techniques (*chapters 3 and 4*). In *chapter 5* we investigated the differences in apparent diffusion coefficient (ADC)-values derived from diffusion weighted imaging (DWI) in patients with either prostatitis and prostate cancer. We investigated the feasibility of an MR-compatible robotic manipulator in a phantom and patients (*chapter 6 and 7*). In addition we addressed the feasibility of an automatic tracking sequence, which has the potential to improve the MR-guided biopsy procedure (*chapter 8*).

Need for MR-guided biopsy

Chapter 2 reports on the detection rate of prostate cancer found with MR-guided prostate biopsy in a large patient population. In total 438 patients with a prostate specific antigen (PSA) level >4 ng/mL and at least one previous negative TRUS-guided biopsy session were included. MR-guided prostate biopsy was performed in 265 of these patients. Prostate cancer detection rates were 25% for the entire study population (n=438) and 41% for the patients (n=265) who underwent MR-guided prostate biopsy. Furthermore, predominantly clinical significant tumours (87%) were detected with MR-guided biopsy.

In *chapter 3* we identified the location of histopathologically proven prostate cancer detected with MR-guided. In this retrospective study 176 out of 872 patients met the inclusion criteria (elevated PSA level and at least one negative TRUS-guided biopsy session). Prostate cancer was detected in 78% (138/176) of the patients and 73% (202/277) of the cancer suspicious lesions seen on multi-parametric MRI. The majority of the patients had intermediate or high risk cancer (93%; 128/138). Anterior involvement was high (75%; 132/176) and peripheral zone cancers were found in 30% (52/176) of the patients. Cancers with a maximum cancer core length (MCCL) ≥ 6 mm were more likely to be located in the anterior part of the prostate than were cancers with a core length of less than 6 mm (66% vs 6% respectively).

The location of significant prostate cancer lesions missed with MR- and TRUS-guided biopsy in biopsy naïve men at risk is described in *chapter 4*. All subjects underwent multi-parametric MRI and 12-core systematic TRUS-guided biopsy. MR-guided biopsy was performed in all patients with a PI-RADS 3 to 5 lesion on multi-parametric MRI (n=142). In total 191 lesions were found in 108 patients with significant prostate cancer. From these lesions, 74% (141/191) were defined as significant prostate cancer on either MR- or TRUS-guided biopsy. MR-guided biopsy detected 74% (105/141) of these lesions and this was 61% (86/141) with TRUS-guided biopsy, respectively. TRUS-guided biopsy detected significantly more lesions compared to MR-guided biopsy (140 vs 109). However, these lesions were often low-risk/not significant (39%).

Significant lesions missed with MR-guided had most often involvement of dorsolateral (58%) and apical (37%) segments and missed segments with TRUS-guided biopsy were located anteriorly (79%), anterior mid prostate (50%) and anterior apex (23%).

The results from *chapter 3* and *4* have clinical implications for both radiologists and urologists. For example to optimize biopsy scheme for TRUS-guided biopsy and systematic sampling with MRI targeted TRUS-biopsy.

In *chapter 5* we investigated whether it is possible to discriminate between prostatitis and prostate cancer based on ADC values using MR-guided biopsy as the standard of reference. The ADC values calculated from the diffusion weighted images (DWI) acquired during the biopsy procedure were correlated to the histopathology of the biopsy core. This was done by projecting bi-planar confirmation scans with the needle left in situ on the calculated ADC maps. By using this location, a region of interest was drawn manually with the size and extent of the most diffusion-restricted region on the ADC map, representing the biopsied cancer suspicious lesion. We concluded that DWI is a non invasive technique that demonstrated a significant difference in mean ADC of prostatitis ($1.08 \times 10^{-3} \text{ mm}^2/\text{s}$, $\text{SD} \pm 0.18$) and prostate cancer ($0.88 \times 10^{-3} \text{ mm}^2/\text{s}$, $\text{SD} \pm 0.15$). However, its usability in clinical practice is limited due to a high degree of overlap.

Robotic assisted MR-guided biopsy

In *chapter 6* the feasibility of an in-house developed pneumatically actuated MR-compatible robotic manipulator was evaluated in a phantom study. With the robotic manipulator the needle guide direction can be controlled outside the magnet room under real-time MR image guidance. Consequently the patient does not need to be moved in and out of the magnet bore during needle guide manipulation.

The failure mode and effect analysis (FMEA) and safety measurements of the robotic manipulator showed minor items for improvement. The average time needed for manipulation to place the needle guide in the desired position was 5 minutes. The average total procedure time (including set up) to perform a biopsy was less than 30 minutes. For needle placement the average in-plane error was 3.0 mm (range 0-5.6 mm). The manipulator prevented the need of moving the phantom in and out of the scanner bore for respectively imaging and manipulation of the needle guide. The results demonstrated great potential to improve the transrectal prostate biopsy procedure. The next step therefore was to establish the clinical feasibility of the system.

Chapter 7 evaluated the accuracy and speed of the novel robotic technique compared to the manual method in patients. The robotic and manual techniques demonstrated comparable results regarding mean targeting error (5.7 vs 5.8 mm, respectively) and mean target displacement (6.6 vs 6.0 mm, respectively). The mean biopsy error was larger (6.5 vs 4.4 mm) when using the robotic technique, although not significant. Mean procedure and manipulation times were 76 minutes and 6 minutes, respectively using the robotic technique and 61 minutes and 8 minutes

with the manual technique. Furthermore, it was observed that most of the target displacement was in the direction of the needle trajectory suggesting that most of the target displacement was caused by needle insertion.

The robotic technique prevented the need of moving the patient in and out of the scanner bore for imaging and manipulation of the needle-guide. In spite of the fact that the results are comparable regarding accuracy and speed, the extended technical effort of the robotic technique makes the manual technique - currently - more suitable to perform MR-guided biopsy.

The total procedure time with the robotic technique was longer compared to the results found in a phantom (*chapter 6*) and with the manual technique. Problems regarding patient positioning, limited range of motion and geometric constraints of the robotic technique have contributed to the limited gain in patients. Furthermore, the interaction with the real-time imaging software, robot controller and MR-console led to an extension of the procedure time. A real-time imaging sequence which has the potential to simplify these interactions was evaluated in the next chapter.

In *chapter 8* the feasibility of a fast real-time tracking sequence was demonstrated in patients. The tracking sequence can determine the 3D-position of the passive needle guide during MR image acquisition and show the imaging plane corresponding to the axis of the needle guide in nearly real-time. The patient remains inside the scanner bore during needle guide positioning and imaging. The median time needed for the entire biopsy procedure was 32 minutes (range 14-48 minutes). The median time for guidance per target (movement of the endorectal marker between two cancer suspicious lesions) was 1.5 minutes (range 0.7-5 minutes). From this study we can conclude that it is feasible to use the automatic tracking sequence to perform MR-guided prostate biopsies. This technique has the potential to accelerate MR-guided prostate interventions.

Suggestions for future research: which direction?

The ability of multi-parametric MRI to identify significant prostate cancer has made it possible to obtain targeted samples from lesions rather than systematically sampling the whole prostate with TRUS-guided biopsy (27). The introduction of the Prostate Imaging Reporting and Data System (PI-RADS) in 2012 was the first step in standardized and objective interpretation of multi-parametric MRI which is crucial to diminish the inter-observer variability in image interpretation (19). This system appears to have a good diagnostic accuracy in cancer detection, but no recommendation regarding the best threshold for biopsy can be provided (28). A newer version of the PI-RADS (version 2.0) classification was recently published and must be evaluated (29). Forthcoming from the results in chapter 4 it might be interesting to investigate a region dependent threshold for biopsy. This may improve cancer detection with multi-parametric MRI. For example, a threshold of PI-RADS 3 for lesions in the apical and dorsolateral regions and a threshold of PI-RADS 4,5 for lesions elsewhere in the prostate. Another approach which should be investigated in future research is computer aided diagnosis where quantitative image parameters are used to determine the likelihood of malignancy for cancer suspicious lesions (30).

In *chapter 2* we found evidence that MR-guided biopsy has a high detection rate in patients with an elevated PSA and repeated negative TRUS-guided biopsy sessions. Later, it was found that also in biopsy naïve men with elevated PSA, multi-parametric MRI followed by MR-guided-biopsy reduces the detection of low-risk cancer compared with TRUS-guided biopsy, while improving the overall detection of intermediate/high-risk cancer (31, 32). These results are in concordance with a recently published systematic review which concluded that multi-parametric MRI is able to detect significant prostate cancer in biopsy-naïve males and men with prior negative biopsies (18). Moreover, multi-parametric MRI of the prostate is an excellent technology for diagnosis, patient selection, treatment planning and follow-up (24). However, it has to be kept in mind that significant tumours can still be missed. Insight into the diagnostic limitations of both modalities (*chapters 3 and 4*) has clinical implications for both radiologists and urologists. For example to optimize biopsy sites for TRUS-guided biopsy and systematic sampling with MRI targeted TRUS-biopsy (33).

MRI targeted TRUS-biopsy is a technique which combines previously obtained multi-parametric MR images and real-time TRUS images to direct the biopsy needle to a cancer suspicious lesion. Currently, multiple devices are available which can broadly be classified by the fusion process as either rigid or non-rigid (34). Rigid fusion does not correct for changes in shape and position of the prostate at the time of biopsy. Non-rigid fusion aims to compensate for prostate deformation at the time of biopsy which can be achieved with elastic registration or by statistical motion modelling. Reported target registration errors of 5.1 (rigid) and 2.4 mm (non-rigid) in the mid plane of the prostate are reported, which increase at the apex and base (35). Even though the fusion algorithm of MRI and TRUS images is an important limitation (36), the overall detection rate of MRI targeted TRUS biopsy was higher compared to standard TRUS-guided biopsy (51% vs 43%) (34). Furthermore, MRI targeted TRUS biopsy detects more clinically significant cancers (33% vs 24%) (34). However, some clinically significant cancers may be missed using this approach, and the necessity of obtaining systematic biopsies in addition should be taken in consideration (33, 37).

Initial research in the field of MRI targeted biopsy has been performed in patients with clinical suspicion for prostate cancer with repeated negative TRUS-guided biopsy sessions. Currently, considerable research has been performed in biopsy naïve patients which found evidence that multi-parametric MRI is capable to mainly detect significant prostate cancer with a high negative predictive value in these patients (38). These results are promising in the field of prostate cancer screening and may contribute to a paradigm shift (39). However, it should be kept in mind that the current research is limited by the lack of a reliable and reasonable gold standard to compare with. Whole mount prostatectomy would be the most reliable tool for histopathologic evaluation but is ethically impossible in patients with no proven cancer on biopsy. An alternative approach is to use 5 mm transperineal template prostate mapping (40). The need for general anaesthesia and increased complication rate makes this a highly invasive technique and presents challenges in recruiting patients for clinical trials when less invasive alternatives are available

(40, 41). Furthermore, a universally accepted definition for significant cancer should be introduced and validated since the variability in definitions in the current research makes it difficult to compare and combine results for generalization to clinical practice.

The next step is to investigate which MRI targeted biopsy technique is the most suitable option for each specific patient. Variables such as number of previous negative TRUS-guided biopsy sessions, costs, lesions size and location on multi-parametric MRI may help to select patients and should be investigated in future research.

Besides tailored patient selection it is important to further evolve MRI targeted biopsy techniques. Most important limitation of the current MR-guided biopsy method is the procedure time on MRI which makes this technique not readily available in routine clinical practice yet. The robotic manipulator described in this thesis has the potential to shorten procedure time (*chapter 6*). However, due to the limited research performed in patients with the robotic manipulator (*chapter 7*), the current clinical value of this technique is unclear. Therefore, more clinical research needs to be done to investigate whether the implementation of robotics will improve MR-guided biopsy. Before further research is done in patients, some important aspects to improve the robotic manipulator are required. Most essential are size reduction, broader range of motion and integration of imaging, intervention planning and robotic manipulation within one user interface. A novel robotic manipulator, which incorporated these suggestions for improvement, is now being tested in our clinical practice.

The automatic needle guide tracking sequence described in *chapter 8* integrates imaging and intervention planning. This sequence has the potential to further incorporate imaging and robotic targeting. The next step is therefore to apply this tracking sequence during the robotic intervention.

Another interesting aspect, that needs further investigation to improve MR-guided biopsy accuracy, came forth of the results presented in *chapter 7*. It was found that movement of the target was mainly caused by needle insertion. Special techniques for needle insertion, such as rotating needles and tapping devices have been investigated to minimize target displacement (42-44). When these insertion techniques can be performed inside the scanner bore under real-time imaging, needle insertion will no longer be a blind process, as it is at the moment, and biopsy accuracy may be improved. Alternatively, deformation models of the prostate to predict tissue deformation due to needle insertion may help to overcome this problem (45).

The combination of tumour identification with imaging and accurate needle placement has not only changed the diagnostic process but also the concept of prostate cancer treatment. Minimally invasive therapies are increasingly applied for treatment of localized prostate cancer (14, 15). Major advantages of treatment in the MR scanner are the ability of soft tissue imaging for treatment guidance and monitoring (for example temperature mapping) (24). Likewise biopsy, accurate needle placement is required during treatment.

Conclusions

The following overall conclusions can be drawn:

1. MR-guided biopsy of 3T multi-parametric MRI detected cancer suspicious lesions has a high detection rate of 41% for predominantly clinically significant prostate cancer (87%) in patients with an elevated PSA and at least one previous negative TRUS-guided prostate biopsy session (*chapter 2*).
2. Most cancers (75%) detected with MR-guided biopsy in patients with an elevated PSA and at least one negative TRUS-guided biopsy session, are located in the anterior part of the prostate (*chapter 3*).
3. MR- and TRUS-guided biopsy both have difficulties in detecting apical lesions in biopsy naive men at risk (*chapter 4*).
4. In biopsy naive patients at risk MR-guided biopsy most often missed cancer with involvement of the dorsolateral part (58%) and TRUS-guided biopsy with involvement of the anterior part (79%) (*chapter 4*).
5. Diffusion weighted imaging is a non invasive technique that demonstrated a significant difference in mean ADC values between prostatitis ($1.08 \times 10^{-3} \text{ mm}^2/\text{s}$) and prostate cancer ($0.88 \times 10^{-3} \text{ mm}^2/\text{s}$). However, its usability in clinical practice is limited due to a high degree of overlap (*chapter 5*).
6. The MR compatible robotic manipulator allows a high accuracy and short total procedure time in a phantom (*chapter 6*).
7. It is feasible to perform transrectal prostate biopsy with real-time 3T MR imaging guidance with the aid of a remote-controlled, pneumatically actuated MR-compatible robotic manipulator in patients (*chapter 7*).
8. Although comparable results regarding accuracy and speed were found, the extended technical effort of the robotic manipulator makes the manual technique – currently – more suitable to perform MR-guided biopsies (*chapter 7*).
9. During MR-guided biopsy most target displacement is in the direction of the needle trajectory suggesting that most of the target displacement is caused by needle insertion (*chapter 7*).
10. It is feasible to use an automatic needle guide tracking sequence to perform 3T MR-guided prostate biopsies (*chapter 8*).

With multi-parametric MR imaging it has become possible to identify significant prostate cancer suspicious lesions with reduced detection of insignificant disease. Successively, MR-guided biopsy is a suitable technique for prostate cancer diagnosis. Robotic assisted MR-guided biopsy has the potential to reduce procedure time and increase accuracy, which currently limits the clinical availability. Furthermore, minimally invasive therapies are increasingly applied for treatment of localized prostate cancer. Consequently, the symbiosis of robotics and multi-parametric MRI will play an important role in the future during diagnosis and focal treatment of prostate cancer.

References

1. Ferlay J, Soerjomataram I, Dikshit R, et al. Cancer incidence and mortality worldwide: sources, methods and major patterns in GLOBOCAN 2012. *Int J Cancer*. 2015;136(5):E359-86.
2. Siegel RL, Miller KD, Jemal A. Cancer statistics, 2015. *CA Cancer J Clin*. 2015;65(1):5-29.
3. Integraal kankercentrum Nederland. Nederlandse Kankerregistratie Available from: <http://cijfersoverkanker.nl/>
4. Centraal Bureau voor de Statistiek. Doodsoorzaken. Available from: <http://statline.cbs.nl/>.
5. Schroder FH, Carter HB, Wolters T, et al. Early detection of prostate cancer in 2007. Part 1: PSA and PSA kinetics. *Eur Urol*. 2008;53(3):468-77.
6. Schroder FH, van der Maas P, Beemsterboer P, et al. Evaluation of the digital rectal examination as a screening test for prostate cancer. Rotterdam section of the European Randomized Study of Screening for Prostate Cancer. *J Natl Cancer Inst*. 1998;90(23):1817-23.
7. Djavan B, Ravery V, Zlotta A, et al. Prospective evaluation of prostate cancer detected on biopsies 1, 2, 3 and 4: when should we stop? *J Urol*. 2001;166(5):1679-83.
8. Taira AV, Merrick GS, Galbreath RW, et al. Performance of transperineal template-guided mapping biopsy in detecting prostate cancer in the initial and repeat biopsy setting. *Prostate Cancer Prostatic Dis*. 2010;13(1):71-7.
9. Loeb S, Bjurlin MA, Nicholson J, et al. Overdiagnosis and overtreatment of prostate cancer. *Eur Urol*. 2014;65(6):1046-55.
10. Berglund RK, Masterson TA, Vora KC, et al. Pathological upgrading and up staging with immediate repeat biopsy in patients eligible for active surveillance. *J Urol*. 2008;180(5):1964-7; discussion 7-8.
11. Divrik RT, Eroglu A, Sahin A, et al. Increasing the number of biopsies increases the concordance of Gleason scores of needle biopsies and prostatectomy specimens. *Urol Oncol*. 2007;25(5):376-82.
12. Kvale R, Moller B, Wahlqvist R, et al. Concordance between Gleason scores of needle biopsies and radical prostatectomy specimens: a population-based study. *BJU Int*. 2009;103(12):1647-54.
13. Lattouf JB, Saad F. Gleason score on biopsy: is it reliable for predicting the final grade on pathology? *BJU Int*. 2002;90(7):694-8.
14. Marshall S, Taneja S. Focal therapy for prostate cancer: The current status. *Prostate Int*. 2015;3(2):35-41.
15. Sankineni S, Wood BJ, Rais-Bahrami S, et al. Image-guided focal therapy for prostate cancer. *Diagn Interv Radiol*. 2014;20(6):492-7.
16. Bomers JG, Sedelaar JP, Barentsz JO, et al. MRI-guided interventions for the treatment of prostate cancer. *AJR Am J Roentgenol*. 2012;199(4):714-20.
17. Kanthabalan A, Emberton M, Ahmed HU. Biopsy strategies for selecting patients for focal therapy for prostate cancer. *Curr Opin Urol*. 2014;24(3):209-17.
18. Futterer JJ, Briganti A, De Visschere P, et al. Can Clinically Significant Prostate Cancer Be Detected with Multiparametric Magnetic Resonance Imaging? A Systematic Review of the Literature. *Eur Urol*. 2015;68(6):1045-53.
19. Barentsz JO, Richenberg J, Clements R, et al. ESUR prostate MR guidelines 2012. *Eur Radiol*. 2012;22(4):746-57.
20. Hambrock T, Somford DM, Huisman HJ, et al. Relationship between apparent diffusion coefficients at 3.0-T MR imaging and Gleason grade in peripheral zone prostate cancer. *Radiology*. 2011;259(2):453-61.
21. Delongchamps NB, Rouanne M, Flam T, et al. Multiparametric magnetic resonance imaging for the detection and localization of prostate cancer: combination of T2-weighted, dynamic contrast-enhanced and diffusion-weighted imaging. *BJU Int*. 2011;107(9):1411-8.
22. Katahira K, Takahara T, Kwee TC, et al. Ultra-high-b-value diffusion-weighted MR imaging for the detection of prostate cancer: evaluation in 201 cases with histopathological correlation. *Eur Radiol*. 2011;21(1):188-96.
23. Delongchamps NB, Singh A, Haas GP. The role of prevalence in the diagnosis of prostate cancer. *Cancer Control*. 2006;13(3):158-68.
24. Muller BG, van den Bos W, Pinto PA, et al. Imaging modalities in focal therapy: patient selection, treatment guidance, and follow-up. *Curr Opin Urol*. 2014;24(3):218-24.
25. Beyersdorff D, Winkel A, Hamm B, et al. MR imaging-guided prostate biopsy with a closed MR unit at 1.5 T: initial results. *Radiology*. 2005;234(2):576-81.
26. Woods TO. Standards for medical devices in MRI: present and future. *J Magn Reson Imaging*. 2007;26(5):1186-9.
27. Dianat SS, Carter HB, Macura KJ. Magnetic Resonance-Guided Prostate Biopsy. *Magn Reson Imaging Clin N Am*. 2015;23(4):621-31.
28. Hamoen EH, de Rooij M, Witjes JA, et al. Use of the Prostate Imaging Reporting and Data System (PI-RADS) for Prostate Cancer Detection with Multiparametric Magnetic Resonance Imaging: A Diagnostic Meta-analysis. *Eur Urol*. 2015;67(6):1112-21.
29. Weinreb JC, Barentsz JO, Choyke PL, et al. PI-RADS Prostate Imaging - Reporting and Data System: 2015, Version 2. *Eur Urol*. 2016;69(1):16-40.
30. Lemaitre G, Marti R, Freixenet J, et al. Computer-Aided Detection and diagnosis for prostate cancer based on mono and multi-parametric MRI: a review. *Comput Biol Med*. 2015;60:8-31.
31. Pokorny MR, de Rooij M, Duncan E, et al. Prospective study of diagnostic accuracy comparing prostate cancer detection by transrectal ultrasound-guided biopsy versus magnetic resonance (MR) imaging with subsequent MR-guided biopsy in men without previous prostate biopsies. *Eur Urol*. 2014;66(1):22-9.
32. Siddiqui MM, Rais-Bahrami S, Turkbey B, et al. Comparison of MR/ultrasound fusion-guided biopsy with ultrasound-guided biopsy for the diagnosis of prostate cancer. *JAMA*. 2015;313(4):390-7.
33. Salami SS, Ben-Levi E, Yaskiv O, et al. In patients with a previous negative prostate biopsy and a suspicious lesion on magnetic resonance imaging, is a 12-core biopsy still necessary in addition to a targeted biopsy? *BJU Int*. 2015;115(4):562-70.
34. Valerio M, Donaldson I, Emberton M, et al. Detection of Clinically Significant Prostate Cancer Using Magnetic Resonance Imaging-Ultrasound Fusion Targeted Biopsy: A Systematic Review. *Eur Urol*. 2015;68(1):8-19.
35. Hu Y, Ahmed HU, Allen C, et al. MR to ultrasound image registration for guiding prostate biopsy and interventions. *Med Image Comput Comput Assist Interv*. 2009;12(Pt 1):787-94.
36. van de Ven WJ, Hulsbergen-van de Kaa CA, Hambrock T, et al. Simulated required accuracy of image registration tools for targeting high-grade cancer components with prostate biopsies. *Eur Radiol*. 2013;23(5):1401-7.
37. Filson CP, Natarajan S, Margolis DJ, et al. Prostate cancer detection with magnetic resonance-ultrasound fusion biopsy: The role of systematic and targeted biopsies. *Cancer*. 2016.
38. Futterer JJ, Briganti A, De Visschere P, et al. Can Clinically Significant Prostate Cancer Be Detected with Multiparametric Magnetic Resonance Imaging? A Systematic Review of the Literature. *Eur Urol*. 2015.

39. Grenabo Bergdahl A, Wilderang U, Aus G, et al. Role of Magnetic Resonance Imaging in Prostate Cancer Screening: A Pilot Study Within the Goteborg Randomised Screening Trial. *Eur Urol*. 2015.
40. Sivaraman A, Sanchez-Salas R, Barret E, et al. Transperineal template-guided mapping biopsy of the prostate. *Int J Urol*. 2015;22(2):146-51.
41. Pepe P, Aragona F. Morbidity after transperineal prostate biopsy in 3000 patients undergoing 12 vs 18 vs more than 24 needle cores. *Urology*. 2013;81(6):1142-6.
42. Abolhassani N, Patel R, Moallem M. Control of soft tissue deformation during robotic needle insertion. *Minim Invasive Ther Allied Technol*. 2006;15(3):165-76.
43. Lagerburg V, Moerland MA, van Vulpen M, et al. A new robotic needle insertion method to minimise attendant prostate motion. *Radiother Oncol*. 2006;80(1):73-7.
44. Meltsner MA, Ferrier NJ, Thomadsen BR. Observations on rotating needle insertions using a brachytherapy robot. *Phys Med Biol*. 2007;52(19):6027-37.
45. Misra S, Macura KJ, Ramesh KT, et al. The importance of organ geometry and boundary constraints for planning of medical interventions. *Med Eng Phys*. 2009;31(2):195-206.

SAMENVATTING EN CONCLUSIES

Dit proefschrift beschrijft enkele aspecten van de symbiose tussen beeldvorming en robotica bij magnetische resonantie (MR)-geleide prostaatbiopsie. De noodzaak van MR-geleide biopsie wordt aangetoond in *hoofdstuk 2*. Verschillen in locatie en agressiviteit tussen MR-geleide biopsie en transrectale echografie (TRUS)-geleide biopsie worden in *hoofdstukken 3 en 4* beschreven teneinde inzicht te krijgen in de tekortkomingen van beide technieken. In *hoofdstuk 5* beschrijven we de verschillen in 'apparent diffusion coefficient' (ADC)-waarden verkregen tijdens 'diffusion weighted imaging' (DWI) teneinde onderscheid te kunnen maken tussen prostatitis en prostaat kanker. De toepasbaarheid van een MR-compatibele robot wordt aangetoond in een fantoom- en patiëntenstudie (*hoofdstuk 6 en 7*). Daarnaast is de bruikbaarheid van een automatische 'tracking' sequentie aangetoond, die de MR-geleide biopsieprocedure mogelijk kan verbeteren (*hoofdstuk 8*).

Noodzaak van MR-geleide biopsie

Hoofdstuk 2 rapporteert over de detectieratio van prostaatkanker, gevonden met MR-geleide prostaatbiopsie, in een grote patiëntenpopulatie. In totaal werden 438 patiënten geïnccludeerd, die zowel een prostaatspecifiek antigeen (PSA) > 4 ng/mL hadden, als tenminste 1 eerdere negatieve transrectale ultrageluid (TRUS)-geleide biopsiesessie hadden ondergaan. MR-geleide prostaatbiopsie werd uitgevoerd bij 265 van deze patiënten. De detectieratio van prostaatkanker voor de gehele onderzoekspopulatie (n=438) was 25% en respectievelijk 41% voor de patiënten (n=265) die de MR-geleide prostaatbiopsie ondergingen. Bovendien zijn de tumoren, die met MR-geleide biopsie werden gediagnosticeerd, hoofdzakelijk klinisch significant (87%). De resultaten van deze studie tonen aan dat, bij patiënten met een verhoogd PSA en 1 of meer negatieve TRUS-geleide biopsiesessies, MR-geleide biopsie een hogere prostaatkanker detectieratio heeft dan herhaalde TRUS-geleide biopsie. Tevens detecteert MR-geleide biopsie meer klinisch significante prostaattumoren.

Hoofdstuk 3 beschrijft de locatie van prostaatkanker, gediagnosticeerd met 3 tesla (3T) MR-geleide biopsie in patiënten met een verhoogd PSA en tenminste 1 negatieve TRUS-geleide biopsiesessie. Retrospectief werden 176 patiënten geïnccludeerd. Prostaatkanker is vastgesteld bij 78% (138/176) van de patiënten en bij 73% (202/277) van de laesies gezien op de multi-parametrische MRI. Bij het grootste deel van de patiënten is een klinisch significante tumor (93%; 128/138) gediagnosticeerd. In 75% (132/176) van de patiënten is kanker gevonden in het ventrale deel van de prostaat en in 30% (52/176) van de patiënten zijn periferezone tumoren gevonden. Tumoren met een maximale kanker core lengte (MCCL) ≥ 6 mm zijn voornamelijk (66%) in het ventrale deel van de prostaat gevonden.

In *hoofdstuk 4* zijn de locaties van significante prostaatkankerlaesies, die worden gemist met MR- of TRUS-geleide biopsie, onderzocht. Bij alle (n=223) mannen, met een klinische verdenking op prostaatkanker die niet eerder een prostaatbiopsie hadden ondergaan, werd een multi-parametrische MRI gemaakt en een 12-core systematische prostaat biopsie verricht. Bij alle patiënten met een PI-RADS 3 - 5 laesie op de multi-parametrische MRI (n=142) werd een MR-geleide biopsie verricht.

Bij 108 van de 142 patiënten werd de diagnose significante prostaatkanker gesteld. In deze patiëntengroep zijn 191 verschillende tumoren gevonden. Van deze tumoren is 74% (141/191) gedefinieerd als significante prostaatkanker. Bij MR-geleide biopsie is 74% (105/141) van deze tumoren significant en bij TRUS-geleide biopsie is dit 61% (86/141). TRUS-geleide biopsie detecteerde weliswaar meer tumoren dan MR-geleide biopsie (140 vs 109) maar een groot deel van deze tumoren zijn niet significant (39%). Significante tumoren, gemist met MR-geleide biopsie, zijn vaak gelegen in de dorsolaterale en apicale segmenten van de prostaat. Met TRUS-geleide biopsie werden vooral significante tumoren gemist in het ventrale (79%) deel van de prostaat. Met name in de ventrale mid prostaat (50%) en het ventrale deel van de apex (23%). De resultaten van de hoofdstukken 3 en 4 hebben klinische implicaties voor zowel de uroloog als de radioloog. Bijvoorbeeld voor het optimaliseren van het biopsie schema, gebruikt bij TRUS-geleide biopsie en MRI-gerichte TRUS-biopsie.

In *hoofdstuk 5* is onderzocht of het mogelijk is om onderscheid te maken tussen prostatitis en prostaatkanker op basis van ADC-waarden, verkregen tijdens MR-geleide biopsie. De ADC-waarden, berekend uit de diffusie gewogen beelden (DWI) van de MR-geleide biopsie, werden gecorreleerd aan de histopathologie van het biopsiemonster. Dit werd gedaan door de controle MRI-scan (in twee richtingen), met de naald in situ, op de berekende ADC-afbeelding te projecteren. De biopsielocatie werd gebruikt om handmatig een regio met grootte en omvang van de diffusierestrictie in te tekenen op de ADC-afbeelding die de kankerverdachte laesie weergeeft. DWI is een niet-invasieve techniek, die een significant verschil laat zien tussen gemiddelde ADC-waarden van prostatitis ($1,08 \times 10^{-3} \text{ mm}^2/\text{s}$, $\text{SD} \pm 0,18$) en prostaatkanker ($0,88 \times 10^{-3} \text{ mm}^2/\text{s}$, $\text{SD} \pm 0,15$). Echter, de bruikbaarheid in de klinische praktijk wordt beperkt door een hoge mate van overlap van de ADC-waarden.

Robot geassisteerde MR-geleide biopsie

In *hoofdstuk 6* is de toepasbaarheid van een pneumatisch aangedreven MR-compatibele robot bepaald in een fantoom. Vanuit de controlekamer kan met de robot de richting van een naaldgeleider onder real-time MRI worden aangepast. Het is daarbij niet meer nodig om het fantoom uit de MR-tunnel te schuiven om de naaldgeleider te verplaatsten.

Uit de analyse naar potentiële gevaren (FMEA) en de veiligheidsmetingen van de robot kwamen enkele verbeter punten naar voren. Uit de proef in het fantoom blijkt dat de gemiddelde tijd die nodig was om de naaldgeleider in de gewenste positie te brengen 5 minuten is; De gemiddelde totale proceduretijd (inclusief opbouwen) om een biopsie uit te voeren was minder dan 30 minuten; De nauwkeurigheid (in-plane error) voor het plaatsen van de naald was gemiddeld 3,0 mm (range 0-5,6 mm). De robot voorkomt de noodzaak om een patiënt in en uit de scanner te schuiven voor respectievelijk beeldvorming en manipulatie van de naaldgeleider. Deze resultaten bewezen de potentie om de transrectale prostaatbiopsieprocedure te verbeteren. De volgende stap is derhalve de klinische toepasbaarheid van dit systeem te onderzoeken.

Hoofdstuk 7 vergelijkt de nauwkeurigheid en snelheid van de nieuwe robottechniek met de handmatige methode in patiënten. De robotmethode en de handmatige methode toonden vergelijkbare resultaten met betrekking tot de gemiddelde fout (respectievelijk 5,7 vs 5,8 mm) voor de positionering van de naaldgeleider en gemiddelde doelwit verplaatsing (respectievelijk 6,6 vs 6,0 mm). De gemiddelde biopsiefout was groter (6,5 vs 4,4 mm) bij gebruik van de robot, echter niet significant. De mediaan van de proceduretijd en manipulatielijd waren respectievelijk 76 minuten en 6 minuten met behulp van de robot en 61 minuten en 8 minuten met de manuele methode. Verder werd waargenomen dat de meeste doelwit verplaatsing in de richting van het naaldtraject was. Dit suggereert dat de meeste verplaatsing werd veroorzaakt door het inbrengen van de naald.

De robot voorkomt de noodzaak om de patiënt in en uit de scanner te schuiven voor respectievelijk beeldvorming en manipulatie van de naaldgeleider. Ondanks vergelijkbare resultaten met betrekking tot de nauwkeurigheid en snelheid preferereert op dit moment de manuele techniek voor MR-geleide biopsieën. De extra technische handelingen maken het gebruik van de robot minder geschikt.

De totale proceduretijd met de robot bij patiënten is langer dan bij de fantoomstudie (*hoofdstuk 6*). Problemen met betrekking tot positionering van de patiënt, beperkte bewegingsmogelijkheid en ruimtelijke beperkingen van de robot zijn hieraan debet. De interactie tussen de real-time imaging software, de robotcontroller en de MR-console veroorzaakt een verlenging van de proceduretijd. Een real-time imaging sequentie, die deze interacties vereenvoudigt wordt geëvalueerd in het volgende hoofdstuk.

Hoofdstuk 8 toont de toepasbaarheid van een snelle real-time 'tracking' sequentie aan in een patiëntenonderzoek. De 'tracking'-sequentie berekent tijdens de MR-beeldacquisitie de 3D-positie van de passieve naaldgeleider en geeft bijna real-time het beeldvlak weer dat overeenkomt met de richting van de naaldgeleider. De patiënt blijft in de MR-tunnel tijdens het positioneren van de naaldgeleider en de beeldvorming. De mediane tijd, die nodig is voor de gehele biopsieprocedure was 32 minuten (range 14-48 minuten). De mediane tijd voor manipulatie per laesie (manipulatie van de endorectale marker tussen twee kankerverdachte laesies) was 1,5 minuten (range 0,7-5 minuten). Uit deze studie kunnen we concluderen dat het mogelijk is om met de automatisch 'tracking' sequentie MR-geleide prostaatbiopsieën uit te voeren. Deze techniek heeft potentie om MR-geleide prostaatinterventies te verbeteren.

Conclusies

De volgende algemene conclusies kunnen worden getrokken:

1. MR-geleide biopsie van 3T multi-parametrische MRI-gedetecteerde kankerverdachte laesies heeft een detectieratio van 41% voor overwegend klinisch significante prostaatkanker (87%) bij patiënten met een verhoogd PSA en ten minste 1 eerdere negatieve TRUS-geleide prostaatbiopsiesessie (*hoofdstuk 2*).
2. De meeste prostaatkankers (75%) gedetecteerd met MR-geleide biopsie bij patiënten met een verhoogd PSA en ten minste 1 negatieve TRUS-geleide biopsiesessie, bevinden zich in het ventrale deel van de prostaat (*hoofdstuk 3*).
3. Zowel MR- als TRUS-geleide biopsie missen apicale tumoren in patiënten met een klinische verdenking op prostaat kanker, die nog niet eerder een prostaat biopsie hebben ondergaan (*hoofdstuk 4*).
4. In patiënten die niet eerder een prostaatbiopsie hebben ondergaan worden met MR-geleide biopsie vooral tumoren gemist die in het dorsolaterale deel van de prostaat (58%) zijn gelegen. Met TRUS-geleide biopsie zijn de gemiste tumoren vooral gelegen in het ventrale deel van de prostaat (79%) (*hoofdstuk 4*).
5. Diffusiegewogen beeldvorming is een niet-invasieve techniek, die een significant verschil in gemiddelde ADC-waarden tussen prostatitis ($1,08 \times 10^{-3} \text{ mm}^2/\text{s}$) en prostaatkanker ($0,88 \times 10^{-3} \text{ mm}^2/\text{s}$) laat zien. Echter, de bruikbaarheid in de klinische praktijk wordt beperkt door een hoge mate van overlap in ADC-waarden (*hoofdstuk 5*).
6. De MR-compatibele robot zorgt voor een hoge nauwkeurigheid en korte totale proceduretijd in een fantoom (*hoofdstuk 6*).
7. Het is mogelijk om transrectale prostaatbiopsie met real-time 3T MR-beeldvorming uit te voeren in patiënten met behulp van een op afstand bedienbare, pneumatisch aangedreven MR-compatible robot (*hoofdstuk 7*).
8. Hoewel vergelijkbare resultaten met betrekking tot de nauwkeurigheid en snelheid werden gevonden, maken de extra technische handelingen voor het gebruik van de robot de manuele techniek op dit moment meer geschikt voor MR-geleide biopsieën (*hoofdstuk 7*).
9. Tijdens MR-geleide biopsie werd de meeste verplaatsing van de laesie in de richting van het naaldtraject gevonden, wat suggereert dat de meeste verplaatsing wordt veroorzaakt door het inbrengen van de naald (*hoofdstuk 7*).
10. Het is mogelijk om met een automatische 'tracking' sequentie 3T MR-geleide prostaatbiopsieën uit te voeren (*hoofdstuk 8*).

Met multi-parametrische MRI is het mogelijk om kankerverdachte laesies te identificeren. MR-geleide biopsie is een geschikte techniek om deze verdachte gebieden te bioperen. De klinische beschikbaarheid van MR-geleide biopsie is momenteel beperkt vanwege de lange proceduretijd en nauwkeurigheid. Robotgeassisteerde MR-geleide biopsie is mogelijk en heeft de potentie deze beperkingen te verbeteren. Daarnaast worden minimaalinvasieve therapieën steeds meer toegepast in de behandeling van prostaatkanker. Derhalve zal de symbiose van robotica en multi-parametrische MRI in de toekomst mogelijk een belangrijke rol spelen bij zowel de diagnose als de focale behandeling van prostaat kanker.

DANKWOORD

Wietske, ik realiseer mij al te goed dat het gekozen traject veel flexibiliteit van jou heeft gevraagd. Wanneer ik weer eens gefrustreerd was wist jij mij te motiveren en inspireren. Jij weet mijn grenzen soms beter dan ikzelf. Gelukkig heb ik hier geen bewijs voor; maar zonder jou was dit proefschrift er niet geweest. Ik ben zo blij met jou en wat vind ik het fijn om samen met jou en onze dochter Mies te zijn.

Prof. dr. J.O. Barentsz, beste Jelle, jouw enthousiasme voor het onderzoek naar de prostaat heeft mij geïnspireerd. Net zoals jouw naamgenoot kijk jij voorbij de horizon, daardoor is het je gelukt om de prostaat in kaart te brengen. Jij hebt ervoor gezorgd dat ik mij als Technisch Geneeskundige heb kunnen ontwikkelen. Naast het wetenschappelijk deel van mijn onderzoek heb ik, door jouw inzet, veel klinische ervaring op kunnen doen. Daarnaast wil ik jou bedanken voor jouw flexibiliteit waardoor ik in staat ben geweest om naast mijn promotie de studie geneeskunde te volgen.

Dr. J.J. Fütterer, beste Jurgen, ik wil jou in het bijzonder bedanken voor de begeleiding. Je snelle commentaar op een eerste versie van een artikel, inventiviteit maar ook de structurerende gesprekken hebben ertoe geleid dat ik nu mijn proefschrift heb afgerond. Mede dankzij jouw vertrouwen heb ik veel klinische ervaring op kunnen doen. Jij was altijd op de hoogte van wat er speelde. Toen ik net aan de geneeskunde opleiding was begonnen zei jij; "misschien wordt je wel huisarts". Ik was daar helemaal niet mee bezig en had als doel om interventie radioloog te worden. Inmiddels zit ik middenin de opleiding tot huisarts wat mij erg gelukkig maakt!

Dr. Ir. T.W. Scheenen, beste Tom, jij hebt mij laten zien dat MRI een interessante afbeeldingstechniek is. Bij jou kon ik terecht wanneer ik een bepaalde sequentie nodig had voor de experimenten met de robot. Door samen achter de MRI te zitten is voor mij de theorie achter deze modaliteit zichtbaar geworden. Bedankt voor de ondersteunde woorden, met name aan het einde van mijn promotie, jij wist mijn gevoelens goed te verwoorden.

Dr. S. Misra, Sarthak, jij hebt mij geholpen met de technische aspecten tijdens het onderzoek. Je kritische blik heeft mij scherp gehouden.

Pieter Vos en Henk Jan Huisman, jullie hulp was onmisbaar wanneer ik weer eens bepaalde gegevens uit MRCAD nodig had. Beste Dennis, altijd enthousiast en vol met ideeën. Dankzij jouw creativiteit is de robot werkelijkheid geworden.

Beste Jonne en Reinoud, wij kennen elkaar van de opleiding Technische Geneeskunde waar wij in 2003 als pioniers aan begonnen. Ik hecht veel waarde aan de gesprekken die wij hebben over ieders onderzoek, de ontwikkelingen omtrent Technische Geneeskundige maar ook de gezelligheid daarbuiten tijdens een diner, dagje uit of een borrel. Jonne, onze samenwerking binnen het bestuur van de Nederlandse Vereniging voor Technische Geneeskunde ten behoeve van het kwaliteitsregister is vruchtbaar gebleken.

Reinoud dankzij jouw adviezen is het mij gelukt om naast de studie Geneeskunde dit proefschrift te schrijven. Een betere studietoelichting kon ik mij niet wensen. Daarnaast wil ik Elsemieke en jou bedanken voor de gastvrijheid.

Collegae en kamer genoten Joyce, Derya, Wendy, Marcel, Maarten, Ansje, Thomas, Caroline, Esther, Kristian, Martin, Wulphert, Martijn, Tim en Jan, wetenschap heeft ons bij elkaar gebracht maar dit lijkt wel gerandomiseerd gebeurd. Het is leuk om binnen zo'n gevarieerd team te werken.

Beste prof. dr. Prokop, mede dankzij uw vertrouwen in de Technisch Geneeskundige heb ik mij ook zodanig kunnen ontplooien.

Beste Marijke en Manita, jullie hebben heel wat gepuzzeld om de biopten met de robot te organiseren.

Laboranten van de MRI, ik wil jullie bedanken voor de hulp tijdens de MR-geleide prostaat biopten. Ik heb veel van jullie geleerd over het bedienen van de MRI scanner, daarnaast was het ook gewoon gezellig.

Solange en Leonie, bedankt voor jullie steun, op de een of andere manier konden jullie altijd wel een gaatje vinden in de drukke agenda's van Jelle en Jurgen.

Dr. C.A. Hulsbergen-van de Kaa, hartelijk dank voor de ondersteuning vanuit de pathologie.

Beste cogroep 163, leuk om met jullie de ontwikkeling tot arts te hebben kunnen delen.

Gerda en Jan Willem, dank voor jullie begrip en ondersteuning om mijn proefschrift tijdens het eerste jaar van de huisartsenopleiding af te kunnen ronden.

De Lochem boys, het is leuk om te zien dat een ieder zich op geheel eigen wijze heeft ontwikkeld en wanneer wij weer bij elkaar zijn het ouderwets gezellig is. Steven, design en wetenschap lijken vaak ver uit elkaar te liggen maar jij bent het levende bewijs dat dit niet zo is. Onze hechte vriendschap betekent veel voor me. Geert, ik bewonder je grafische werk en ben vereerd dat jij dit proefschrift vorm hebt weten te geven.

Hans, Marion, Jikke, Jitze, Hilke, Sebastiaan en Tjerk dank voor het luisteren maar vooral voor de gezelligheid. Ik ben blij dat ik jullie bij Wietske heb gekregen.

Jasper en Floor bedankt voor jullie gastvrijheid, ik kon regelmatig bij jullie aanschuiven met het eten en er was ook altijd wel een bedje vrij. Floor, ik hoop dat de gesprekken over robots die Jasper en ik regelmatig voerden niet te saai voor je waren.

Mijn ouders, Mart en Hennie, hebben mij altijd gesteund en staan altijd weer paraat als ik ze nodig heb, ik ben jullie dankbaar. Van jullie moest ik doen wat ik leuk vind, door jullie ben ik gekomen waar ik nu sta.

CURRICULUM VITAE



Martijn Gerjan Schouten is geboren op 22 mei 1985 te Groningen. In 2003 behaalde hij zijn VWO diploma aan het Staring College te Lochem. Aansluitend begon hij aan de nieuwe opleiding Technische Geneeskunde aan de Universiteit Twente, welke in dit jaar van start ging. In 2010 behaalde hij zijn Master of Science titel na een stage op de afdeling Radiologie van het Radboud UMC. Deze wetenschappelijke stage resulteerde in een publicatie en bleek tevens de fundatie te zijn van dit proefschrift. Onder leiding van prof. dr. Barentsz en dr. Fütterer is hij in 2010 begonnen met het huidige project over MR-geleide prostaat biopsie. Daarnaast is hij in 2011 begonnen aan de opleiding Geneeskunde aan de Katholieke Universiteit Nijmegen en legde hij in 2015 de artsen eed af. In 2016 is hij begonnen aan de huisartsenopleiding.

[← BACK TO TABLE OF CONTENTS](#)

[MRI-GUIDED PROSTATE BIOPSY: WHICH DIRECTION?](#)

PUBLICATIONS

Schouten MG, van de lees M, Pokorny M, Hoogenboom M, Barentsz JO, Thompson LC, Fütterer JJ. Why and where do we miss significant prostate cancer with multiparametric magnetic resonance imaging followed by magnetic resonance-guided and transrectal ultrasound-guided biopsy in biopsy naive men? Eur. Urol 2017

Schouten MG, Hoeks CMA, Bomers JGR, Hulsbergen-van de Kaa CA, Witjes JA, Thompson LC, Rovers MM, Barentsz JO, Fütterer JJ. Location of prostate cancers determined by multiparametric and MRI-guided biopsy in patients with elevated prostate-specific antigen level and at least one negative transrectal ultrasound-guided biopsy. AJR Am J Roentgenol 2015; 205(1):57-63

Zamecnik P, **Schouten MG**, Krafft AJ, Maier F, Schlemmer HP, Barentsz JO, Bock M, Fütterer JJ. Automated real-time needle-guide tracking for fast 3-T MR-guided transrectal prostate biopsy: a feasibility study. Radiology. 2014; 273(3):879-86

Nagel KN, **Schouten MG**, Hambrock T, Litjens GJ, Hoeks CM, ten Haken B, Barentsz JO, Fütterer JJ. Differentiation of prostatitis and prostate cancer by using diffusion-weighted MR imaging and MR-guided biopsy at 3 T. Radiology. 2013; 267(1):164-72

Jahya A, **Schouten MG**, Fütterer JJ, Misra S. On the importance of modelling organ geometry and boundary conditions for predicting three-dimensional prostate deformation. Comput Methods Biomech Biomed Engin. 2014; 17(5):497-506

Hoeks CM, **Schouten MG**, Bomers JG, Hoogendoorn SP, Hulsbergen-van de Kaa CA, Hambrock T, Vergunst H, Sedelaar JP, Fütterer JJ, Barentsz JO. Three-Tesla Magnetic Resonance-Guided Prostate Biopsy in Men With Increased Prostate-Specific Antigen and Repeated, Negative, Random, Systematic, Transrectal Ultrasound Biopsies: Detection of Clinically Significant Prostate Cancers. Eur Urol. 2012; 62(5):902-9

Schouten MG, Bomers JGR, Yakar D, Huisman HJ, Bosboom D, Scheenen TWJ, Misra S, Fütterer JJ. Evaluation of a robotic technique for transrectal MRI-guided prostate biopsies. Eur. Radiol. 2012; 22:276-283

Yakar D, **Schouten MG**, Bosboom D, Scheenen T, Barentsz JO, Fütterer JJ. Feasibility of a pneumatically actuated MR-compatible robot for MR-guided prostate biopsy. Radiology 2011; 260:241-247

Yakar D, Debats O, Bomers JGR, **Schouten MG**, van Lin E, Fütterer JJ, Barentsz JO. Predictive value of MRI in the localization, staging, volume estimation, assessment of aggressiveness, and guidance of radiotherapy and biopsies in prostate cancer. Invited review J Magn Reson Imaging 2012; 35:20-31

Schouten MG, Ansems J, Renema WKJ, Bosboom D, Scheenen TWJ, Fütterer JJ. The accuracy and safety aspects of a novel robotic technique for needle guide positioning to perform transrectal prostate biopsy. Med. Phys. 2010; 37:4744-4750.



MRI-guided prostate biopsy: which direction?

Martijn G. Schouten

